THE REGULATION OF NEURAL-SPECIFIC GLYCOSYLATION IN *DROSOPHILA MELANOGASTER*

by

SARAH RUTH BAAS

(Under the Direction of Michael Tiemeyer)

ABSTRACT

The addition of carbohydrate structures (glycans) to proteins is an essential post-translational modification that begins in the endoplasmic reticulum and is completed through Golgi remodeling. Glycosylation can be cell-specific, tissue-specific, and developmental stage-specific. Altered glycosylation patterns are a hallmark of many cancers as well as many neuronal and muscular diseases, and developmental disorders. However, the mechanisms that regulate glycosylation in a tissue-specific manner are not well understood. A genetic screen in *Drosophila melanogaster* yielded a mutation called *sugar-free frosting* (*sff*), the *Drosophila* homolog of *SAD* kinase. Analysis of all of the N-linked glycans in *sff* mutant embryos revealed a shift towards more complex structures, a shift determined to stem from altered Golgi compartmentation. Many signaling pathways impinge on *sff/SAD* function, allowing the cellular microenvironment to exert minute control over the N-glycosylation patterns of neurons. One of those pathways receives signaling from a Toll-like receptor (Tollo) expressed on a neighboring non-neural cell. Pharmacological studies indicate that the signal relayed to the neural cell is a biogenic amine. In addition, White, which contributes to eye pigment biosynthesis, interacts with Sff/SAD and influences the phenotypes associated with the *sff* mutation. White also

influences N-glycan expression. Therefore, White, biogenic amines, and Sugar-free frosting/SAD kinase, define nodes in a pathway that modulates neural-specific glycosylation in *Drosophila*.

INDEX WORDS: SAD kinase, glycosylation, HRP-epitope, Golgi, White, Biogenic amines

THE REGULATION OF NEURAL-SPECIFIC GLYCOSYLATION IN *DROSOPHILA MELANOGASTER*

by

SARAH RUTH BAAS

B.S., Virginia Tech, 2004

A Dissertation Submitted to the Graduate Faculty of The University of Georgia in Partial Fulfillment of the Requirements for the Degree

DOCTOR OF PHILOSOPHY

ATHENS, GEORGIA

2010

THE REGULATION OF NEURAL-SPECIFIC GLYCOSYLATION IN *DROSOPHILA MELANOGASTER*

by

SARAH RUTH BAAS

Major Professor:	Michael Tiemeyer
Committee:	Steven Dalton Michael Pierce Richard Steet Lance Wells

Electronic Version Approved:

Maureen Grasso
Dean of the Graduate School
The University of Georgia
May 2010

ACKNOWLEDGEMENTS

Above all, I must give God the glory. Every day I am in awe of the wonder of His creation and am blessed to be able to add a tiny piece of knowledge to our understanding of this intricate and marvelous world.

Secondly, I must of course thank my advisor, Dr. Michael Tiemeyer. After working in the lab only a week, I knew I wanted to stay- I have never regretted that decision. I could not have asked for a better mentor and I thank you for your never-ending optimism and childlike glee at every experimental result. It will be very difficult to leave the lab and I will be eternally grateful to you for everything.

I am grateful to the members of my doctoral committee: Dr. Steve Dalton, Dr. Michael Pierce, Dr. Rich Steet, and Dr. Lance Wells. Thank you for all your advice and input. You have certainly stretched my abilities but I thank you for seeing where I needed to be and helping me to get there.

I thank all the members of the Tiemeyer lab, past and present. Especially Mary, my cubby buddy. To the mass spec side of our lab- Toshi, Kazuhiro, and Mindy- thanks for all your help in teaching me to become an analytical chemist. To Varshika, my apprentice. When I leave the lab, I know I am leaving the sff project in good hands!

I am eternally grateful to my dear family, for their endless love and support. I could not have survived these last years without you! And when I say family, I cannot leave out my precious dog Bree. To my mother, I admire you so much and I strive to have as much faith and strength as you. To my father, for his incredible insightfulness and overflowing love. I may

have beat you to a Ph.D, but you will always be one of the most gifted and intelligent people I have ever met. To my dear sister Robyn, I love you too much for words. Finally, thank you to all my dear friends. You have helped make this journey easier with laughter and encouragement.

Oh I almost forgot…I must thank all the flies that have participated in all the experiments, against their will. Sorry I killed you, but at least most of you drowned in alcohol, so you died drunk and happy. Except the sffs, they might be too depressed. Oh well, at least some of you were treated with antidepressants!

TABLE OF CONTENTS

LIST OF TABLES

Page

LIST OF FIGURES

Page

CHAPTER 1

INTRODUCTION AND LITERATURE REVIEW

The scope of this dissertation deals with the importance of N-linked glycosylation and the signaling pathways and mechanisms involved in regulating tissue-specific N-glycan expression. Before splashing into N-glycosylation, a toe dip into other types of glycosylation will be presented.

Carbohydrates are broadly appreciated as energy sources: monosaccharides such as glucose, disaccharides like fructose and lactose, and polysaccharides like glycogen. But carbohydrates are decidedly more vast and complex and have many diverse functions. To begin with, all eukaryotic cells are covered in a thick layer of carbohydrate called the glycocalyx. It consists of glycoproteins, proteoglycans, and glycosphingolipids. Each of these classes will be briefly discussed, before delving into glycoproteins exclusively.

Glycolipids and Proteoglycans

Glycosphingolipids, a type of glycolipid, consist of a glycan (simply meaning saccharide or carbohydrate) attached to a lipid ceramide tail. These are embedded in the cell membrane with there being are more than 200 glycolipids that have been identified (Varki et al., 1999). Certain glycosphingolipids have been found to be associated with certain receptors, contributing to their function. For example, the ganglioside GM3 inhibits tyrosine phosphorylation of the epidermal growth factor receptor, although the mechanism of action is not well understood (Varki, Cummings et al. 1999).

Proteoglycans have a core protein with glycosaminoglycan (GAG) chains attached. GAGs are polysaccharides consisting of repeating units of hexosamine and a hexose or a hexuronic acid. Examples include heparan sulfate and chondroitin sulfate. The majority of the proteins at the neuronal synapse (to be discussed later) bind heparin or they are heparan sulfate proteoglycans (Martin, 2002). These include syndecan, dally-like, and agrin. Agrin is a heparan sulfate proteoglycan that is essential to neuromuscular junction (NMJ) morphogenesis as mouse knockouts fail to form NMJs and cannot breathe, dying at birth (Guatam et al., 1996). Agrin activates muscle-specific kinase (MuSK), whose signaling leads to the aggregation of nicotinic acetylcholine receptors (Glass et al., 1996).

O-linked glycans

Proteins that are post-translationally modified with carbohydrate structures are called glycoproteins. There are two predominant ways by which carbohydrates can be linked to proteins: O-linked and N-linked. O-linked glycans are attached to serine or threonine residues, while N-linked glycans are attached to asparagine (asn) residues. The proteoglycans discussed above are a type of O-glycan. Mucin type O-glycans are initiated by a N-acteylgalactosamine (GalNAc) attached to serine or threonine (Carraway and Hull, 1989). Galactose is added in a β1-3 linkage forming a disaccharide called Core 1. Additional monosaccharides are extended or branched to form different core structures, numbered 2 through 8. A single GlcNAc can also be added to serine/threonine resides. This modification, known as O-GlcNAc, is present on nuclear and cytosolic proteins and has been shown to be reciprocal with phosphorylation in some contexts (Snow and Hart, 1998). O-GlcNAc addition modifies signaling pathways involved in diabetes and neurodegenerative disease. There are also O-mannose initiated structures, most

famously on α-dystroglycan; many forms of congenital muscular dystrophy stem from aberrant glycosylation of α-dystroglycan (Martin, 2007; Wells, 2009).

Another important O-linked modification is the addition of fucose, catalyzed by O-fucosyltransferases (O-FucTs) add fucose onto epidermal growth factor (EGF) repeats and thrombospondin-1 repeats on proteins (Becker and Lowe, 2003). Both humans and *Drosophila* have two O-FucTs (referred to as POFUTs). Another example of a protein that is O-fucosylated is Notch, which plays important roles in development, particularly in cell fate determination. O-fucosylation is essential for proper Notch signaling such that knocking out POFUT1 in mice or OFUT1 in *Drosophila* produces phenotypes that mimic defects in Notch (Luo et al., 2006). GlcNAc addition to the fucose, catalyzed by the enzyme Fringe, is also essential for proper Notch signaling. Surprisingly, in the fly OFUT1 is also required for proper folding of the Notch protein (Okajima et al., 2005). OFUT1 binds to Notch and chaperones it out of the ER, helping it to fold; this function does not require its fucosyltransferase activity.

α3 Fucosyltransferases are involved in synthesizing the ligands for selectins (Becker and Lowe, 2003). Selectins are cell adhesion receptors found on platelets (P-selectin), endothelial cells (E and P-selectin), and leukocytes (L-selectin). The ligands, which are modified forms of sialyl Lewis^x, bind to selectins, which help mediate the rolling of leukocytes on the endothelium after their attachment to the vessel wall (Becker and Lowe, 2003; Wangers and Kansas, 2000). After their tumbling, the leukocytes are activated by chemokines and eventually migrate into the tissues. FucT IV and VII are essential for normal leukocyte trafficking, determined by generating mouse knockouts of *FUT4* and *FUT7* genes (Javaud et al., 2003).

N-linked glycans

N-linked glycosylation is the primary focus of this dissertation, so it will be discussed in detail. The first focus will be on N-glycan maturation. These events are generally well conserved across species, so the events in mammals will be discussed now, with differences in *Drosophila* discussed later. N-linked glycans begin their life membrane bound as a dolichol oligosaccharide precursor (Varki et al., 1999) (**Fig 1.1**). One GlcNAc is transferred from UDP-GlcNAc to a dolichol phosphate by GlcNAc1-phoshotransferase on the cytosolic face of the endoplasmic reticulum (ER). A second GlcNAc is added by the GlcNAc transferase Alg (consisting of Alg 13 and Alg14)(Bickel et al., 2005). Next, five mannoses are added, four in all for a final total of nine mannoses; GDP-mannose is the donor. The entire structure is then flipped such that the oligosaccharides are exposed to the lumen of the endoplasmic reticulum. Dol-P-Man then adds its mannose onto the precursor, four in all. Three glucoses are added next, in the same fashion using a Dol-P-Glc donor. The precursor is now ready to be attached to an asparagine residue on the appropriate protein. Oligosaccharyltransferase (OST) transfers the precursor to a nascent protein.

The next step to forming a mature N-linked glycoprotein is folding. First, glucosidase I and II remove the terminal two glucoses. The proteins calnexin or calreticulin, which bind to the premature glycoprotein, then recognize the last remaining glucose. If the polypeptide is not folded correctly, a glucosyltransferase adds glucose back onto the structure; otherwise the last glucose is removed.

Once the premature glycoprotein is properly folded, it now serves as the substrate for various glycosyltransferases and mannosidases to generate the three classes of N-linked glycans (**Fig. 1.2**). High mannose types are the simplest N-linked glycans and terminate in mannose

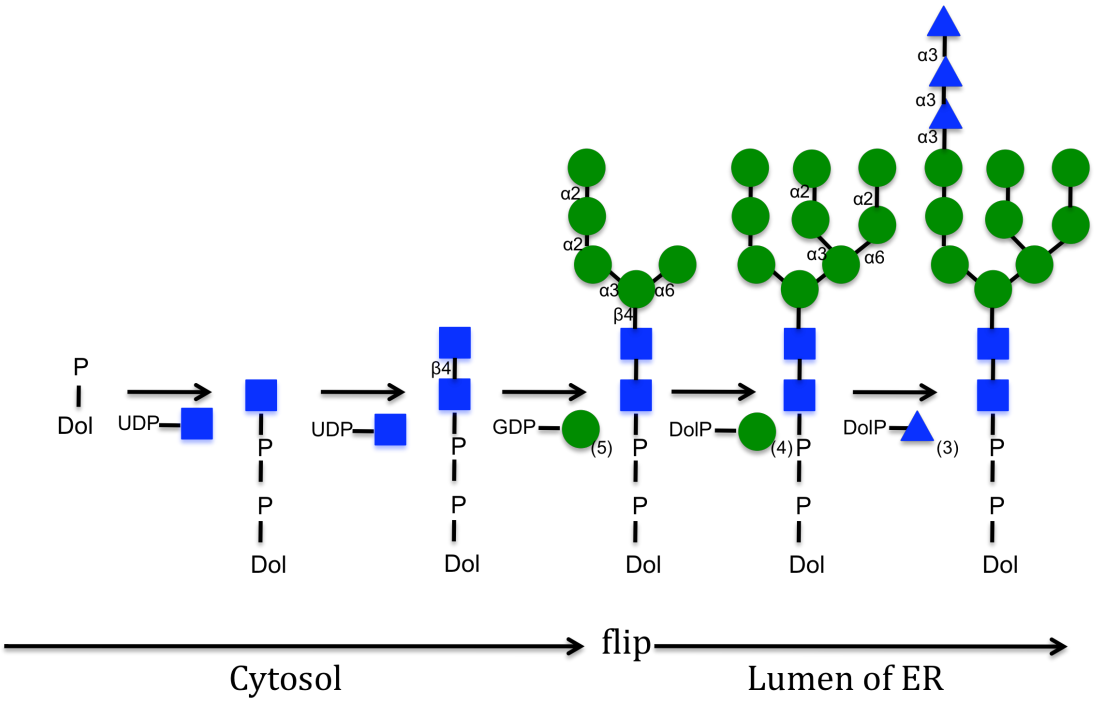

Figure 1.1 Initial steps in N-glycan biosynthesis
The dolichol oligosaccharide precursor is synthesized by the transfer of 2 GlcNAcs (blue) and 9 mannoses (green) from nucleotide sugar donors onto dolichol phosphate. The orientation of the precursor is flipped during synthesis so that it faces the lumen of the ER. Glucoses (yellow) are added to a terminal mannose, after which the oligosaccharide is transferred to a nascent polypeptide. Adapted from Varki et al., 1999.

residues. The remaining classes of N-linked glycans are diversifications of a $Man_5GlcNAc_2$-Asn, which is generated from the activities of class I α-mannosidases. More complex glycan processing occurs in various compartments of the Golgi apparatus. GlcNAc transferase I (GnTI) adds a GlcNAc in a β1-2 linkage to the terminal mannose on the 3' arm. The glycan can be trimmed down by cleavage of terminal mannoses by α-mannosidase II. $GlcNAc_1Man_3GlcNAc_2$-Asn is an example of the hybrid class, with a high mannose arm and a complex arm with GlcNAc. GnT II, III, IV, V, and VI all add GlcNAc from UDP-GlcNAc at specific points on the mannose tree and each adds it in a certain linkage. Sialic acid can be added by sialyltransferase (from CMP-sialic acid) and fucose can be added to the internal GlcNAc, by fucosyltransferase using GDP-Fuc. The structures that have these modifications on both branches are called complex N-glycans. GnTI and II must both act to produce a complex structure (Varki et al., 1999).

Drosophila as a model system

Drosophila melanogaster, or fruit fly, is a commonly used model system, particularly for genetic studies. It has a small genome and only 4 chromosomes. Its generation time is also short, making it easy to manipulate and get results fairly quickly (as opposed to the mouse, for example). The *Drosophila* life cycle consists of 17 embryonic stages, 3 larval stages, a pupal stage, and an adult stage. The experiments discussed later will mainly focus on the embryo, but there will also be a few experiments conducted with 3rd instar larvae and adults. Thus, this dissertation will present the effects of a mutation across the entire life cycle of *Drosophila*.

N-glycans of _Drosophila_

By mass spectrometry (methods to be discussed later), 42 N-glycans present in the embryo have been identified and their prevalence expressed as a percent of the total profile (Aoki et al., 2007).

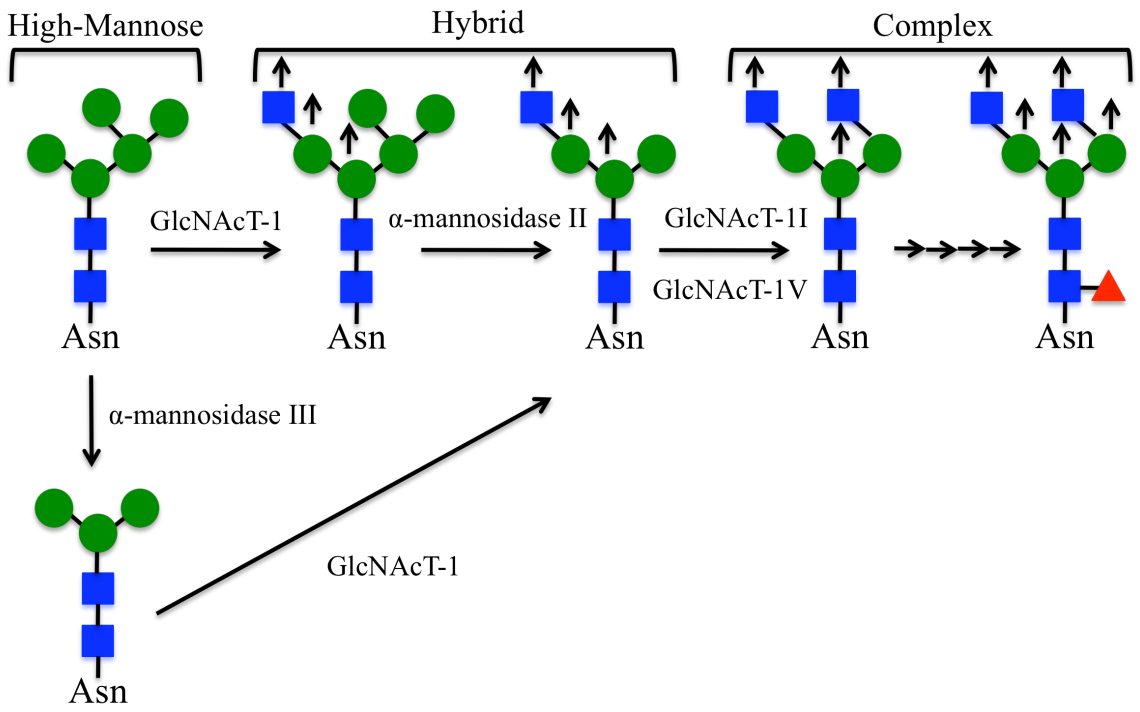

Figure 1.2 Three classes of N-linked glycans
N-linked glycans are classified into high-mannose (only terminal mannoses), hybrid (some branches that terminate in mannose and some that contain GlcNAc or other sugars) and complex (all branches terminate in sugars other than mannose). The diversification of N-linked glycans involves both the removal and addition of different monosaccharides. The arrows indicated on the structures represent sites that can be extended further. Adapted from Varki et al., 1999.

The N-glycome of *Drosophila* is much simpler than vertebrates as the most abundant structures are high mannose type. There are two sialylated structures but they are just barely detectable above background (Aoki et al., 2007). Many of the enzymes required to synthesize these structures have not yet been identified and characterized. Analysis of all of these glycans enables the effect of various mutations on the prevalence of each structure to be determined in order to gain a better understanding of the role of a specific protein in regulating N-glycosylation.

There are some differences between mammalian N-linked glycan structures and glycosyltransferases (discussed above) and *Drosophila*. *Drosophila* has a unique enzyme called Fused Lobes (Fdl) (Leonard et al., 2006). Fdl is a hexosaminidase that can remove the GlcNAc added by GnTI (**Fig 1.3**). The presence of Fdl helps explain the simplicity of the glycans in *Drosophila* because the enzyme can prevent further elaboration of structures to the more complex. Another reason is that the expression of glycosyltransferases, such as sialyltransferase, is very restricted (Koles et al., 2004).

Another uniqueness of *Drosophila*, as well as other invertebrates and also plants, is the ability to add α1-3 linked fucose to the internal GlcNAc of the chitobiose core, in addition to α1-6 (**Fig 1.3**). In *Drosophila* this modification is added by a fucosyltransferase called FucTA. There are 3 other fucosyltransferase annotated in the *Drosophila* genome, B, C, and D; only FucTA is able to add this modification in *vivo* (Rendic et al., 2006; Rendic et al.). α-3 linked fuc is the defining component of a family of N-glycans known as HRP-epitopes. This family contains hybrid, paucimannose, and complex structures, which are expressed predominantly in the nervous system of the *Drosophila* embryo; they are also expressed in the later stages, and in other invertebrates such as the grasshopper (Snow et al., 1987). HRP-epitopes are recognized by

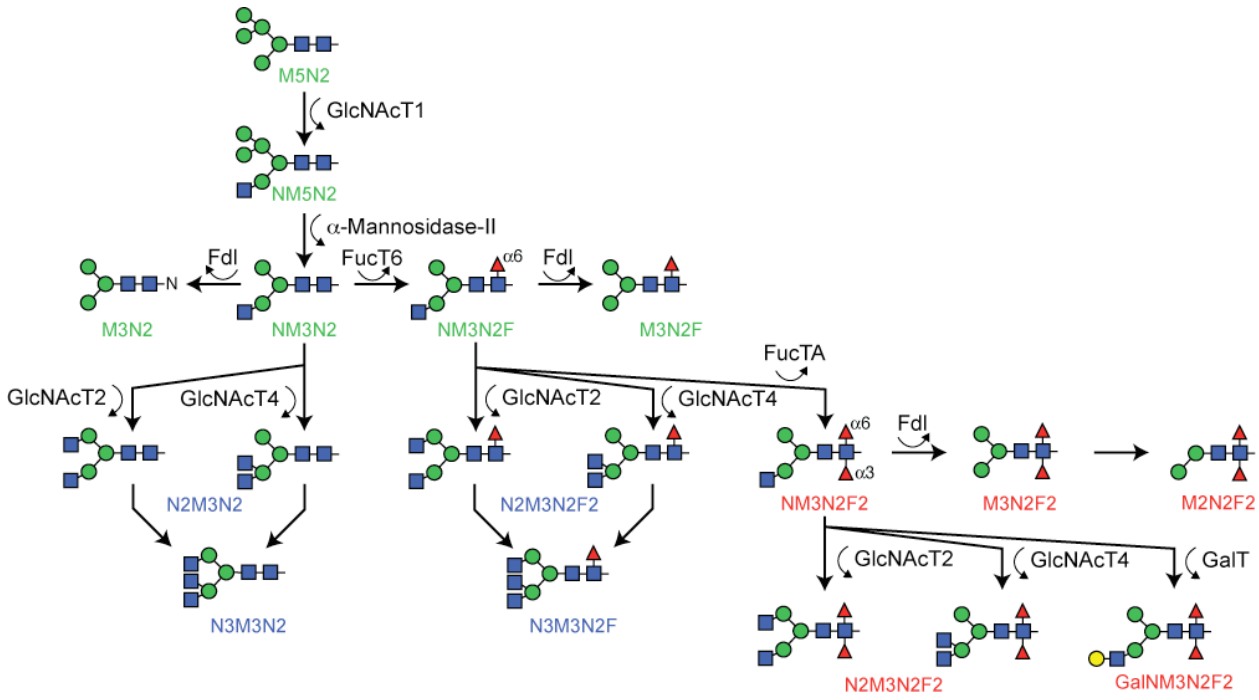

Figure 1.3 N-glycan processing pathways in *Drosophila*
The figure above depicts some of the N-glycan processing pathways present in *Drosophila*. Particularly noted is the activity of Fused lobes (fdl) that cleaves the GlcNAc added by GlcNAcT1, reverting structures to simpler types (structures named in green). The activities of GlcNAcT2 and 4 generate more complex glycans (structures named in blue). FucTA adds α-3 linked fucose onto the internal GlcNAc to generate the HRP-epitopes (structures named in red).

antibodies generated against the plant glycoprotein horseradish peroxidase (HRP) and are one of the main focuses of the experiments that are described in this dissertation, and therefore will be discussed in more detail later.

Development of the *Drosophila* embryonic nervous system

The main focus of this dissertation will be the regulation of tissue-specific glycosylation in the nervous system of *Drosophila*, particularly the embryonic nervous system. Therefore, it is necessary to discuss nervous system development throughout the *Drosophila* life cycle, but the main focus will remain on the embryonic nervous system, which consists of the ventral nerve cord and peripheral nervous system.

The ventral nerve cord (VNC) of *Drosophila* arises from the neurogenic region of the ectoderm. The middle neurogenic region gives rise to the neurons and glial cells at the midline of the VNC while the flanking regions are responsible for all of the other neurons (Compos-Ortega, 1993). The dorsal-ventral and anterior-posterior patterning of the embryo divides the cells in this region into a grid consisting of seven rows and three columns (Karcavich, 2005). Each section is referred to an equivalence group, and one neuroblast (NB), the stem cell precursor of the nerve cord, delaminates from each group; the rest of the cells become epidermal cells. This decision is controlled by proneural genes, members of the basic helix-loop-helix family of transcription factors, and neurogenic genes, members of the Notch signaling pathway (Skeath and Thor, 2003; Technau et al., 2006). The proneural genes are a complex called *achaete-scute* (*ac/sc*) and consist of *achaete* (*ac*), *scute* (*sc*) and *lethal of scute* (*l'sc*) (Skeath and Thor, 2003). In each equivalence group, the cell that has the highest expression of *ac/sc* will become the neuroblast. The remaining cells are prevented from becoming a NB by the activity of Notch. With its fate sealed, the NB expresses Delta, the ligand for Notch. Delta binds to the

Notch receptor on the neighboring cell, and through a series of cleavages, Notch translocates to the nucleus and interacts with two proteins, Suppressor of Hairy and Mastermind. This complex then activates expression of *Enhancer of Split* genes, which repress transcription of the *ac/sc* genes (Skeath and Thor, 2003). Lacking *ac/sc* expression, the cells adopt the epidermal cell fate. Decapentaplegic (DPP), which is secreted in the dorsal non-neural ectoderm, also promotes ectoderm differentiation by suppressing genes required for neural development (Kim et al., 2004). Similarly, Short Gastrulation (Sog)/Chordin is expressed in the ventral neurectoderm and promotes the neural fate by blocking DPP activity (Kim et al., 2004).

After gastrulation, approximately three hours after the start of embryogenesis (stage 8), the neuroblasts double in size and migrate to the interior of the embryo, to a region known as the subectodermal proliferative zone, located between the ectoderm and the mesoderm (Brody and Odenwald, 2002; Feurstenberg et al., 1998; Hartenstein, 1993). This process is called delamination and occurs during stage 9-10 in five waves. (3 hours, 40 minutes to 5 hours, 20 minutes) (Brody and Odenwald, 2002; Hartenstein, 1993; Hartenstein and Campos-Ortega, 1997). The result is about thirty NBs per hemisegment.

After their journey, neuroblasts divide in a stem cell-like fashion to produce cells called ganglion mother cells (GMCs), which bud off from the basal side of the neuroblast; this occurs between stages 9 and 13, four to ten hours after the start of embryogenesis (Feurstenberg et al., 1998; Hartenstein, 1993). The neuroblast divides about 5 times, growing smaller after each division and pushing its daughter cells farther into the interior of the embryo (Hartenstein and Campos-Ortega, 1997). The division is asymmetric, as it results in specific proteins and mRNA localizing exclusively into the ganglion mother cell. This includes Prospero, which functions to limit the proliferative ability of the GMC to a single division, giving rise to two neurons and/or

glial cells (Feurstenberg et al., 1998; Skeath and Thor, 2003). This exclusivity of Prospero involves the protein Miranda, which binds to it and holds it in the apical cortex of the neuroblast at late interphase. As mitosis begins, Prospero and Miranda are pulled to the basal side. As a result, these two proteins are only localized to the ganglion mother cell (Feurstenberg et al., 1998; Skeath and Thor, 2003)(Figure 1). *Prospero* mRNA is also partitioned into the GMC via the same mechanism, but this appears to be independently regulated. Surprisingly, *prospero* is only transcribed in the neuroblast, where it serves no purpose, and not in the GMC, where it is essential (Feurstenberg et al., 1998). Another protein, Numb, is also asymmetrically partitioned into the GMC, in much the same way that Prospero is. However, these two proteins are independent, as *propero* mutants correctly localize Numb protein and vice versa (Feurstenberg et al., 1998). Numb dictates the cell fates of the progeny of the ganglion mother cell, a topic to be discussed presently.

The gene expression pattern of the ganglion mother cell is dependent on the time of its birth, and is determined by its neuroblast parent. Neuroblasts express a set of genes in a transient manner and in a reproducible order so that as time progresses the resultant progeny will only express the gene from that time frame (**Figure 1.4**). In contrast to the transient expression in the neuroblast, the expression in the ganglion mother cell is not transient and endures for the life of the cell and is passed on to its progeny. There are five genes in this temporal set, and consist of *Hunchback* (*Hb*), *Kruppel* (*Kr*), *Pdm*, *Castor* (*Cas*), and *Grainyhead* (*Gh*), presented in the order that they are expressed (Brody and Odenwald, 2002; Edenfeld et al., 2002; Pearson and Doe, 2004; Skeath and Thor, 2003). All of the genes encode transcription factors. Therefore, each GMC that is produced from a neuroblast will have a unique identity according to its time of birth, as only about one GMC is produced during each expression interval. Interestingly, this

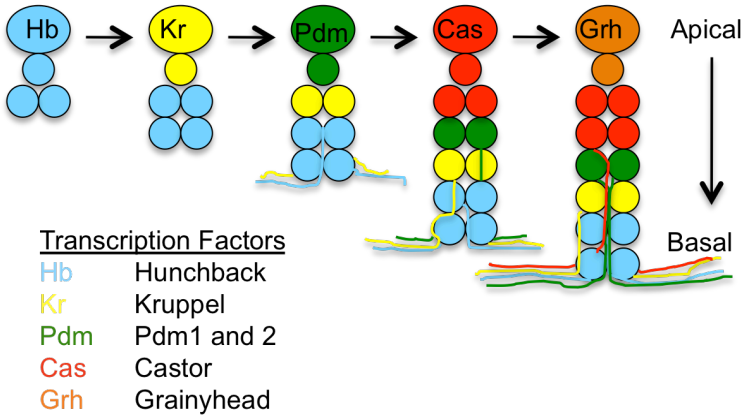

Figure 1.4 Transient gene expression in the neuroblast yields unique progeny
Ganglion mother cells express one transcription factor from a set temporally expressed by its parent neuroblast. The neuroblast expresses *hunchback* first, followed by *kruppel*, *pdm*, *castor*, and *grainyhead*. Only one ganglion mother cell is born during each expression time point. Figure adapted from Brody and Odenwald, 2002.

gene expression does not coincide with cell fate (Pearson and Doe, 2004). For example, a GMC that expresses *Hb* can give rise to interneurons, motorneurons, or glia just as a GMC that expresses *Cas*. The ability of the neuroblast to express a set of genes in a timely and transient manner due to the fact that each transcription factor can activate the next in line, while repressing the one in line behind that (Edenfeld et al., 2002; Skeath and Thor, 2003). For example, *Hb* activates *Kr* expression, while repressing *Pdm*. The effect of this timely march is a "genetic layering" of the ventral nerve cord, with the neural and glial progeny of the GMCs expressing *Hb* at the basal edge, followed by *Kr, Pdm*, and *Cas* moving apically, with *Gh* residing at the apical edge (Skeath and Thor, 2003)(Figure 2). It seems that the progression of gene expression in the neuroblast is more dependent on the cell cycle, rather than developmental timing (Brody and Odenwald, 2002). This observation was the result of an experiment in which the cell cycle of the neuroblast was arrested. After the cycle was reinitiated, the neuroblast continued onto the next gene in line, instead of skipping ahead to catch up with the developmental process. With all that is known, many questions still remain unanswered, such as how the permanence of the gene expression in the GMC is achieved while the expression in the neuroblast is so fleeting (Pearson and Doe, 2004).

After the GMC has been entrusted with a specific genetic identity, it divides asymmetrically to produce two postmitotic cells, which also adopt the same expression pattern. The postmitotic cells include motor neurons, which extend their axons into the periphery (about 40 total/ 5% of total), interneurons, which extend axons within the VNC to innervate other axons (about 150/hemisegment or 90%) and glial cells, which act as support cells to neurons by providing nutrients as well as factors to help guide the axons (about 5%) (Compos-Ortega, 1993; Skeath and Thor, 2003). The cell cycle of a ganglion mother cell is approximately 100 minutes,

and involves the same genetic partitioning as the neuroblast performed when giving rise to its progeny (Hartenstein and Campos-Ortega, 1997). As previously stated, one of the factors that is exclusively inherited into the GMC is the Numb protein. This protein, as well as a very busy protein- Notch, is responsible for determining the fate of the progeny of the GMC. Numb is asymmetrically localized to only one daughter cell via a similar mechanism as before, involving the protein Inscuteable and tethering to the basal cortex during mitosis (Skeath and Thor, 2003). Notch is symmetrically divided into both daughter cells, and its signaling events specify one fate of the daughter neurons. However, in the daughter that has received Numb, Notch signaling is blocked; Numb blocks Notch signaling by binding Notch to α-adaptin, causing it to be endocytosed (Skeath and Thor, 2003). Lacking Notch signaling, this daughter cell will adopt a different fate from that of its sibling. One example of this is the progeny of the ganglion mother cell GMC1-1a (Skeath and Thor, 2003). Normal Notch signaling in one daughter produces the neuron pCC, whose axons pioneer one of the longitudinal pathways at the midline, whereas the cell with Numb (and thus with inactive Notch signaling) will become the neuron aCC, which is initially found at the midline but then sends its axon to the periphery.

The longitudinal glial cells, which flank either side of the midline of the ventral nerve cord, arise from neuroblast-like precursors called glioblasts. Unlike neuroblasts, their division is symmetric and the result is a pair of daughter cells. Subsequent divisions yield a total of eight to 10 glia per hemisegment (Compos-Ortega, 1993). The glioblast expresses the transcription factors *fushi tarazu* (*ftz*), *prospero* (*pros*), and *orthodenticle* (*otd*), which are presumed to play a role in the specification of the glioblast and its progeny; mutations in *pros* or *otd* result in the absence of longitudinal connectives (Compos-Ortega, 1993).

The midline of the ventral nerve cord arises independently from the rest of the nerve cord, and is specified by a region in the neurogenic portion of the ectoderm known as the mesectodermal ridge (Hartenstein and Campos-Ortega, 1997). At stage five, about two hours after the start of embryogenesis, when the cellular blastoderm has formed, the midline precursor cells are arranged in two columns of four cells per segment that separate the neurogenic region of the ectoderm from the mesoderm (Compos-Ortega, 1993; Hartenstein and Campos-Ortega, 1997). After gastrulation (stage 8) the two columns join together at the midline, in a single row of eight cells. These cells then delaminate and join the other neuroblasts further into the embryo, leaving a hole that is eventually filled by epidermal cells (Campos-Ortega, 1993). The number of precursor cells is variable per segment, ranging from six to ten, with an average of 7.5 midline precursor cells (Hartenstein and Campos-Ortega, 1997). Of these, six divide once while one, referred to as the median neuroblast, divides in a stem cell-like manner to produce five to eight neurons. The six progenitor cells, in totality, give rise to three ventral unpaired median (VUM) progenitors, two midline glia progenitor cells, one midline precursor 1 (MP1) cell, and one progenitor cell that gives rise to two unpaired median interneurons (UMI). The midline glia progenitors each give rise to two glial cells, the MP1 precursor produces two MP1 daughter neurons, and the VUM progenitors give rise to one motorneuron and one interneuron each (Campos-Ortega, 1993; Hartenstein and Campos-Ortega, 1997).

All cells in the ventral midline of the nerve cord initially express the genes *single-minded* (*sim*) and *slit*, but after neural differentiation has occurred (around stage 13), only the glial cells express these genes (Campos-Ortega, 1993). Slit, together with its receptor roundabout (robo), play a role in axon pathfinding, preventing axons from crossing the midline. Axons are allowed to cross the midline with the aid of another protein, commissureless (comm). *Sim*, which is a

member of the basic helix-loop-helix family of transcription factors, seems to be the master regulatory gene for the midline as mutations result in lethality due to the failure of midline cells to properly differentiate into neurons and glia (Nambu et al., 1991). *sim* expression is activated by a cascade of transcription factors, beginning with *Dorsal*, which promotes the ventral expression of the factors *twist* and *snail*. These two proteins control *sim* activation, which is expressed at the blastoderm stage in stripes of ventral midline precursors (Campos-Ortega, 1993).

The commissures of the ventral nerve cord, which resemble rungs on a ladder, are formed during stage 12, between eight and ten hours after the start of embryogenesis (Goodman and Doe, 1993). The six midline glial cells, two each of MGA, MGM, and MGP, serve as landmarks to orient the axons as they traverse the midline. These glial cells, flanked by neuronal cell bodies, enwrap the axons of the commissures and their birth positions are exactly the opposite of where they finally rest. In their final positions, the MGA cells are located above the anterior commissure, sandwiched between the SP1 neurons, the MGM glia are found in between the anterior and posterior commissures, flanked by RP3/RP1, and the MGP are below the posterior commissure, with aCC/pCC neurons on either side. The posterior commissure forms first and is pioneered by the first axons of the CNS. These axons extend their growth cones toward the ventral unpaired median neurons (VUM), which are located just below where the commissures will form, and just above where the MGP glia are initially positioned. The axons then extend around the anterior end of the VUMs across the midline. The anterior commissure forms second, by axons that extend toward the MGA glial cells, crossing just posterior to them in a straight line. The two commissures are then separated by the movement of the MGM and MGA glia- the

MGA migrate to rest above the anterior commissure while the MGM move down to squeeze in between the commissures. (Goodman and Doe, 1993).

The longitudinal pathways form in concert with the commissures so that when the two commissures separate during stage 13, the linear pathways are already complete (Goodman and Doe, 1993) (**Figure 1.5**). There are three longitudinal pathways- MP1, vMP2, and FN3. The former two have been characterized the most, so they will be discussed in detail. The vMP2 pathway is pioneered by the pCC and vMP2 growth cones while the MP1 fascicle is formed by MP1 and dMP2 growth cones (Goodman and Doe, 1993; Lin et al., 1994). These two pathways remain separate within a segment, but fasciculate in between. pCC, along with aCC, are located just posterior to the posterior commissure. aCC extends its growth cone around pCC before exiting to the periphery, while pCC extends anteriorly, remaining close to the midline. Meanwhile, dMP2 and MP1, located just below the anterior commissure (along with vMP2), fist extend laterally before migrating posteriorly to from the MP1 pathway. vMP2, moving diagonally away from the midline, joins pCC and extends upwards to greet the descending dMP2 and MP1 from the segment above to form the combined pathway; the glial cell LGX marks the location for this rendezvous (Goodman and Doe, 1993; Lin et al., 1994). There is also a triplet of neurons- U1, U2, and U3- located between the cell bodies of aCC/pCC and MP1/vMP2/dMP2. These neurons send their growth cones laterally and join aCC as they exit to the periphery.

By stage 14, the formation of the commissural axon tracks are complete and the nerve cord begins to condense. The brain begins to fold away from the anterior end and curls over toward the posterior end, with the optic lobes nestled almost on top of the anterior portion of the axon scaffold.

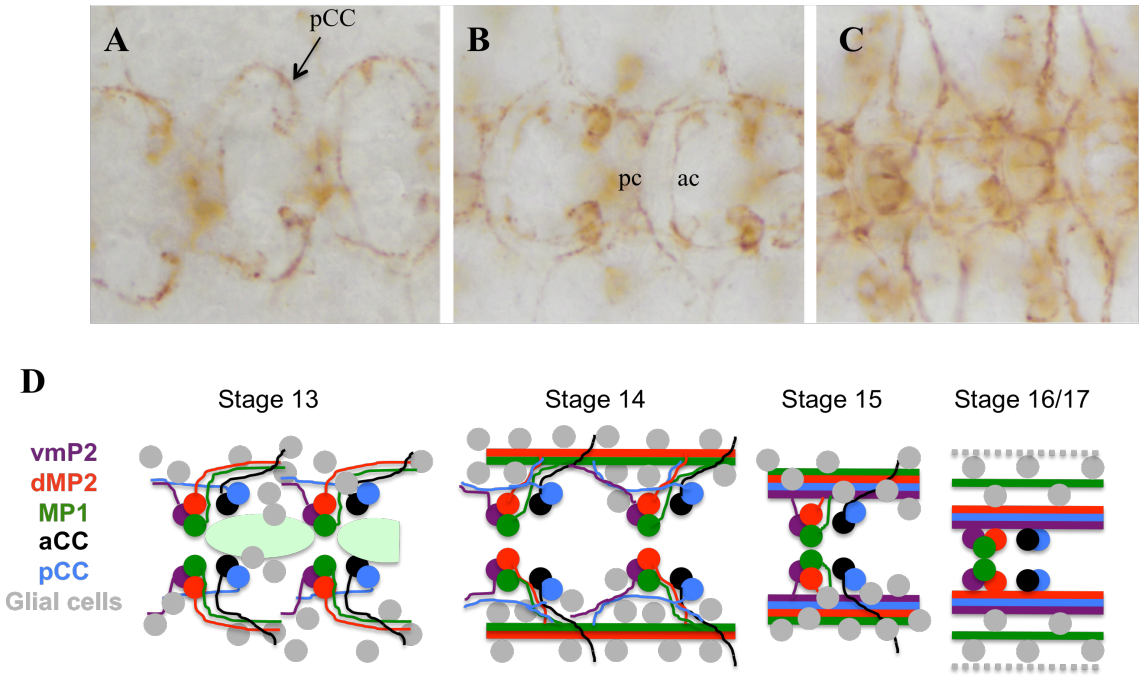

Figure 1.5 Formation of the longitudinal axon tracts of the embryonic nerve cord
A-C. The ventral nerve cord of the embryo at stage 13 (**A**), 14 (**B**), and 15 (**C**) stained with 22C10 antibody (neuronal marker). The pCC growth cone is visible in (**A, arrow**). At stage 14, the anterior (ac) and posterior commissures (pc) are almost complete. (**D**) Illustration of the pioneering of neurons that form the longitudinal axon tracts of one segment of the embryonic nerve cord starting at stage 13. The illustrations roughly correspond to the images in A-C. There are three pathways, MP1, vMP2, and FN3. MP1 is formed by the migration of MP1 and dMP2 growth cones while vMP2 is formed by aCC and pCC. Several glial cells serve as landmarks to orient the axons to the appropriate place. Illustration adapted from Sánchez-Soriano, 2007.

The early development of the *Drosophila* ventral nerve cord involves intricate timing and regulation of gene expression such that the final result is a group of cells in which each cell has a unique expression pattern. This pattern is dependent on the cell's position within the embryo and its time of birth. Tightly regulated and asymmetric cell divisions ensure that specific proteins are correctly partitioned into the daughter cells so that each daughter adopts her own cell fate. The early events in the embryo are critical in building the correct framework for generating a fully functional adult ventral nerve cord.

The larval and adult nervous system of *Drosophila*

After the last embryonic stage, three larval stages follow, called instars. The larvae are free moving and their number one priority is to eat. The larvae burrow through their food (in the laboratory this would be a vial filled with molasses or cornmeal media). Once the larva has finished eating, it crawls out of the food and up the side of the vial, where a casing is formed around it; this is the pupal stage. After a few days, an adult emerges from the case. Adults can live about ten weeks; males live longer than females.

De novo neurogenesis occurs first in the embryo, but again during the larval stage (Sánchez-Soriano et al., 2007). In order to advance to the final adult stage significant reorganization occurs. The larva has structures called imaginal disks that give rise to adult structures. These include the eye-antennal disc, 3 leg discs, and wing, labial, haltere, and genital dic and are located near the brain lobes. The central nervous system is one of the few organs that remain from embryo to adult. The neurons that are made in the embryo persist into the later stages, and many new neurons are added, arising from the same neuroblasts (Hartenstein, 1993). These neuroblasts reemerge in 1st instar larvae and start proliferating. Neural differentiation of the daughter cells (into adult neurons) does not begin until the pupal stage. The optic lobe,

which in the embryo is very small, enlarges and becomes two separate lobes, with the optic lobe anlage in between. The optic lobes now flank what will become the rest of the brain. The outer optic anlage will become the lamina and part of the medulla, and the inner anlage will form the medulla, lobula, and lobula plate. In adults, the optic lobe anlage becomes the supraesophageal ganglion, and below is the subesophageal ganglion. This structure is connected to the thoracio-abdominal ganglion, which extends into the main body of the fly (Hartenstein, 1993).

The optic lobe of the brain receives signals from the eye. In adults, the lobes are beneath the eyes and are subdivided into distinct layers from outermost to innermost- the lamina, medulla, lobula, and lobula plate neuropiles (Monastirioti 1999). In the embryo the optic lobe is very small and nonfunctional. During the larval stages, the optic lobe becomes two separate lobes. The eyes are not formed yet, but will arise from imaginal discs that are located near the brain the anterior of the larvae. The photoreceptor cells (R-cells) in the eye disk project through the optic stalk to different synaptic layers of the brain. R1-R6 axons migrate to terminate to form the lamina plexus, which consists of rows of epithelial and marginal glial cells. The glial cells help target the axons. When these cells are disrupted, R1-R6 extend past the lamina plexus and into the medulla (Poeck et al., 2001). R7 and R8 axons pass through the lamina plexus and terminate in the medulla.

Lamina neurons arise from neuroblasts in the outer proliferation center (Fan et al., 2005). The neuroblasts give rise to lamina precursor neurons, which in turn divide to produce mature lamina neurons. R-cells signaling, involving Hedgehog and Spitz, causes the lamina neurons to proliferate and differentiate; glial cells also respond to differentiate and migrate. Cells of the lobula complex arise from the inner proliferation center.

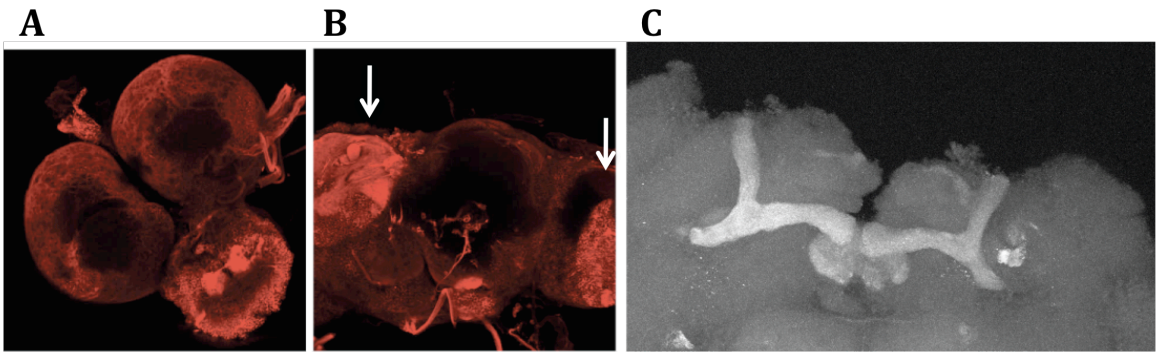

Figure 1.6 Morphology of the larval and adult brain of *Drosophila melanogaster*.
A-B. Confocal images of brains stained with anti-HRP antibody. (**A**) 3rd instar larval brain with the 2 brain lobes and the rest of the CNS extending out from the lobes. (**B**) Adult brain with the two optic lobes (arrows) flanking the main brain segment. (**C**) 1D4 staining of an adult brain highlighting the mushroom bodies (L-shaped structure).

As mentioned in the above, the optic lobe anlage forms between the optic lobes during larval development. During this formation, the developing lamina and medulla are close to the lobula complex primordium (Fan, Soller et al. 2005). The mature lobula complex in the adult does not receive any direct input from the R-cells. However, during the transient meeting of the lamina, medulla, and lobula complex primordium, the targeting of R-cells can be influenced by cells in the lobula complex primordium. Evidence of this relationship stems from work on mutations in *slit*, *robo*, and *egghead*. In *slit* or *robo* mutants, R-cell projection is disrupted because of a break in the boundary between the lamina and lobula, causing cells to mix across the compartments of the two optic lobes (Tayler et al., 2004). The role of a glycosyltransferase, egghead, in the role of optic lobe development will be discussed later.

The *Drosophila* neuromuscular junction

Neurons communicate to other neurons and to muscles by sending electrical signals along their axon bodies. At the nerve terminal, the electrical signal is converted to a chemical signal, and neurotransmitter molecules are released and received by the acceptor cell. The space between the signal-generating cell and the signal-receiving cell is called the synaptic cleft; the former is called the presynaptic side and the latter is the postsynaptic side. In neuron-neuron communication a signal is sent down the length of the axon and is received by a dendrite of the receiving neuron. The active zone is where the vesicles containing the neurotransmitters release their contents into the synapse. The active zone is very close to the postsynaptic density area, which is separated by extracellular space that can be as small as 30nm (Zhai and Bellen, 2004).

Vesicle fusion occurs on the pre-synaptic plasma membrane that is juxtaposed to the postsynaptic density (Zhai and Bellen 2004). Along with a site for vesicle fusion, the plasma membrane of the presynaptic nerve terminal contains voltage-gated Ca^{2+} channels, which are

required for exocytosis. Vesicles fuse to the plasma membrane upon Ca^{2+} entry, a fusion that is facilitated by the SNARE complex and involves t-SNAREs syntaxin and SNAP-25, and v-SNAREs such as synaptobrevin. A direct interaction between these molecules and Ca^{2+} channels at the presynaptic plasma membrane has been demonstrated (Catterall, 1999; Jarvis et al., 2002). SNAP-25 and syntaxin have been shown in neuronal cell culture to define sites where secretory vesicles dock and fuse by forming cholesterol-dependent clusters in the plasma membrane (Lang et al., 2001).

Several adhesion molecules are present at both pre- and postsynaptic nerve terminals and help align the active zone and postsynaptic density, as well as mediate signaling events and neurotransmission. The adhesion molecules present include cadherins (Shapiro and Colman, 1999), protocadherins (Frank and Kemler, 2002), neural cell adhesion molecule (Rougon and Hobert, 2003), fasciclin II (Davis et al., 1997), down syndrome adhesion molecule (Schmucker et al., 2000), syndecans (Hsueh and Sheng, 1999), neuroglian (Walsh and Doherty, 1997), integrins (Chavis and Westbrook, 2001), and sidekicks (Yamagata et al., 2002).

Beneath the plasma membrane of the active zone is the cytomatrix, where synaptic vesicles dock and fuse (Zhai and Bellen, 2004). General cytoskeletal proteins like actin, tubulin, myosin, spectrin, and β-catenin are found here. Scaffolding proteins, not unique to just presynaptic terminals, are also in the cytomatrix and include SAP90/PSD95/Dlg, SAP97, and CASK/LIN-2. CASK interacts with calcium channels and syndecan-2. Several other proteins are also at the cytomatrix, helping vesicles to dock, prime, fuse, and release. These proteins include RIM1, Munc13, Bassoon, Piccolo, and CAST/ERCs. Rab 3 interacting molecule 1 (RIM1) and Munc13 are involved in vesicle priming, Bassoon and Piccolo in neurotransmitter release. ERCs include ELKs, Rab6 interacting protein 2, and CAST. These proteins bind Rab6

and involved in general traffic in all cells. RIM1 has several binding partners, including ERCs. RIM1 also binds synaptotagmin to aid vesicle release, Liprinsα, which regulates active zone size, and Rab3. A mouse knockout of RIM1 has a very mild synaptic phenotype, which suggests RIM1 may not be essential for neurotransmitter release (Schoch et al., 2002; Zhai and Bellen, 2004). There are no homologs for Bassoon and Piccolo in *Drosophila*, but another protein called Bruchpilot (Brp) is presumed to combine the functions of these proteins and ERCs (Wagh DA et al., 2006).

Synaptic vesicles are tethered onto electron-dense projections that extend from the cytomatrix. Their shape is unique to each organism and dependant on neuronal cell type, in *Drosophila* they have a "T" shape and are called T bars. T bars are not found at every active zone, and it has been suggested that those that do contain T bars have a stronger output (Govind and Meiss, 1979; Quigley and Pearce, 2001). Also, the number of T bars have been shown to be altered in response to changes in light stimulation (Brandstatter and Meinertzhagen, 1995; Rybak and Meinertzhagen, 1997).

The most well characterized neuromuscular junction (NMJ) in *Drosophila* is between two muscles of the abdominal wall in 3rd instar larvae (**Figure 1.7**). The synaptic units are called boutons and look like small round beads decorated along the branches of the nerve terminal. Bouton number can increase by budding or forming de novo (Zito et al., 1999). A protein called Highwire/RPM1 is responsible for maintaining appropriate bouton number and size at both the *Drosophila* and *C. elegans* NMJ (Murthy and Camili, 2003). The NMJ is glutamatergic, and glutamate is actually spontaneously released hours before actual synaptic contacts have been formed (Waites et al., 2005).

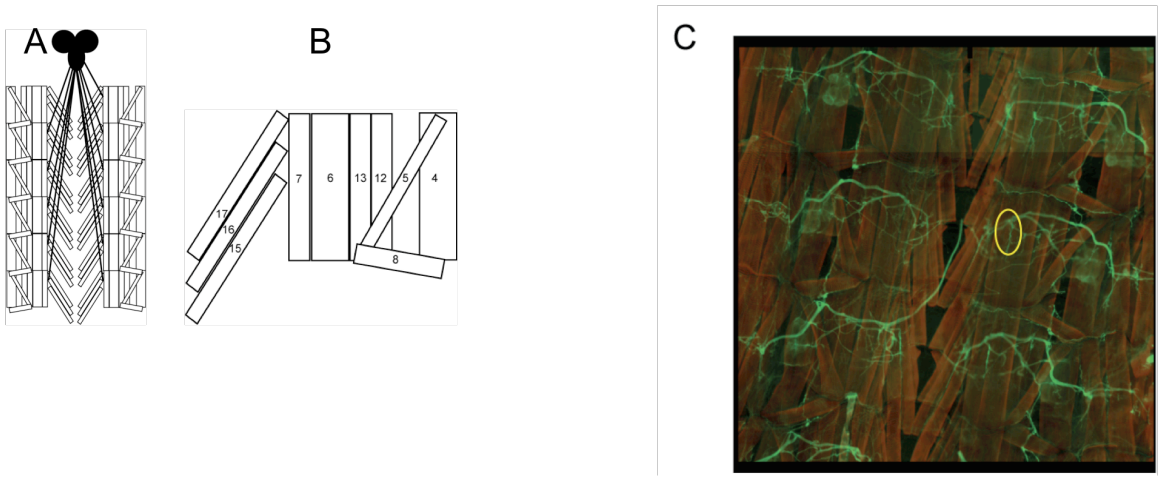

Figure 1.7 Anatomy of the larval musculature and the neuromuscular junction
(**A**). Pictoral representation of the muscles of the abdominal wall and the neurons that extend from the brain. The muscles are arranged in a repeating pattern of 17 muscles. (**B**) Representation of one segment. Particularly note muscles 6 and 7. (**C**) Fusion of several confocal images taken of the abdominal muscles of the wall of a 3rd instar larva. Anti-HRP antibody (green) stains the nerves and phalloidin (red) stains the muscles. The yellow circle surrounds one of the NMJs between muscles 6 and 7.

Glycans and the nervous system of *Drosophila*

Results to be presented in this dissertation describe the neurobiological defects of a mutation in a protein that is required for proper expression of N-linked glycans in the neural cells of *Drosophila*. Neurological defects of mutations in several genes regulating N-linked and other types of glycosylation have been reported, and a few will be highlighted here.

As mentioned earlier, Fused Lobes is a hexosaminidase that can cleave the GlcNAc added by GlcNAc transferase 1 (Leonard et al., 2006). *Fdl* mutants have a fusion of the β lobes of the mushroom body in the adult brain, hence the name. However, there is some speculation as to whether the *fdl* gene is actually responsible for the fused lobes phenotype. Work from another group reports that the phenotype is attributed by another gene, *achintya/vismay* (*achi*) (Donaldson et al., 1999). This finding was based on a deficiency line that removes both genes. Achi is a transcription factor that is a member of the aly-class meotic-arrest loci that activate transcription of differentiation-specific genes and genes involved in meiotic cell cycle progression (Jiang et al., 2007). The coding region for *achi* actually lies within the coding region for *fdl*. Thus, it is unclear whether a mutation in *fdl* has any neuronal defect.

Fused lobes removes the GlcNAc added by GlcNAc transferase I. In *Drosophila*, mutations in the gene encoding this transferase, *mgat1*, cause neurological defects (Sarkar et al., 2006). Null mutations in *mgat1* are viable, but the males are sterile and have a reduced life span. The flies also have an adult locomotor defect. *Mgat1* mutants also have a fusion of the β lobes of the mushroom body. There is a maternal contribution of GlcNAcT I in null embryos, but removal eliminates anti-HRP expression in the embryo. Even though high mannose N-glycans represent over half of all N-linked glycans in *Drosophila*, these studies indicate that complex

glycans are also vital. Thus N-glycans modified by GlcNAc transferase I are required for life span, locomotor ability, and brain development in *Drosophila*.

Glycosphingolipids are also important for proper nervous system function. The first two genes required for the synthesis of glycosphingolipids in *Drosophila* are the glycosyltransferases *egghead* (*egh*) and *brainiac* (*brn*) (**Figure 1.8**). *Egghead* encodes a mannosyltransferase that synthesizes the mactosylceramide core of glycosphingolipids (Wandall et al., 2003). *Brainiac* encodes a GlcNAc transferase that extends the structure generated by Egghead (Muller et al., 2002). Mutations in these genes result in maternal-effect neurogenic phenotypes and embryonic lethality (Goode et al., 1996a; Goode et al., 1996b). The proliferation of neural cells in both of these mutants was affected, so much so that other cell lineages were affected. Both *egh* and *brn* mutants affect epithelial morphogenesis during oogenesis. The mutants have abnormal neurogenesis, compound egg chambers, and dorsal appendage fusion phenotypes. It was found that these defects stem from disruption of Notch and EGFR signaling.

Egghead also plays a role in optic lobe development (Fan et al., 2005). As discussed earlier, R-cells in the eye disk project through the optic stalk to different synaptic layers of the brain. R1-R6 axons migrate to terminate and form the lamina plexus, which consists of rows of epithelial and marginal glial cells. In *egghead* mutants, R1-R6 cells migrate past the marginal glial cells and into the medulla (Fan, Soller et al. 2005). The glial cells at the interface between the lamina plexus and the lobula cortex is also disorganized, allowing R1-R6 axons to pass through. Also, the distal cells of the lobula cortex invade the lamina. Surprisingly, the function of egghead is not required in the lamina plexus, but in the lobula complex primordium. Experiments involving *egghead* and *brainiac* reveal that the activity both glycosyltransferases

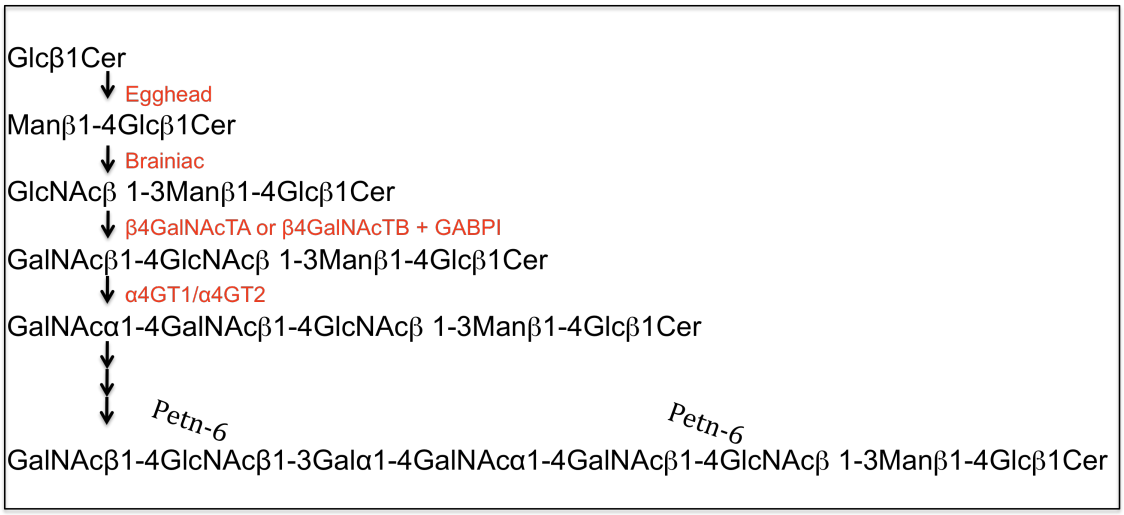

Figure 1.8 Glycosphingolipid synthesis in *Drosophila*
Schematic of the steps in glycosphingolipid synthesis and the enzymes that catalyze the reactions. Particularly noted are Egghead, Brainiac and the β4GalNacTs, as mutations in these enzymes induce neural phenotypes. Adapted from Chen et al., 2007.

are required in the lobula complex primordium for correct migration of R1-R6 axons in the developing lamina. Studies in vertebrates have demonstrated that glycosphingolipids function in cell adhesion, growth, differentiation, cell interaction and signaling (Watts 2003). All of these functions may contribute to correct axon guidance in the developing optic lobes of *Drosophila*.

The glycosphingolipid precursor structure initiated by Egh and Brn is extended by β4GalNAc transferases. There are two enzymes in *Drosophila* homologous to the vertebrate β1,4-galactosyltransferase family, β4GalNAcTA and β4GalNAcTB. These enzymes actually transfer GalNAc to a terminal GlcNAc (forming LacdiNAc) instead of Gal like the vertebrate enzymes (Haines and Irvine, 2005). LacdiNAc has been found on N-linked glycans and glycolipids in *Drosophila* (Seppo et al., 2000). β4GalNAcTB is the major enzyme involved in glycosphingolipid synthesis, while GalNAcTA plays a minor role (Stolz et al., 2008). Unlike *brn* and *egh* null mutants, which are embryonic lethal, *β4GalNAcTA* and *B* single and double mutants are viable.

β4GalNAcTA mutants have several neurological defects (Haines and Stewart, 2006). Larvae crawl backwards and frequently swing their heads. The larval neuromuscular junction has reduced branching, size, and bouton number. Muscular defects were also detected in mutants. Adult flies have locomotor defects and often have trouble righting themselves after a fall. Although the underlying mechanisms for these defects have not yet been elucidated, it is clear that there are substrates in the nervous system of *Drosophila* that require proper glycosylation by the addition of β1,4 GalNac by this enzyme.

β4GalNAcTB mutations affect oogenesis, similar to *egh* and *brn* mutants (Chen et al., 2007). *β4GalNAcTB* mutants have dorsal appendage fusion, which was also seen in *egh* and *brn* mutants. EGFR signaling between the oocyte and follicle cells in these mutants is compromised.

Interestingly, the activity of β4GalNAcTB requires the activity of another protein, GABPI, which is similar to Asp-His-His-Cys (DHHC) acetyltransferases. GABPI shuttles β4GalNAcTB into the Golgi where it can bind to substrates (Johswich et al., 2009). Lacking GABP1 assistance, β4GalNAcTB remains trapped in the ER (Johswich et al., 2009).

Heparan sulfate proteoglycans (HSPG) also play a role in the nervous system of *Drosophila*. *Syndecan* and *dally-like* are expressed in the lobula cortex and are involved in the formation of the visual system (Fan et al., 2005). They also play roles at the synapse (Johnson et al., 2006). Syndecan helps in the growth of presynaptic terminals and Dally-like helps regulate active zone formation and function. Both of these HSPGs bind to a protein tyrosine phosphatase receptor called LAR. Syndecan and Dally-like have opposing roles: the latter inhibits LAR and the former promotes LAR function. The binding affinity of Dally-like for LAR is higher than that of Syndecan for LAR, but both HSPGs act through LAR to control synapse morphogenesis and function at the neuromuscular junction in *Drosophila* larvae (Johnson et al., 2006).

So far genes involved in N-glycan or glycolipid biosynthesis as well as proteoglycans play important roles in nervous system function in *Drosophila*. Proteins that bind carbohydrates, called lectins, also contribute. One example is gliolectin (Sharrow and Tiemeyer, 2001; Tiemeyer and Goodman, 1996). Giolectin binds N-glycans and is expressed by the glial cells of the developing nerve cord. As discussed earlier, the axon pathfinding events that form the commissures and midline of the embryonic ventral nerve cord require appropriate cues from glial cells to guide the axons to the appropriate location. Although the commissures and longitudinal form in the absence of *gliolectin*, there are definitely abnormalities. In the *gliolectin* null mutant, the formation of commissures is disrupted and some commissures appear fused (Sharrow and

Tiemeyer, 2001). The formation of the longitudinal pathways is also delayed. Thus Gliolectin is necessary to ensure the fidelity of the formation of the ventral nerve cord.

SAD kinases

The results presented later provide evidence for the first mutation in the *Drosophila* homolog of a protein called Synapses of the Amphid Defective kinase (SAD). Therefore it is necessary to present the current knowledge of SAD kinase and its previously identified function in neuronal synapses and neuronal polarity. SAD kinase is a serine/threonine kinase and belongs to the group of calcium calmodulin dependent kinases, more specifically the family of AMPK/SNF1 kinases (Manning et al., 2002). They, along with other members of the serine/threonine kinase family, contain an essential conserved lysine residue in the ATP binding site (Hanks et al., 1998). Aside from the kinase domain, SAD kinases have two other conserved regions called SCR1 and SCR2. They also have a Ubiquitin associated (UBA) domain immediately proximal to the kinase domain. The UBA domain, a part of SCR1, helps stabilize SAD's phosphorylating ability (Rider, 2006). SAD kinases are also present in higher organisms, including mouse and humans; the *Drosophila* gene with the closest homology is *CG6114*, which until this point had not been characterized and no mutants have been described. The kinase domain of SAD-1 and CG6114 share 85% identity and two other conserved regions are 44% identical (Crump et al., 2001). In humans SAD is also called BRSK1 and 2, for Brain Specific Kinase.

SAD kinase function at the synapse

SAD was first identified in *Caenorhabditis elegans* (*C. elegans*), in a screen for mutations that affect synaptic vesicle clustering in the ASI chemosensory neurons (Crump et al., 2001). *SAD-1* mutants were not severely affected in locomotion, but synaptic vesicles were more diffuse and disorganized. There are two *SAD* kinases in rats, *SAD-A* and *B*, both solely expressed in the

brain (Inoue et al., 2006). *SAD-B* is expressed in several regions of the brain, including the hippocampus, cerebellum, olfactory bulb, and the cortex. Cellular localization of SAD-B using immunogold staining showed that it is present at the presynaptic nerve terminal, specifically at the cytomatrix of the active zone. A soluble pool of the enzyme is also detectable within neuronal cell bodies, indicating the possibility of additional SAD functions at non-synaptic locations (Inoue et al., 2006; Kishi et al., 2005). Studies also suggest that SAD-B aids in neurotransmitter release and helps control the size of the readily releasable pool of vesicles. One of the binding partners identified for SAD-B is RIM1, which aids in vesicle priming (Inoue et al., 2006).

SAD kinase function in neuronal polarity

SAD is related to PAR kinases, which have conserved roles in polarity. The kinase domain of SAD is 50% identical to the kinase domain of Par-1, which is involved in embryonic polarity. Another SAD kinase, POPK-1 in ascidians, also has a role in polarity (Nakamura et al., 2005). Morpholino knockdown of *POPK-1* alters the proper localization of maternal mRNAs at the posterior pole in the embryo. Overexpression of *SAD-1* in *C. elegans* resulted in synaptic vesicle proteins in dendrites, suggesting SAD-1 is involved in neuronal polarity (Crump et al., 2001).

As in rats, there are two *SAD* kinases, *SAD-A* and *B*, in mouse, and a double knockout has been generated (Kishi et al., 2005). Both *SAD-A* and *B* mRNA are highly expressed in brain and spinal cord, with *SAD-B* also expressed in the testis, albeit at low levels. In the cortex of the brain, expression is high in the preplate, where new neurons are being formed. In neurons, *SAD* is expressed in dendrites and axons.

Mouse *SAD* double knockouts have very little movement and die within two hours of birth (Kishi et al., 2005). The forebrain was smaller in mutants and the layers of the cortical

plates were disorganized. Neurons taken from the mutant cortex or hippocampus were cultured and stained with markers for axons (dephospho-tau) and dendrites (MAP2). Neurons lacking SAD did not polarize correctly and the markers were intermixed. This result recapitulated the result seen in *C. elegans* and confirms SAD's role in establishing neuronal polarity. Overexpression of SAD in culture led to an increase in phosphorylation of the microtubule associated protein (MAP) Tau, at serine 262 (Kishi et al., 2005). Axons have low levels of phosphorylated Tau, so it seems somewhat contradictory for SAD to phosphorylate Tau in axons to aid in polarity. Phosphorylation of Tau at serine 262 causes Tau to dissociate from microtubules. It is likely that SAD regulates other proteins, like other MAPs to help polarize neurons (Wildonger et al., 2008). SAD-A and SAD-B seem to function redundantly in neuronal polarity. However, as aforementioned it appears that SAD-B is also involved in synaptic function.

SAD phosphorylation of substrates is proposed to be mediated by a scaffolding protein called Neurabin (NAB) (Hung et al., 2007). NABs are F-actin binding proteins that have been shown to interact with several proteins including Rac3, protein-phosphatase-1 (PP1), the Rho-specific GEF Lfc and the Rac-specific GEF Taim1. In mammals there are two NABs, Neurabin 1 and Spinophilin (Neurabin II). Both are localized to the postsynaptic density of the neuronal synapse. They recruit PP1 and Lfc to dendritic spines, helping to regulate morphology and motility. Spinophilin also interacts with G-protein coupled D2 dopamine receptors and $\alpha 2$ adrenergic receptors. Single knockout mice are viable, but *NAB1* knockouts have a defect in long-term potentiation and *Sphinophilin* knockouts have defects in long-term depression (Hung et al., 2007).

A yeast two-hybrid screen conducted using *C. elegans* proteins found that SAD-1 binds to the only Neurabin in *C. elegans* (Hung et al., 2007). SAD-1 binds to NAB through its C-terminal region. This interaction is required for neuronal polarity, but not for SAD's role in synaptic transmission. *NAB* mutants also have a defect in polarity, but the phenotype is not completely identical to *SAD-1* mutants, and some types of neurons are differentially affected by the two mutations, suggesting that NAB binds other proteins, that the interaction between SAD-1 and NAB is only required in some neurons (Hung et al., 2007).

Neurabin does have a single homolog in *Drosophila melanogaster*. mRNA expression begins at stage 11, along the midline in mesectodermal cells and in one neuroblast (Clements et al., 2003). Expression continues to increase until stage 14, where it decreases. Expression is present again in 3rd instar larvae, in the CNS and in small amounts in a few imaginal discs. Null mutations in *dNAB* result in larval locomotor defects, and early larval lethality. Even hypomorphic mutants have adult lethality and severe locomotor defects. Overexpression or reduction of *dNAB* disrupts eye development. Also, in *dNAB* null mutants, the number of lateral neurons expressing the *even-skipped* marker gene is reduced. Therefore NAB seems to function similarly in *Drosophila* to aid in neuronal polarity, albeit its role seems more restricted to specific lineages. It is unclear whether NAB's function in mediating SAD activity is conserved in *Drosophila*.

Teasing apart SAD's dual function

So far, two distinct functions of SAD kinases have been discussed. Early in development SAD, along with Neurabin, Tau, and members of two separate signaling pathways, help determine axon/dendrite identity. Later, in mature neurons, SAD phosphorylates proteins like RIM at the active zone to release neurotransmitter filled vesicles. SAD has different binding partners for

each function, indicating that the regulatory pathways involved in neuronal polarity and synaptic function are separate.

In order to assess the temporal requirements for SAD function in neuronal polarity and synaptic organization, an analog-sensitive version of the kinase in *C. elegans* was generated (Kim et al., 2008). The generation of an analog-sensitive kinase allows the inhibition of kinase activity by the administration of ATP analogs. Utilizing this method, the authors determined that inactivation of SAD when neurons are polarizing resulted in defects that could not be reversed by reactivation of SAD by a heat-shock inducible construct. In contrast, inactivation of SAD later, when synapses are fully formed and functional, causes defects but those defects are reversible. The authors demonstrated that SAD-1 activity promotes synaptic organization both during establishment of synapses and in maintenance of synapse activity.

Regulators of SAD activity and expression

Work from several laboratories has helped to define SAD's role in neuronal polarity and synaptic transmission, and regulatory pathways are now emerging (**Figure 1.9**). Although *SAD* kinase is expressed both in axons and dendrites, it is only activated in axons, by a kinase called LKB1 (Barnes et al., 2007). *LKB1* knockout mice have similar phenotype to *SAD* knockouts in that they are unable to form polarized neurons. Overexpression of *LKB1* results in neurons with multiple axons. LKB1 is activated by PKA, which is activated in response to extracellular signals such as brain-derive neurotrophic factor (BDNF) (Wildonger et al., 2008). *In vitro*, PKA phosphorylates SAD-A/BRSK2, increasing its activity (Guo et al., 2006). However, treatment of HEK293 and CCL13 cells with forskolin, an activator of PKA, had no effect on SAD-A/BRSK2

or SAD-B/BRSK1 activity (Bright et al., 2008). Also, LKB1 activation by PKA is not required for LKB1 activation of SAD. Studies by the same group also found that SAD kinases can be dephosphorylated (and hence inactivated) by Protein phosphatase 2C.

Another pathway leads to SAD activation (Wildonger, Jan et al. 2008). In response to extracellular signals, PI3K phosphorylates Akt, which then phosphorylates Tuberous Sclerosis complex 2 (Tsc2). Tsc2 is in a complex with Tsc1 and is inactivated upon phosphorylation by Akt. This allows the GTPase Rheb to bind GTP, leading to the inactivation of Target of Rapamycin complex 1 (TORC1). TORC1 activation results in an increase in *SAD* translation, and a corresponding increase in SAD protein levels. Several experimental findings led to this model pathway for SAD regulation. For example, In *Tsc2* mutants, the levels of *SAD-A* and *SAD-B* are increased. Also, treatment of these *Tsc2* mutant neurons with rapamycin reduced *SAD* levels to normal. This suggests that TORC1 does not regulate basal levels of *SAD* and that there are other modes of regulation, particularly in dendrites where this pathway is not active (Wildonger, Jan et al. 2008).

Another kinase found to activate SAD is Ca^{2+}/calmodulin-dependent protein kinase kinase (CaMKK) (Fujimoto et al., 2008). Affinity chromatography purification of rat brain extract identified SAD-B as a binding partner for CaMKK. SAD-B was phosphorylated *in vitro* by CaMKK at Threonine 189 in the activation loop. *In vivo* experiments confirmed these results. Ca^{2+} influx helps control neurotransmitter release, so activation of SAD-B by CaMKK may be one means of this control.

Other functions for SAD Kinases

SAD kinase is emerging as a multi-function protein. Roles in neuronal polarity and synaptogenesis have already been discussed. Recently, another role for SAD has been published,

Table 1.1 Overview of the domains and binding partners of SAD kinase

Illustrated are the three conserved domains of SAD kinase, their important motifs, and the proteins that have been reported to interact with those domains.

Conserved Regions	Domains/ Motifs	Function	Interacting Proteins
Kinase	KXGS (for substrate recognition)	Activation of kinase domain phosphorylation of substrate	Upstream: LKB1, CaMKKα, Protein Phosphatase 2C Downtream: Tau, other MAPs?, γ−tubulin
SCR 1	UBA domain	Increases the efficiency of substrate phosphorylation by stabilizing the kinase domain	Not known
SCR 2	PDZ binding domain	PDZ binding domain	NAB-1, RIM1

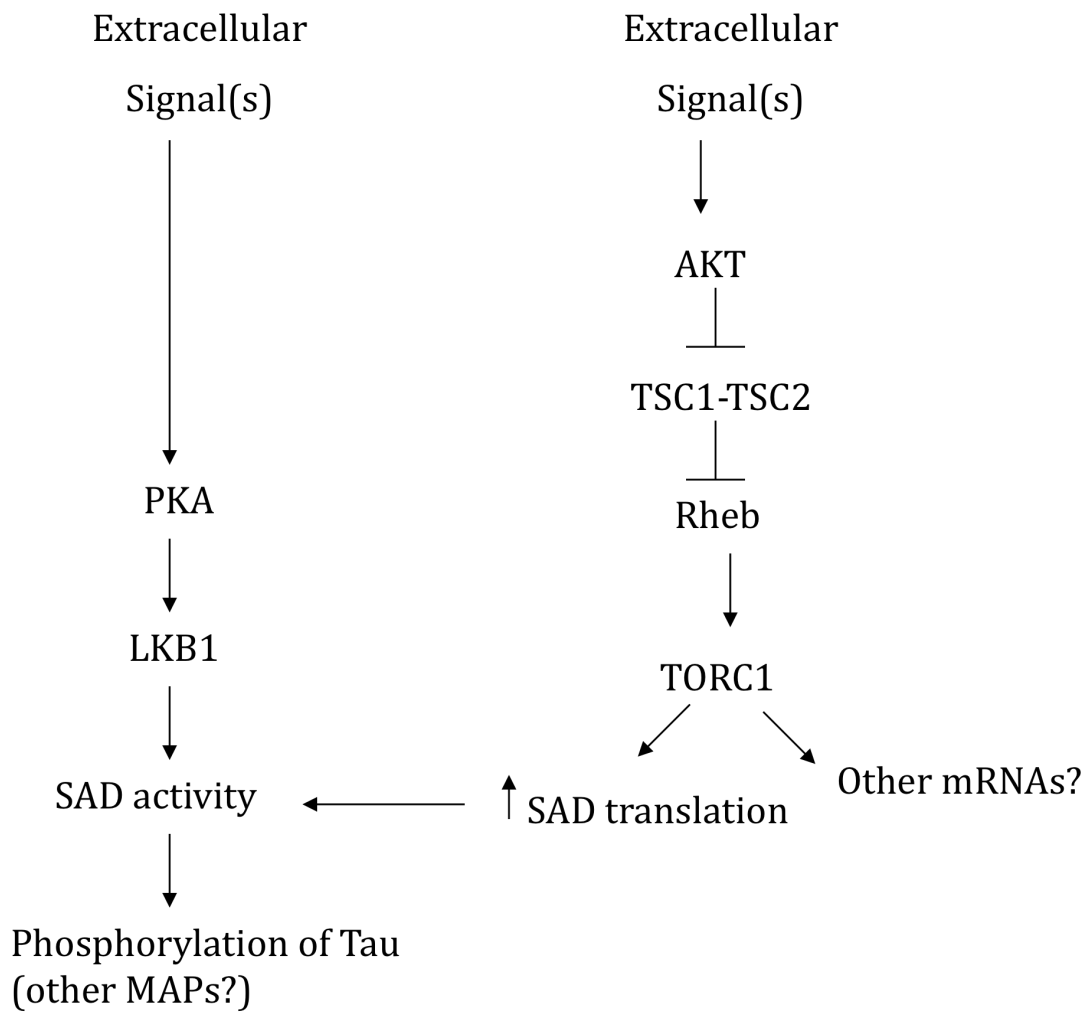

Figure 1.9 Pathways leading to SAD activation
Two signaling pathways have been reported to lead to the activation of SAD kinase function in neuronal polarity. Either through PKA or AKT, *SAD* expression is up regulated, leading to phosphorylation of Tau and other microtubule associated proteins (MAPs). Adapted from Wildonger, 2008.

in cell cycle regulation (Alvarado-Kristensson et al., 2009). Enhancement of *SAD-B* expression induces several cell types in the brain to divide abnormally, indicating that SAD-B may be involved in cell division (Alvarado-Kristensson, Rodriguez et al. 2009). SAD kinases are homologous to the Hsl1 kinases in *Saccharomyces cerevisiae*, which mediate Swe1 degradation and Cdk1 activation during entry into mitosis (Lew, 2000). It has already been demonstrated that SAD kinases in mouse and human phosphorylate Wee1 and CDC25B/C, which inhibits Cdk1 activity and hence mitosis entry (Lu et al., 2004). Recently another role for SAD-B has been identified, which involves phosphorylation of γ-tubulin (Alvarado-Kristensson, Rodriguez et al. 2009). γ-tubulin regulates αβ-tubulin nucleation and aids centrosomal duplication and spindle formation. SAD-B phosphorylates γ-tubulin on serine 131, which results in relocation of γ-tubulin to the centrosome and is necessary for centrosome amplification. The authors found that increasing or decreasing *SAD-B* expression disrupts entry into S phase. Therefore SAD-B must be tightly regulated for proper S phase entry and progression.

In chapter two, data will be presented that reveal yet another function for this very busy SAD kinase. This role is the regulation of neural-specific N-glycan expression in *Drosophila*. Data presented there implicate SAD function in the regulation of Golgi trafficking or dynamics, helping with vesicular traffic much like it does at the synapse.

HRP-Epitope and Tollo

Chapter two introduces a mutation in *SAD* that affects expression of HRP-epitopes, therefore more details about HRP-epitopes and what is known about how their expression is regulated will be presented here. As mentioned previously, HRP-epitopes are N-linked glycans that all have an α-3 linked fucose on the internal GlcNAc of the chitobiose core. This modification is added by Fucosyltransferase A (FucTA). HRP-epitopes are expressed throughout the entire *Drosophila*

life cycle. In the embryo, anti-HRP staining is evident in the ventral nerve cord and peripheral nervous system, as well as non-neural tissue including the anal pads, posterior hindgut, and garland gland.

Proteins bearing the HRP-epitope

Some of the proteins bearing the HRP-epitope have been identified. This work was performed using an anti-HRP antibody column (Desai et al., 1995). Extracts from *Drosophila* embryos were passed through the column and then separated by SDS-PAGE. The proteins were then identified by mass spectrometry, but the authors suggest there are other proteins that remain unidentified (Desai, Popova et al. 1995).

The proteins identified that carry the HRP-epitope are fasciclin (Fas) I and II, neurotactin, neuroglian, DPTP10D, DPTP69D, and DPTP99A (Desai, Popova et al. 1995). Fas I and II are cell adhesion molecules, but Fas I is a bit divergent since it does not share homology with other such proteins. However it is homologous to a human osteoblast protein, OSF-2 (Takeshita et al., 1993). Fas I is one of the three most abundant HRP-modified proteins (Desai, Popova et al. 1995). Fas II is a homolog of the neural cell adhesion molecule (NCAM) and plays a role in axon pathfinding as mutants for *Fas II* display fasciculation defects in the longitudinal axon pathways of the *Drosophila* embryonic nerve cord (Lin et al., 1994). Fas II also regulates the influence of pioneer neurons on follower neurons. That is, growth cones of pioneer motor neurons in the embryo are more complex than the growth cones of axons that follow, and it has been demonstrated that this relationship is regulated by Fas II (Sanchez-Soriano and Propkop, 2005).

The other proteins to share the top spots with Fas I as most abundant HRP-modified proteins are neurotactin and DPTP69D. Neurotactin is a heterophilic adhesion molecule and is

expressed in the CNS and a small subset of PNS neurons in the *Drosophila* embryo; it is also expressed during germ band extension in ectodermal cells (Desai, Popova et al. 1995). Neurotactin is closely related to the vertebrate adhesion molecule L1, and has Ig and fibronectin (FN) type II domains (Fas II also has these domains). DPT69D is a receptor-linked tyrosine phosphatase not found in vertebrates, and also has Ig and FN domains. DPT69D is only expressed on axons in the developing nerve cord. Its expression continues in the larval stage, where it is expressed in the brain, nerve cord, photoreceptor axons, and optic lobes.

Based on the expression patterns of the proteins identified thus far, the staining pattern of anti-HRP antibody in the CNS is the sum of neurotactin, DPTP69D, and Fas I. In the PNS, Fas I and neurotactin contribute (Desai et al., 1995). It is unclear at this point whether or not the HRP-modification contributes the function of these proteins. Fas I and II are always glycosylated, but outside of the nervous system they do not have HRP-epitope glycans (Bastiani et al., 1987; McAllister et al., 1992). So it seems that the HRP-epitope modification is neural specific, with the exception of the garland gland, anal pads and posterior hindgut, and it remains to be determined whether this expression is necessary for neuronal identity. It is of interest to note that in vertebrates, a different glycan, the L2/HNK-2 epitope, decorates neuronal proteins N-CAM, L1, and myelin-associated glycoprotein (Kruse et al., 1984).

Regulation of HRP-epitope expression

Previously, only two mutants had been identified that affect HRP-epitope expression in *Drosophila*. *Neurally altered carbohydrate* (*nac*) mutants lack anti-HRP staining in larval, pupal and adult stages (Katz et al., 1998). Adults exhibit fasciculation defects in wing sensory axons, which suggests the HRP-epitope may play a role in axon pathfinding (Whitlock, 1993). Analysis of wing discs revealed misrouting of axons as well as ectopic neurons (Whitlock, 1993).

The second mutant is the balancer chromosome *TM3*, which abolishes anti-HRP staining in the CNS and PNS while retaining garland gland, hindgut, and anal pad staining. Deletion analysis of the 3rd chromosome identified *tollo* as the gene in TM3 responsible for the mutant phenotype (Seppo et al., 2003). *Tollo,* also called *Toll-8*, is a member of the Toll-like receptor signaling family. *Tollo* is a Finnish word for "stupid" since mutants linger near the bottom of the vial and have difficulty extricating themselves from their food.

In-*situ* hybridization revealed *tollo* mRNA in ectodermal cells, not neural cells. Based on this finding, a model has been proposed in which Tollo in ectodermal cells is activated and signals to surrounding neural cells to express the HRP-epitope. Tollo's function in the HRP-epitope expression pathway represents a novel function for a Toll-like receptor (TLR) as their classic role is in the innate immune response. However, the first TLR, Toll-1, was discovered for its involvement in dorsal/ventral patterning of the *Drosophila* embryo (Anderson et al., 1985). The *Drosophila* canonical TLR signaling pathways are activated in response to gram-negative bacteria and fungi and result in the expression of the antifungal drosomycin in an NF-κB dependant manner (Beinke and Ley, 2004; Imler and Zheng, 2003; Jang IH, 2006).

Unlike mammalian TLRs, activation requires the cysteine knot growth factor späetzle as a ligand, which activates the Toll/IL-1 receptor (TIR) cytoplasmic signaling domain. Späetzle is synthesized as a pro-ligand that is proteolytically cleaved by either Persephone or späetzle-processing enzyme (Imler and Zheng 2003; Jang IH 2006). Once activated, the TLR associates with the adaptor myeloid differentiation primary response protein 88 (MyD88) and Tube. Pelle, an IRAK-4 homolog, facilitates degradation of the IκB homolog Cactus. With Cactus degraded, Dorsal (NF-κB homolog) is free to enter the nucleus and activate transcription

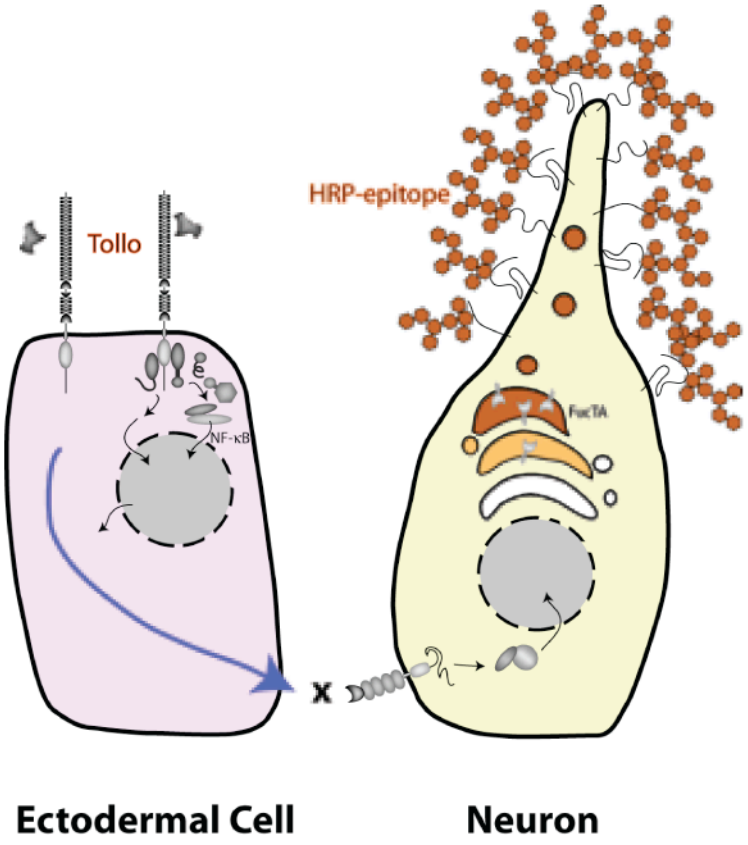

Figure 1.10 HRP-epitope expression pathway
Tollo, a Toll-like receptor expressed on an ectodermal cell, signals through a non-canonical pathway to release a yet unidentified factor, X, which binds to a neighboring differentiating neural cell. The signaling cascade in the neural cell results in the addition of HRP-epitopes on proteins. The signal may involve the activation of FucTA, the enzyme that adds the characteristic modification (α-3 linked fucose) that defines the family of HRP-epitopes. The data presented in this dissertation offers new evidence for what events are triggered in the neural cell, as well as an hypothesis as to the identity of factor X.

(Belvin and Anderson, 1996; Imler and Zheng, 2003). Deleting either *tube* or *pelle* doesn't affect HRP staining, indicating Tollo may be acting through a non-canonical pathway (**Fig. 1.10**).

SUMMARY AND SCOPE OF DISSERTATION

This chapter has given a brief overview of glycosylation, particularly N-glycosylation in *Drosophila*. Also, the development of the *Drosophila* nervous system was discussed and the contribution of glycosylation to neural function. SAD kinase was introduced as being involved in neuronal polarity and synaptic function, based on previous reports of SAD homologs from *C. elegans* and mouse.

Chapter two of this dissertation reports the first mutation reported for the *Drosophila SAD kinase*, that we have named *sugar-free frosting* (*sff*). The *sff* mutant, aside from having neurological phenotypes similar to SAD homologs, also has alterations in the N-glycosylation profile in embryos. Expressed exclusively in neural cells, SAD/sff modulates glycan expression by regulating traffic through the Golgi apparatus. Mechanisms that regulate tissue-specific glycan expression are not well understood, and Sff/SAD sheds some light onto how glycan processing events can be manipulated to direct glycan expression in tissues.

Chapter three expands on the findings presented in chapter two by introducing two regulators that, along with sff, modulate neural-specific glycan expression in the *Drosophila* embryo. The phenotypes presented in chapter two for the *sff* mutant are all affected by a protein called White. Data is also presented that introduces biogenic amines as potential regulators of neural glycosylation. The final chapter of this dissertation discusses future experiments and major findings of the work are summarized and placed in a broader context and significance.

REFERENCES

Alvarado-Kristensson, M., Rodriguez, M., Silio, V., Valpuesta, J., and Carrera, A. (2009). SADB phosphorylation of γ-tubulin regulates centrosome duplication. Nature Cell Biology *11*, 1081-1092.

Anderson, K., Jurgens, G., and Nusslein-Volhard, C. (1985). Establishment of dorsal-ventral polarity in the *Drosophila* embryo: Genetic studies on the role of the Toll gene product. Cell *42*, 779-789.

Aoki, K., Perlman, M., Lim, J., Cantu, R., Wells, L., and Tiemeyer, M. (2007). Dynamic developmental elaboration of N-linked glycan complexity in the *Drosophila melanogaster* embryo. J Biol Chem *282*, 9127-9142.

Barnes, A., Lilley, B., Pan, Y., Plummer, L., Powell, A., Raines, A., Sanes, J., and Polleux, F. (2007). LKB1 and SAD kinases define a pathway required for the polarization of cortical neurons Cell *129*, 549-563.

Bastiani, M., Harrelson, A., Show, P., and Goodman, C. (1987). Expression of fasciclin I and II glycoprotein's on subsets of axon pathways during neuronal development in the grasshopper. Cell *48*, 745-755.

Becker, D., and Lowe, J. (2003). Fucose: biosynthesis and biological function in mammals. Glycobiology *13*, 41R-53R.

Beinke, S., and Ley, S. (2004). Functions of NF-κB1 and NF-κB2 in immune cel biology Biochem. J *382*, 393-409.

Belvin, M., and Anderson, K. (1996). A conserved signaling pathway: the *Drosophila* Toll-dorsal pathway. Annu Rev Cel. Dev. Biol. *12*, 393-416.

Bickel, T., Lehle, L., Schwarz, M., Aebi, M., and Jakob, C.A. (2005). Biosynthesis of Lipid-linked Oligosaccharides in Saccharomyces cerevisiae Alg13p AND Alg14p form a complex required for the formation of GlcNAc2-PP-dolichol. J. Biol. Chem *280*, 34500-34506.

Brandstatter, J., and Meinertzhagen, I. (1995). The rapid assembly of synaptic sites in photoreceptor terminals of the fly's optic lobe recovering from cold shock. Proc Natl Acad Sci USA *92*, 2677-2681.

Bright, N., Carling, D., and Thornton, C. (2008). Investigating the role of Brain-specific kinase 1 and 2 by phosphorylation. J. Biol. Chem *283*, 14946-14954.

Brody, T., and Odenwald, W. (2002). Cellular diversity in the developing nervous system: a temporal view from *Drosophila*. Development *129*, 3763-3770.

Carraway, K., and Hull, S. (1989). O-glycosylation pathway for mucin-type glycoproteins. Bioessays *10*, 117-121.

Catterall, W. (1999). Interactions of the presynaptic Ca2+ channels and snare proteins in neurotransmitter release. Ann NY Acad Sci *868*, 144-159.

Chavis, P., and Westbrook, G. (2001). Integrins mediate functional pre- and postsynaptic maturation at a hippocampal synapse. Nature *411*, 317-321.

Chen, Y., Pendersen, J., Wandall, H., Levery, S., Pizzette, S., Claussen, H., and Cohen, S. (2007). Glycosphingolipids with extended sugar chain have specialized functions in development and behavior of *Drosophila*. Dev. Biol. *306*, 736-749.

Clements, M., Duncan, D., and Milbrandt, J. (2003). *Drosophila* NAB (dNAB) is an orphan transcriptional co-repressor required for correct CNS and eye development. Devel. Dynam. *226*, 67-81.

Compos-Ortega, J. (1993). Early neurogenesis in *Drosophila melanogaster*. In The development of *Drosophila melanogaster*, M.B.a.A. Arias, ed. (NY: Cold Spring Harbor Loaboratory Press).

Crump, J., Zhen, M., Yishi, J., and Bargmann, C. (2001). The SAD-1 kinase regulates presynaptic vesicle clustering and axon termination. Neuron *29*, 115-129.

Davis, G., Schuster, C., and Goodman, C. (1997). Genetic analysis of the mechanisms controlling target selection: target-derived Fasciclin II regulates the pattern of synapse formation. Neuron *19*, 561-573.

Desai, C., Popova, E., and Zinn, K. (1995). A *Drosophila* receptor tyrosine phosphatase expressed in the embryonic CNS and larval optic lobes is a member of the set of proteins bearing the "HRP" carbohydrate epitope. J. Neurosci *14*, 7272-7283.

Donaldson, M., Wood, H., Kulakosky, P., and Shuler, M. (1999). Use of mannosamine for inducing the addition of outer arm N-acetylglucosamine onto N-linked oligosaccharides of recombinant proteins in insect cells. Biotechnol. Prog *15*, 168-173.

Edenfeld, G., Pielage, J., and Klambt, C. (2002). Cell lineage specification in the nervous system. Curr. Opin. Gen. Dev. *12*, 473-477.

Fan, Y., Soller, M., Flister, S., Hollman, M., Muller, M., Bello, B., Egger, B., White, K., Schafer, M., and Reichert, H. (2005). The *egghead* gene is required for compartmentalization in *Drosophila* optic lobe development. Dev. Biol. *287*, 61-73.

Feurstenberg, S., Broadus, J., and Doe, C. (1998). Asymmetry and cell fate in the *Drosophila* embryonic CNS. Int. J. Dev. Biol. *42*, 379-383.

Frank, M., and Kemler, R. (2002). Protocadherins. Curr. Opin. Cell Biol. *14*, 557-562.

Fujimoto, T., Yurimoto, S., Hatano, N., Sueyoshi, N., Kameshita, I., Mizutani, K., Kobayashi, R., and Tokumitsu, H. (2008). Activation of SAD kinase by Ca2+/Calmodulin-dependent protein kinase kinase. Biochemistry *47*.

Glass, D., DeChiara, T., Stitt, T., DiStefano, P., Valenzuela, D., and Yancopoulos, G. (1996). The receptor tyrosine kinase MuSK is required for neuromuscular junction formation and is a functional receptor for agrin Cold Spring Harb. Symp. Quant. Biol. *61*, 435-434.

Goode, S., Melnick, M., Chou, T., and Perrimon, N. (1996a). The neurongenic genes egghead and brainiac define a novel signaling pathway essential for epithelial morphogenesis during *Drosophila* oogenesis. Development *122*, 3863-3879.

Goode, S., Morgan, M., Liang, Y., and Mahowald, A. (1996b). 1996 Brainiac encodes a novel secreted protein that cooperates with Grk TGF alpha in the genesis of the follicular epithelium. Dev. Biol. *178*, 35-50.

Goodman, C., and Doe, C. (1993). Embryonic development of the *Drosophila* central nervous system. In The development of *Drosophila melanogaster*, M. Bate, and A. Arias, eds. (New York: Cold Spring Harbor Laboratory Press).

Govind, C., and Meiss, D. (1979). Quantitative comparison of low- and high-output neuromuscular synapses from a motorneuron of the lobster (Homarus americanus). Cell Tissue Res *198*, 455-463.

Guatam, M., Noakes, P., Moscoso, L., Rupp, F., Scheller, R., Merlie, J., and Sanes, J. (1996). Defective neuromuscular synaptogenesis in agrin-deficient mutant mice. Cell *85*, 525-535.

Guo, Z., Tang, W., Yuan, J., Chen, X., Wan, B., Gu, X., Luo, K., Wang, Y., and Yu, L. (2006). BRSK2 is activated by cyclic AMP-dependent protein kinase A through phosphorylation at Thr260. Biochem Biophys Res Commun *347*, 867-871.

Haines, N., and Irvine, K. (2005). Functional analysis of *Drosophila* beta 1,4-N-acetylgalactosaminyl transferases Glycobiology Glycobiology *15*, 335-346.

Haines, N., and Stewart, B. (2006). Functional roles for β1,4-N-Acetylgalactosaminyltransferase-A in *Drosophila* larval neurons and muscles. Genetics *175*, 671-679.

Hanks, S., Quinn, A., and Hunter, T. (1998). The protein kinase family: conserved features and deduced phylogeny of the catalytic domains. Science *241*, 42-52.

Hartenstein, V. (1993). Atlas of *Drosophila* development (NY: Cold Spring Harbor Laboratory Press).

Hartenstein, V., and Campos-Ortega, J. (1997). The embryonic development of *Drosophila melanogaster*, 2 edn (Berlin: Springer Verlag).

Hsueh, Y., and Sheng, M. (1999). Regulated expression and subcellular localization of syndecan heparan sulfate proteoglycans and the syndecan-binding protein CASK/LIN-2 during rat brain development. J. Neurosci *19*, 7415-7425.

Hung, W., Hwang, C., Po, M., and Zhen, M. (2007). Neuronal polarity is regulated by a direct interaction between a scaffolding protein, neurabin, and a presynaptic SAD-1 kinase in *Caenorhabditis elegans*. Development *134*, 237-249.

Imler, J., and Zheng, L. (2003). Biology of Toll receptors: lessons from insects and mammals. J. Leuk. Biol. *74*, 1-9.

Inoue, E., Mochida, S., Takagi, H., Higa, S., Deguchi-Tawarada, M., Takao-Rikitsu, E., Inoue, M., Yao, I., Takeuchi, K., Kitajima, I.*, et al.* (2006). A presynaptic kinase associated with synaptic vesicles and the active zone cytomatrix that regulates neurotransmitter release. Neuron *50*, 261-275.

Jang IH, C.N., Kim SH, Nam HJ, Lemaitre B, Ochiai M, Kambris Z, Brun S, Hashimoto C, Ashida M, Brey PT, Lee WJ. (2006). A Spätzle-processing enzyme required for toll signaling activation in *Drosophila* innate immunity. Dev. Cell *10*, 45-55.

Jarvis, S., Barr, W., Feng, Z., Harmid, J., and Zamponi, G. (2002). Molecular determinants of syntaxin 1 modulation of N-type calcium channels. J. Biol. Chem *277*, 44399-44407.

Javaud, C., Dupuy, F., and Maftah, A. (2003). The fucosyltransferase gene family: an amazing summary of the underlying mechanisms of gene evolution. Genetica *118*, 157-170.

Jiang, J., Benson, E., Bausek, N., Doggett, K., and White-Cooper, H. (2007). Tombola, a tesmin/TSO1-family protein, regulates transcriptional activation in the *Drosophila* male germline and physically interacts with always early. Development *134*, 1549-1559.

Johnson, K., Tenney, A., Ghose, A., Duckworth, A., Hiashi, M., Parfitt, K., Marcu, O., Heslip, T., Marsh, J., Schwarz, T.*, et al.* (2006). The HSPGs syndecan and dallylike bind the receptor phosphatase LAR and exert distinct effects on synaptic development. Neuron *49*, 517-531.

Johswich, A., Kraft, B., Wuhrer, M., Berger, M., Deelder, A., Hokke, C., Gerardy-Schahn, R., and Bakker, H. (2009). Golgi targeting of *Drosophila melanogaster* beta4GalNAcTB requires a DHHC protein family-related protein as a pilot. J. Cell Biol. *184*, 173-183.

Karcavich, R. (2005). Generating neuronal diversity in the *Drosophila* central nervous system: a view from the ganglion mother cells. Devel. Dynam. *232*, 609-616.

Katz, F., Moats, W., and Jan, Y. (1998). A carbohydrate epitope expressed uniquely on the cell surface of *Drosophila* neurons is altered in the mutant nac (neurally altered carbohydrate). EMBO J *7*, 3471-3477.

Kim, I., Kim, I., Kim, S., Kwon, Y., Han, P., Jeon, S., and Kim, S. (2004). CNS midline cells contribute to maintenance of the initial dorsoventral patterning of the *Drosophila* ventral neuroectoderm. J. Neurobiol. *62*, 397-405.

Kim, J., Lilley, B., Zhang, C., Shokat, K., Sanes, J., and Zhen, M. (2008). A chemical-genetic strategy reveals distinct temporal requirements for SAD-1 kinase in neuronal polarization and synapse formation. Neural Dev *3*, 23-37.

Kishi, M., Pan, Y., Crump, J., and Sanes, J. (2005). Mammalian SAD kinases are required for neuronal polarization. Science *307*, 929-932.

Koles, K., Irvine, K., and Panin, V. (2004). Functional characterization of *Drosophila* sialyltransferase. J Biol. Chem *279*, 4346-4357.

Kruse, J., Mailhammer, R., Wernecke, H., Faissner, A., Sommer, I., Goridis, C., and Schachner, M. (1984). Neural cell adhesion molecules and myelin-associated glycoprotein share a common carbohydrate moiety recognized by polyclonal antibodies L2 and HNK-1. Nature *316*, 146-148.

Lang, T., Bruns, D., Wenzel, D., Riedel, D., Holroyd, P., Thiele, C., and Jahn, R. (2001). SNAREs are concentrated in cholesterol-dependent clusters that define docking and fusion sites for exocytosis. EMBO J *20*, 2202-2213.

Leonard, R., Rendic, D., Rabouille, C., Wilson, I., Preat, T., and Altmann, F. (2006). The *Drosophila fused lobes* gene encodes an N-acetylglucosaminidase involved in N-glycan processing. J. Biol. Chem *281*, 4867-4875.

Lew, D. (2000). Cell-cycle checkpoints that ensure coordination between nuclear and cytoplasmic events in S. cerevisiae. Curr Opin Genet Dev *10*, 47-53.

Lin, D., Fetter, R., Kopczynski, C., Grenningloh, G., and Goodman, C. (1994). Genetic Analysis of fasciclin 2 in *Drosophila*: defasciculation, refasciculation, and altered fasciculation. Neuron *13*, 1055-1069.

Lu, R., Niida, H., and Nakanishi, M. (2004). hSAD1 kinase is involved in UV-induced damage checkpoint function. J. Biol. Chem *279*, 31164-31170.

Luo, Y., Koles, K., Vorndam, W., Haltiwanger, R., and Panin, V. (2006). Protein O-fucosyltransferase 2 adds O-fucose to thrombospondin type 1 repeats. J. Biol. Chem *281*, 9393-9399.

Manning, G., Plowman, G.D., Hunter, T., and Sudarsanam, S. (2002). Evolution of protein kinase signaling from yeast to man. TRENDS in Biochemical Sciences *27*, 514-520.

Martin, P. (2002). Glycobiology of the synapse. Glycobiology *12*, 1R-7R.

Martin, P. (2007). Congenital muscular distrophies involving the O-mannose pathway. Curr Mol Med *7*, 417-425.

McAllister, L., Goodman, C., and Zinn, K. (1992). Dynamic expression of the cell adhesion molecule fasciclin I during embryonic development in *Drosophila*. Development *115*, 267-276.

Muller, R., Altmann, F., Zhou, D., and Hennet, T. (2002). The *Drosophila melanogaster* brainiac protein is a glycolipid-specific beta 1,3-N-acetylglucosaminyltransferase J. Biol. Chem *277*, 32417-32420.

Murthy, V., and Camili, P. (2003). Cell biology of the presynaptic terminal. Annu Rev Neurosci *26*, 701-728.

Nakamura, Y., Makabe, K., and Nishida, H. (2005). POPK-1/SAD-1 kinase is required for the proper translocation of maternal mRNAs and putative germ plasm at the posterior pole of the ascidian embryo. Development *132*, 4731-4742.

Nambu, J., Lewis, J., Wharton, K., and Crews, S. (1991). The *Drosophila single-minded* gene encodes a helix-loop-helix protein that acts as a master regulator of CNS midline development. Cell *67*, 1157-1167.

Okajima, T., Xu, A., Lei, L., and Irvine, K. (2005). Chaperone activity of protein O-fucosyltransferase 1 promotes notch receptor folding. Science *307*, 1599-1603.

Pearson, B., and Doe, C. (2004). Specification of temporal diversity in the developing nervous system. Annu. Rev. Cell Dev. Biol. *20*, 619-647.

Poeck, B., Fischer, S., Ghunning, D., Zipursky, S., and Salecker, I. (2001). Glial cells mediate target layer selection of retinal axons in the developing visual system of *Drosophila*. Neuron *29*, 99-113.

Quigley, P., and Pearce, J. (2001). Synaptic differentiation between two phasic motorneurons to a crayfish fast muscle. Invert. Neurosci *4*, 77-84.

Rendic, D., Linder, A., Paschinger, K., Borth, N., Wilson, I., and Fabini, G. (2006). Modulation of neural carbohydrate epitope expression in *Drosophila melanogaster* cells. J Biol Chem *281*, 3343-3353.

Rendic, D., Sharrow, M., Overcarsh, B., Nguyen, K., Kapurch, J., Aoki, K., Poltll, G., Wilson, I., and Tiemeyer, M. N-linked glycoprotein fucosylation modulates cell signaling during *Drosophila melanogaster* development. submitted.

Rider, M. (2006). The ubiquitin-associated domain of AMPK-related protein kinase allows LKB1-induced phosphorylation and activation. Biochem. J *294*, e7-e9.

Rougon, G., and Hobert, O. (2003). New insights into the diversity and function of neuronal immunoglobulin superfamily molecules. Annu Rev Neurosci *26*, 207-238.

Rybak, J., and Meinertzhagen, I. (1997). The effects of light reversals on photoreceptor synaptogenesis in the fly Musca domestica. Eur J Neurosci *9*, 319-333.

Sanchez-Soriano, N., and Propkop, A. (2005). The influence of pioneer neurons on a growing motor nerve in drosophila requires the neural cell adhesion molecule fasciclin II. J. Neurosci *25*, 78-87.

Sánchez-Soriano, N., Tear, G., Whitington, P., and Prokop, A. (2007). *Drosophila* as a genetic and cellular model for studies on axonal growth. Neural Dev *2*.

Sarkar, M., Leventis, P., Silvescu, C., Reinhold, V., Schacter, H., and boulianne, G. (2006). Null mutations in *Drosophila N-acetylglucosaminyltransferase I* produce defects in locomotion and a reduced life span. J. Biol. Chem *281*, 12776-12785.

Schmucker, D., Clemens, J., Shu, H., Worby, C., Xiao, J., Muda, M., Dixon, J., and Zipursky, S. (2000). *Drosophila* Dscam is an axon guidance receptor exhibiting extraordinary molecular diversity. Cell *101*, 671-684.

Schoch, S., Castillo, P., Jo, T., Mukherjee, K., Geppert, M., Wang, Y., Schmitz, F., Malenka, R., and Sudhof, T. (2002). RIM1α forms a protein scaffold for regulating neurotransmitter release at the active zone. Nature *415*, 321-326.

Seppo, A., Matani, P., Sharrow, M., and Tiemeyer, M. (2003). Induction of neuron-specific glycosylation by Tollo/Toll-8, a *Drosophila* Toll-like receptor expressed in non-neural cells. Development *130*, 1439-1448.

Seppo, A., Moreland, M., Schweingruber, H., and Tiemeyer, M. (2000). Zwitterionic and acidic glycosphingolipids of the *Drosophila melanogaster* embryo. Eur. J. Biochem *267*, 3549-3358.

Shapiro, L., and Colman, D. (1999). The diversity of cadherins and implications for a synaptic adhesive code in the CNS. Neuron *23*, 427-430.

Sharrow, M., and Tiemeyer, M. (2001). Gliolectin-mediated carbohydrate binding at the *Drosophila* midline ensures fidelity of axon pathfinding. Development *128*, 4585-4595.

Skeath, J., and Thor, S. (2003). Genetic control of *Drosophila* nerve cord development. Curr. Opin. Neurobiol. *13*, 8-15.

Snow, D., and Hart, G. (1998). Nuclear and cytoplasmic glycosylation. Int Rev Cytol *181*, 43-74.

Snow, P., Patel, N., Harrelson, A., and Goodman, C. (1987). Neural-specific carbohydrate moiety shared by many surface glycoproteins in *Drosophila* and grasshopper embryos. J Neurosci *7*, 4137-4144.

Stolz, A., Haines, N., Pich, A., Irvine, K., Hokke, C., Deelder, A., Gerardy-Schahn, R., Wuhrer, M., and Bakker, H. (2008). Distinct contributions of β4GalNAcTA and β4GalNAcTB to *Drosophila* glycosphingolipid biosynthesis Glycoconj J *25*, 167-175.

Takeshita, S., Kikuno, R., Tezuka, K., and Amann, E. (1993). Osteoblast-specific factor 2: cloning of a putative bone adhesion protein with homology with the insect protein fasciclin I Biochem. J *294*, 1-8.

Tayler, T., Robichaux, M., and Garrity, P. (2004). Compartmentalization of visual centers in the *Drosophila* brain requires slit and robo proteins. Development *131*, 5395-5945.

Technau, G., Berger, C., and Urbach, R. (2006). Generation of cell diversity and segmental pattern in the embryonic central nervous system of *Drosophila*. Devel. Dynam. *235*, 861-869.

Tiemeyer, M., and Goodman, C. (1996). Giolectin is a novel carbohydrate-binding protein expressed by a subset of glia in the embryonic *Drosophila* nervous system. Development *122*, 925-936.

Varki, A., Cummings, R., Esko, J., Freeze, H., Hart, G., and Marth, J. (1999). Essentials of Glycobiology, 1 edn (New York: Cold Spring Harbor Laboratory Press).

Wagh DA, Rasse TM, Asan E, Hofbauer A, Schwenkert I, Dürrbeck H, Buchner S, Dabauvalle MC, Schmidt M, Qin G*, et al.* (2006). Bruchpilot, a protein with homology to ELKS/CAST, is required for structural integrity and function of synaptic active zones in Drosophila. Neuron *49*, 833-844.

Waites, C., Craig, A., and Garner, C. (2005). Mechanisms of vertebrate synaptogenesis. Annu Rev Neurosci *28*, 251-274.

Walsh, F., and Doherty, P. (1997). Neural cell adhesion molecules of the immunoglobulin superfamily: role in axon growth and guidance. Annu Rev Cel. Dev. Biol. *13*, 425-456.

Wandall, H., Pedersen, J., Park, C., Levery, S., Pizzette, S., Cohen, S., Schwientek, T., and Clausen, H. (2003). *Drosophila egghead* encodes a β 1,4-mannosyltransferase predicted to form the immediate precursor glycosphingolipid structure for brainiac. J. Biol. Chem *278*, 1411-1414.

Wangers, A., and Kansas, G. (2000). Potent induction of alpha(1,3)-fucosyltransferase VII in activated CD4+ T cells by TGF-beta 1 through a p38 mitogen-activated protein kinase-dependent pathway. J. Immunol. *165*, 5011-5016.

Wells, L. (2009). O-glycan complexity and analysis. In Handbook of Glycomics, R. Cummings, and J. Pierce, eds. (London: Academic Press).

Whitlock, K. (1993). Development of *Drosophila* wing sensory neurons in mutants with missing or modified cell surface molecules. Development *117*, 1251-1260.

Wildonger, J., Jan, L., and Jan, Y. (2008). The Tsc1-Tsc2 complex influences neuronal polarity by modulating TORC1 activity and SAD levels. Genes and Dev *22*, 2447-2453.

Yamagata, M., Weiner, J., and Sanes, J. (2002). Sidekicks: synaptic cell adhesion molecules that promote lamina-specific connectivity in the retina. Cell *110*, 649-660.

Zhai, G., and Bellen, H. (2004). The architecture of the active zone in the presynaptic nerve terminal. Physiology *19*, 262-270.

Zito, K., Parnas, S., Fetter, R., Isacoff, E., and Goodman, C. (1999). Watching a synapse grow: noninvasive confocal imaging of synaptic growth in *Drosophila*. Neuron *22*, 719-729.

CHAPTER 2

SUGAR-FREE FROSTING/SAD KINASE DRIVES GOLGI COMPARTMENTATION ESSENTIAL FOR NEURAL-SPECIFIC GLYCAN EXPRESSION IN THE *DROSOPHILA* EMBRYO[1]

[1] Sarah Baas, Mary Sharrow, Varshika Kotu, Meg Middleton, Heather Flanagan-Steet, Kazuhiro Aoki, and Michael Tiemeyer. Submitted.

SUMMARY

Precise glycan structures on specific neural glycoproteins impart functionalities essential for development and plasticity. However, mechanisms controlling neural-specific glycosylation are unknown. A genetic screen for relevant mutations in *Drosophila* generated the *sugar-free frosting mutant* (*sff*) that reveals a new function for protein kinases in regulating substrate flux through specific Golgi processing pathways. Sff kinase is the *Drosophila* homologue of SAD kinase, which regulates synaptic vesicle tethering and neuronal polarity in nematodes and vertebrates. Our *Drosophila sff/SAD* mutant shares phenotypes with these systems, but we detect altered neural glycosylation well before the initiation of synaptogenesis. Aberrant Golgi compartmentation constitutes the underlying mechanism for altered glycosylation. Analogous to synaptic vesicle tethering, we propose that Sff/SAD regulates vesicle tethering at Golgi membranes. Furthermore, neuronal *sff/SAD* expression is dependent on transcellular signaling through a non-neural toll-like receptor, linking neural-specific glycan expression to a kinase activity that is induced in response to environmental cues.

INTRODUCTION

Essential aspects of neural development and plasticity rely on the regulated expression of specific glycan structures linked to glycoproteins, proteoglycans, and glycolipids. The fundamental involvement of glycans in neural cell function begins with neurectoderm differentiation, when the elaboration of distinct glycan structures on the Notch glycoprotein receptor facilitates ligand-specific activation that drives cell fate selection (Okajima and Irvine, 2002). Subsequently, glycans expressed in developing and mature neural tissues impinge on other important cell signaling, migration, adhesion, and synaptic functions (Matani et al., 2007).

Several underlying molecular mechanisms for glycan function are well characterized, including the influence of N-linked polysialic acid on NCAM interactions, the engagement of axonal glycosphingolipid glycans by a specific carbohydrate binding protein on oligodendrocytes, and the activity-dependent deposition of glycosaminoglycans into perineuronal nets (Acheson et al., 1991; Matthews et al., 2002; Vyas et al., 2002). Each of these instances, and others, reveal the prevalence of temporally and/or spatially regulated glycan expression, a rubric which is further supported by the existence of many anti-glycan antibodies (HNK-1, CAT, Jones, A2B5, FORSE-1, anti-HRP) that delineate sub-populations of neuronal or glial cells (Allendoerfer et al., 1999; Constantine-Paton et al., 1986; Jan and Jan, 1982; Kruse et al., 1984; Matthews et al., 2002; Schnitzer and Schachner, 1982; Snow et al., 1987). Furthermore, aberrant glycan expression in humans is associated with an increasingly broad range of pathologies, including mental retardation, congenital muscular dystrophies, multiple sclerosis, and disorders of immune, skeletal, and connective tissues (Dennis et al., 2009; Freeze, 2002; Lee et al., 2007; Michele and Campbell, 2003; Zak et al., 2002). Despite the overwhelming evidence for regulated glycan expression and for the significant consequences of disregulated glycan expression, the mechanisms that govern tissue-specific glycosylation are essentially unknown, particularly during embryonic development.

We have previously reported that a mutation in an ectodermally expressed Toll-like receptor (*tollo/toll-8*) alters N-linked glycosylation in the developing *Drosophila* embryonic nervous system (Seppo et al., 2003). This defect was detected as loss of staining with antibodies that recognize a family of structurally related N-glycans, known as HRP-epitopes, which are normally expressed in a restricted set of embryonic tissues (Jan and Jan, 1982; Snow et al., 1987). The *tollo/toll-8* mutation specifically abolishes HRP-epitope expression in neural tissue

although *tollo/toll-8* is not expressed in neural cells that carry the HRP-epitope. Rather, it is expressed and functions within non-neural ectodermal cells that surround differentiating neurons, establishing the basis for a transcellular signaling pathway that drives neuron-specific glycosylation (Seppo et al., 2003). Such transcellular signaling might drive cell-specific glycan expression through altered transcription of glycan biosynthetic enzymes (glycosyltransferases, nucleotide sugar transporters, etc.) or through mechanisms that modify trafficking through specific glycoprotein processing pathways. The relative contribution of altered transcription and altered cellular organization to tissue-specific glycan expression is completely unresolved in any biological context.

To address this lack of knowledge and to identify the unknown components of this novel transcellular signaling mechanism, we have undertaken a random mutagenesis screen for genes that specifically affect HRP-epitope expression in the *Drosophila* embryonic nervous system. Here, we describe an informative mutation recovered from this screen, called *sugar-free frosting* (*sff*), whose phenotype reveals the importance of regulated Golgi dynamics for neuron-specific glycan expression. The mutation maps to the *Drosophila* homologue of a Ser/Thr kinase known as "Synapses of the Amphid Defective" (SAD-1) in nematodes and vertebrates (Crump et al., 2001; Inoue et al., 2006; Kishi et al., 2005). Our *sff* mutation, which is the first described disruption of the *Drosophila SAD* kinase, interacts genetically with *tollo/toll-8* and modulates glycan complexity in neurons that are receptive to the *tollo/toll-8* transcellular signaling pathway prior to synaptogenesis. Our results lead us to propose that neural-specific glycan expression is sculpted by the relative activities of multiple protein kinases, each acting to facilitate flux through specific Golgi processing pathways. This hypothesis implies a new paradigm in which

cell-specific glycoprotein glycosylation reflects the convergence of signaling pathways onto regulated kinase activities that modulate specific Golgi trafficking routes.

EXPERIMENTAL PROCEDURES

Reagents

Rabbit anti-HRP, HRP-Concanavalin A (ConA), and HRP-conjugated goat anti-rabbit or goat anti-mouse antibodies were obtained from Jackson Laboratories. Monoclonal antibodies 1D4, nC82 (anti-Brp), and 22C10 were obtained from the Developmental Studies Hybridoma Bank (DHSB, University of Iowa). Biotin-conjugated PNA (peanut lectin) was obtained from Vector Laboratories. Alexa-conjugated secondary antibodies (Alexa488, 568, and 633), rabbit anti-GFP (cross-reactive with YFP), and PROLONG anti-fade were obtained from Molecular Probes. TRITC-Phalloidin was from Invitrogen. PNGaseA was from Calbiochem, Trypsin and chymotrypsin were from Sigma.

Drosophila Culture

All strains were reared on standard molasses media at 25^{o}C unless otherwise indicated. Stocks carrying multiple markers for recombination mapping (rucuca), or carrying marked balancer chromosomes for standard husbandry, or carrying defined deficiencies for deletion mapping (third chromosome deletion set, DrosDel, and Exelexis lines), or carrying reporter markers for specific Golgi compartments (Golgi-YFP) were obtained from The Bloomington *Drosophila* Stock Center at Indiana University. The *tollo/toll-8* mutant line is as previously described (Seppo et al., 2003). For confocal characterization of the medial/trans Golgi, the YFP reporter carried by the Golgi-YFP line obtained from Bloomington (third chromosome insertion) was recombined

onto the *sff*^{B22} chromosome (third chromosome mutation). Therefore, for Golgi characterization, wild-type refers to the parental w^{*}; +; Golgi-YFP line. Otherwise, wild-type refers to *OreR*.

Mutagenesis Screen

Males of genotype w^{1118}, +, + were treated with 25 mM ethyl methanesulfonate and mated en masse to females of the genotype w^{1118}; *Kr/*Cyo; *D/TM6b*. Individual male progeny heterozygous for the 2nd and 3rd chromosome markers were backcrossed to w^{1118}; *Kr/*Cyo; *D/TM6b* females to create lines that carried mutagenized 2nd or 3rd chromosomes. Progeny from each individual line were sib-mated to give embryo collections that were stained with anti-HRP antibody. To scrub away accessory mutations, mutant lines of interest were outcrossed to *OreR* for at least 5 generations. Mutants of interest were identified by staining embryo collections harvested from balanced lines (F2 generation) with anti-HRP antibody. Lines showing altered HRP-epitope expression were subsequently stained with Concanavalin A. Only lines that were deficient in anti-HRP staining but normal for Concanavalin A staining were maintained.

Immunohistochemistry, Immunofluorescence, and NMJ Analysis

Embryos from overnight collections were dechorionated, fixed, devitellinized, and stained with antibodies using blocking conditions and wash buffers as previously described (Patel, 1994; Seppo et al., 2003). Primary antibody and other probe dilutions were as follows: anti-HRP, 1:2000 for embryos and 1:1000 for larvae; Peroxidase-conjugated ConA, 1:100; mAb 1D4, 1:3; mAb nc82, 1:100; mAb 22C10, 1:5; TRITC-Phalloidin, 1:100; anti-GFP, 1:5000; biotin-conjugated PNA, 1:100 (0.5 mg/ml final). Alexafluor-conjugated secondary antibodies were used at a 1:500 dilution. Fluorescence-stained preparations were generally mounted in 70% glycerol with 4% DABCO or with PROLONG anti-fade reagent. Peroxidase-conjugated secondary antibodies were used at 1:1000 dilution for anti-rabbit with 3,3-diaminobenzidine

precipitation in the presence of H_20_2 as substrate (Patel, 1994). For histochemical probes (antibodies and ConA) Nomarski (DIC) and light micrographs were obtained on a Zeiss Axioskop microscope fitted with a Q imaging Retiga 2000R camera.

NMJ morphology was assessed in wandering third instar larvae raised at 18°C. Larval dissections were performed as previously described (Kaufmann et al., 2002). Third instar larvae were harvested and pinned dorsal side up onto Sylgard plates in a solution of 128mM NaCl, 2mM KCl, 4mM $MgCl_2$, 35.5mM sucrose, 5mM HEPES, 1mM EDTA. A mid-longitudinal incision was made and internal organs were removed. The resulting pelts were secured by pins and fixed in 4% paraformaldehyde. Larval pelts were stained with anti-HRP antibody, mAb 1D4, and/or TRITC-Phalloidin. The NMJ at muscles 6 and 7 were imaged using a laser scanning confocal microscope (LSC, Olympus FV1000). Images were acquired using a 40x (N.A. 1.30) oil objective. Stacks of optical sections were collected in the z-dimension; the step-size, based on the calculated optimum, was 0.50 mm. Maximum intensity projections were assembled off-line using NIH Image J. For consistency across larvae, quantification of bouton number and primary branching was limited to the NMJs in abdominal segments 3 and 4.

N-glycan analysis

Total N-glycans were prepared from overnight embryo collections (25^{o}C) as previously described (Aoki et al., 2007). Briefly, embryos were homogenized and delipidated by extraction with chloroform:methanol:water::4:8:3 (v/v/v). Proteins were precipitated, collected by centrifugation, and dried to generate a proteinaceous powder. The protein powder was resuspended, boiled, reduced, and digested with trypsin/chymotrypsin. Glycopeptides were enriched by C18 Sep-Pak chromatography and N-linked glycans were released by PNGaseA digestion. Following clean-up by C18 Sep-Pak chromatography, released glycans were

permethylated and analyzed by mass spectrometry using nanospray ionization interfaced to a linear ion trap instrument (NSI-MS^n on an LTQ Ion Trap, Thermo/Fisher). The Total Ion Mapping (TIM) functionality of the instrument control and data acquisition software package (Xcaliber, v 2.0) was used, as described previously, to acquire full N-linked glycan profiles (Aoki et al., 2007). The large collections of MS and MS/MS spectra generated by TIM analyses (approximately 700 spectra per sample) were manually interpreted to assign glycan structures and quantify relative glycan prevalence. Ambiguities were resolved by acquisition of spectra at MS^3–MS^4 as needed.

Deletion Breakpoint Mapping by Single Embryo PCR

Embryos from overnight collections of the non-complementing Δ*brm*[11] or complementing Δ*th*[102] deletion lines were dechorionated and homogenized individually in 10µl 10mM Tris-Cl pH 8.2, 1mM EDTA, 25mM NaCl, 200µg/ml Proteinase K. Homogenates were incubated at 37°C for 20 minutes, followed by a 2 minute incubation at 95°C. Extract was added directly to the PCR reaction; extract from one embryo was enough for 3-4 reactions. PCR for the *trh* gene (tryptophan hydroxylase), which is not disrupted by either deletion, confirmed the integrity of the genomic DNA in the sample and PCR for *brm* (brahma), which lies within the deletion interval of both lines, was used to determine which extracts came from deletion homozygotes. Following lists the genes and primers used to map the deletion breakpoints. Both deletion lines were maintained over balancer chromosomes. Therefore, PCR analysis was performed on multiple single embryo homogenates to obtain results that matched expected Mendelian ratios for the balanced stock.

PCR primer sequences for mapping deletion breakpoints		
Gene	Sense	Antisense
CG9122 (*trh*)	CTAGCCATTGAATACATCACCAGATCGG	GCCAAGTGAATTGTACTACGCATACACCT
CG5942 (*brm*)	CTTGCGGTAACCCTCCTCATCC	GCCAGCATGCAGGACAACC
CG32155	CGCGACTGAACAGTTATGATCG	CGGTGATGGATGCAAACAGG
CG13055	CCTTTGAGATATGTGTAGGAGACG	GGAAATTAAGCACACGCACG
CG13073	GCTGCGATTTGTGCTTATTCC	GCCTCGCAGATATAGATATAGATGG
CG6117 (*Pka-C3*)	CCACTCCAAATATCAAGATTTACCG	GCCAGCAGAAGCATCATTATTACC
CG33989 (*pHCl*)	GGAAGTTGGGTGGGCTTATGC	GGCATACGGGCAATGTGACC
CG6114 (*sff/SAD*)	GCATTCAAAGTGCCTGGTGC	GGTGGAGCACAGGAGTACATGG
CG6114 (*sff/SAD*)	GCGATTGGAGTTTAGTTTGCAGAGC	GCACAGCACATGCCCTAATAAAGC
Primer sequences are given in 5' - 3' direction.		

***In situ* hybridization**

Wild-type genomic sequence corresponding to 2581 bp of the *CG6114* 3' UTR was amplified by PCR (sense: 5'-CGCTGCTCATTGCACAGTGC-3', antisense: 5'-GCTGAGCACGAACGCAACC-3') and cloned into PCR 2.1 TOPO vector (Invitrogen). Clones were recovered bearing insert in both sense and anti-sense orientations relative to the T7 promoter. Digoxigenin-11-UTP-labeled RNA was prepared by in-vitro transcription using T7 polymerase and the DIG RNA Labeling Kit (Roche). Overnight embryo collections (25^{o}C) were prepared and probed with sense and antisense probes as previously described (Kopczynski et al., 1996). For co-localization of mRNA with a neuronal marker, *in situ* hybridization was performed (alkaline phosphatase with BCIP/NBT) prior to staining with mAb 22C10 (peroxidase with H_2O_2/DAB).

Proteomic Analysis by LC-MS/MS

Heads from 8 day old males raised at 18^{o}C were homogenized in 50mM Tris-HCl pH 7.5, 0.25M sucrose, 25mM KCl and Complete Mini Protease Inhibitor Cocktail (Roche) and then centrifuged at 5,000xg for 15 minutes at 4°C. The supernatant was then centrifuged at 105,000xg at 4°C for 45 minutes. The supernatant was reduced with 10mM DTT for 45 min at 50°C, then carboxyamidomethylated with 30mM iodoacetamide in the dark for 45 min, and then digested with 4μl trypsin (Sigma, sequencing grade) in 0.1M Tris-HCl pH 8.2 and 0.01M $CaCl_2$. The peptides were loaded onto a 1 ml C18 column, eluted in 20% 2-propanol, and dried by vacuum centrifugation. Two-dimensional RP/RP-HPLC was performed to separate the total peptide mixture (F1-5) based on hydrophobicity (Lim et al., 2007). In the first dimension, peptides were resuspended and loaded onto a reverse-phase column equilibrated in 100% of 0.1% trifluoroacetic acid in water (C18, 2.1 x 150 mm, 5 mm, Grace Vydac). Peptides were eluted over 55 min with a linear gradient from 5 to 60% of the elution buffer (80% acetonitrile, 0.085% trifluoroacetic acid in water) followed by a linear gradient of elution buffer from 60 to 95% over 10 minutes. Five fractions were collected (F1, 15-32%; F2, 32-40%; F3, 40-45%; F4, 45-55%: F5, 55-85% of elution buffer). Fractionated peptides were resuspended in 39 μl of mobile phase A (0.1% formic acid in water) and 1 μl of mobile phase B (80% acetonitrile, 0.1% Formic acid) and loaded off-line onto a nanospray tapered capillary column emitter (360 X 75 X 15 μm, PicoFrit, New Objective) self-packed with C18 resin (10cm, Waters) using a Nitrogen pressure bomb for 10 min. LC-MS/MS analysis was performed on an LTQ XL Ion Trap mass spectrometer (Thermo/Fisher) with a Surveyor MS pump plus (Thermo Scientific). Peptide fractions were separated over 100 min with a flow rate of 130 μl/min using the following gradient profiles:

Gradient conditions for LC/MS/MS following RP/RP-HPLC							
	%B				%B		%B
Time	F1	F2	F3	Time	F4	Time	F5
0	0	5	5	0	5	0	5
5	4	7	15	5	20	5	28
50	10	14	20	50	24	45	34
75	30	35	42	80	55	65	55
80	55	70	75	85	80	80	85
85	95	95	95	90	95	85	95
90	95	95	95	95	95	90	95
91	5	5	5	96	5	91	5
95	0	0	0	100	0	95	0
Buffer A is 0.1% formic acid in water; Buffer B is 80% acetonitrile, 0.1% formic acid							

Full MS spectra (m/z 300-2000) were collected every 600 msec during the chromatographic run. MS/MS spectra (36% normalized collision energy) were triggered upon detection of any m/z signal that corresponded to any entry into a parent mass list of theoretical CG6114 tryptic peptides that allowed for up to 2 missed cleavages, oxidized methionine, alkylated cysteine, and charge states up to +3. Within this parent mass list are m/z values that are coincident with non-Sff peptides, providing control peptides which allow comparison of Sff peptides with closely eluting components that were not expected to be affected by the *sff* mutation. MS/MS data was searched against the Fly database (*Drosophila melanogaster*, 8-31-09) from Swiss Prot to which CG6114 was added, and against the reverse of this database to assess false discovery. SEQUEST parameters were set with a mass tolerance of 30 ppm, fragment ion cutoff of 0.1%, and allowance for 2 missed cleavages.

Evaluation of Geotaxis Behavior

On the morning of testing, 8 day old males that had been raised at 25^{o} or 18^{o}C were placed individually into empty plastic culture vials containing no media. Following dark-adaptation for

one-hour (under red safe-light) at either 25^{o} or 18^{o}C, the test subjects were gently tapped to the bottom of the vial. The elapsed time for the subject to climb to a mark 3 cm up the side of the vial was recorded. For subjects that did not reach the pre-determined height, the trial was terminated after 2 minutes and the elapsed time was scored as 120 sec.

Immunofluorescence Analysis of Golgi Morphology

To characterize wild-type and *sff*^{B22} Golgi morphology, embryos were dechorionated, fixed, and devitillinized by standard procedures (Patel, 1994). Triple staining for confocal analysis of Golgi compartment markers was performed in the following order: biotin-conjugated PNA (trans marker), rabbit anti-GFP (trans/medial marker), and then mAb 1D4 (HRP-protein), followed by Alexa568-conjugated streptavidin, Alex488-conjugated goat anti-rabbit, and finally Alexa633-conjugated goat anti-mouse. Blocking and dilution buffer for PNA was 0.1% (w/v) BSA, 0.3% (w/v) Triton X-100 in PBS. Blocking and dilution buffers for primary and secondary antibodies were augmented with 5% (v/v) normal goat serum. PNA and primary antibody incubations were overnight at 4^{o}C with end-over-end agitation. Streptavidin and secondary antibody incubations were for 2 hours at ambient temperature. Embryos were cleared in glycerol, dissected, and mounted in anti-fade reagent.

Golgi imaging was also performed using an Olympus FV1000 LSC microscope. Images were acquired in the z-dimension with step-size of 0.45 mm using a 60x (N.A. 1.42) oil objective. Laser intensity, slice thickness, and all other acquisition parameters were identical for imaging wild-type and mutant embryos. Image analysis was accomplished off-line with the Slidebook software package (Intelligent Imaging Innovations, Denver, CO) on non-compressed z-stacks. Confocal stacks were adjusted for background and channel overlap using the software supplier's recommended algorithms.

To quantify overlapping distributions of Golgi compartment markers, the co-localized fluorescence intensity for any two markers was normalized to the total fluorescence intensity of the marker of interest (**Fig. 2.13**). For example, the % co-localization of the trans Golgi marker (PNA) with the medial/trans marker (Golgi-YFP) was calculated by dividing the PNA fluorescence signal intensity detected to be co-localized with Golgi-YFP by the total PNA fluorescence detected within the region of interest. Pearson's Correlation Coefficients were determined using Slidebook software for the fluorescence intensity of pairwise marker combinations across all identified objects within the quantified regions of interest.

RESULTS AND DISCUSSION

Decreased Expression of HRP-Epitopes in *Sugar-Free Frosting* Mutant Embryos

Antibodies generated against the plant glycoprotein horseradish peroxidase (HRP) cross-react with specific asparagine-linked oligosaccharide structures on proteins expressed in the nervous system of many arthropods (Jan and Jan, 1982; Snow et al., 1987). These N-glycans, collectively known as HRP-epitopes, are enriched in neural tissue and carry a3 and a6 linked fucose (Fuc) on the innermost N-acetylglucosamine (GlcNAc) of the chitobiose core (GlcNAcb4GlcNAc, **Fig. 2.2A**). Although the recognized structures are frequently difucosylated, a3-linked Fuc is the dominant antigenic determinant (Kurosaka et al., 1991). HRP-epitopes are expressed throughout the entire *Drosophila* life cycle (Aoki et al., 2007; Fabini et al., 2001). In the embryo, anti-HRP staining is evident in the ventral nerve cord and peripheral nervous system, as well as in a limited set of non-neural tissues, including the garland gland and the hindgut (**Fig. 2.2B-D**).

The restricted distribution of the HRP-epitope provides a platform for identifying genes that govern tissue-specific glycan expression. Therefore, we undertook a random mutagenesis screen, using ethylmethane sulfonate (EMS) as mutagen, to harvest mutations that specifically alter expression of the HRP-epitope without generally affecting N-linked glycosylation. Embryos from the F2 generation derived from individual mutagenized male founders were stained with anti-HRP antibody and examined for loss of HRP-epitope. Mutant lines that exhibited altered HRP-epitope expression were stained with Concanavalin A (ConA), which reports the presence of high-mannose oligosaccharides, to assess the integrity of the core glycosylation machinery.

The first mutation recovered from the screen, initially designated *B22*, is a semi-viable third chromosome line with substantial loss of all neural HRP-epitope expression but normal ConA staining (**Fig. 2.1, Table 2.1**). Residual staining is apparent in late stages within the axon scaffold of the ventral nerve cord. This neural staining is restricted to the dorsal aspect of the nerve cord and imparts the appearance of a thin layer of epitope frosting, prompting us to name the mutation "*sugar-free frosting*" (*sff*). At reduced temperature (21^{o}C), the arrival of residual epitope expression is delayed until slightly later stages than is observed at 25^{o}C (**Fig. 2.2 H-J**).

Increased N-linked Glycan Complexity in *Sugar-Free Frosting* Mutant Embryos

N-linked glycan biosynthesis and processing in *Drosophila* proceeds through steps that are well conserved across the animal kingdom (**Fig. 2.3A**). A major difference between *Drosophila* and vertebrate glycan processing is the activity of an N-acetylhexosaminidase, known as Fused Lobes (Fdl), which removes the GlcNAc residue added by N-acetylglucosaminyltransferase-I (GlcNAcT1). The Fdl enzyme drives the predominance of paucimannose structures in the total

Table 2.1. Viability of *sff* homozygotes

Genotype	# Embryos at start	Pupae	% of Expected	Adults	% of Expected
wild-type	457	373	82	364	80
sff ^{B22}	560	219	39	207	37

"% of Expected" for each genotype at each stage is calculated relative to the total number of embryos at the start of the experiment.

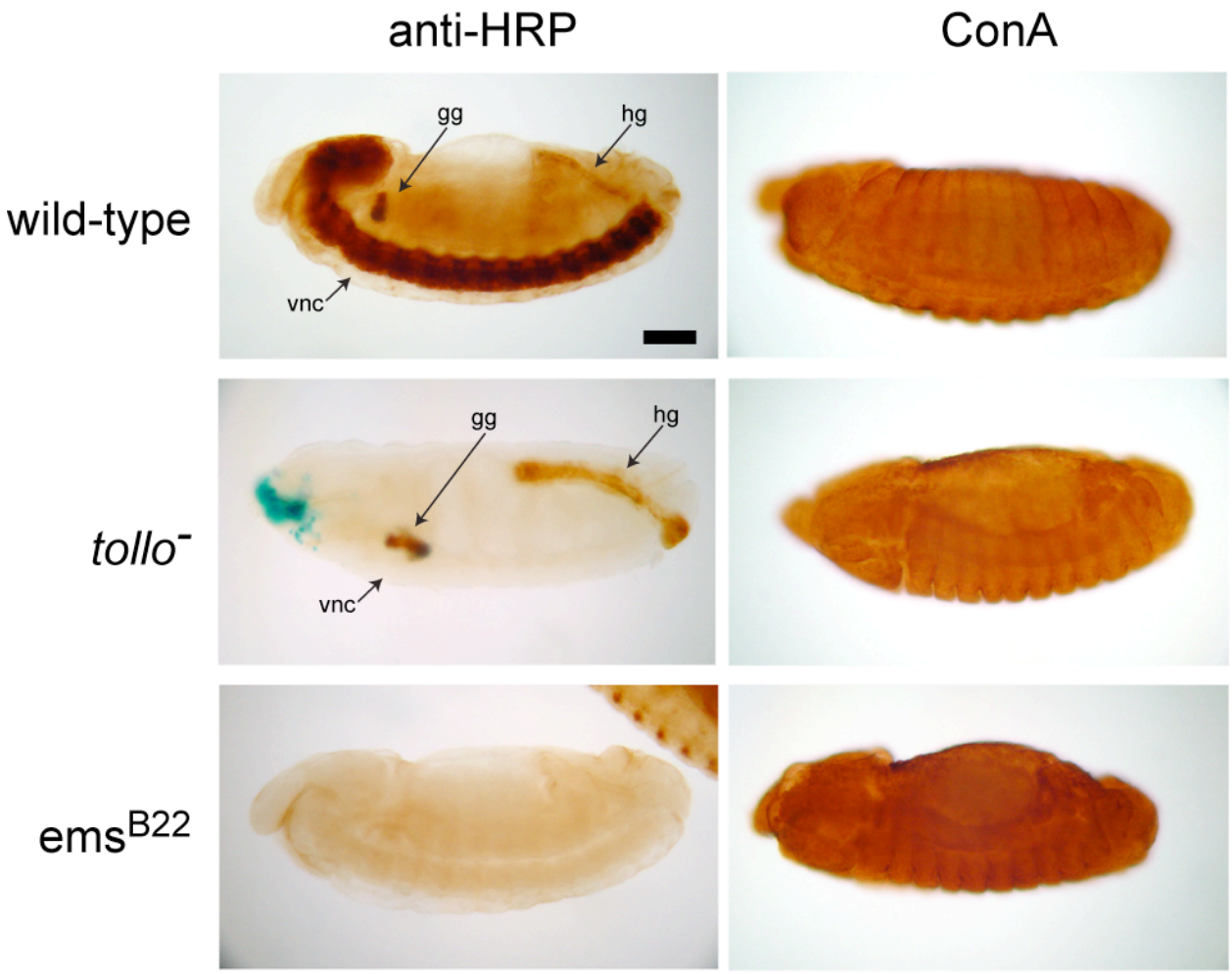

Figure 2.1. The core N-linked glycosylation machinery is intact in *sff* and *tollo/toll-8* mutant embryos.
Staining with the plant lectin Concanavalin A (**ConA**) reveals the presence of high-Man glycans throughout wild-type embryos. The detection of ConA binding requires that the embryo is capable of generating the glycan precursors for glycoprotein glycosylation and processing. The *tollo/toll-8* mutant previously shown to lack HRP-epitopes in the nervous system is not deficient in core glycosylation (Seppo et al., 2003). Similarly, the sff^{B22} mutant (labeled ems^{B22}) is also capable of generating high-Man structures. The ConA staining result is consistent with direct glycan characterization by mass spectrometry. Scale bar corresponds to 60 mm.

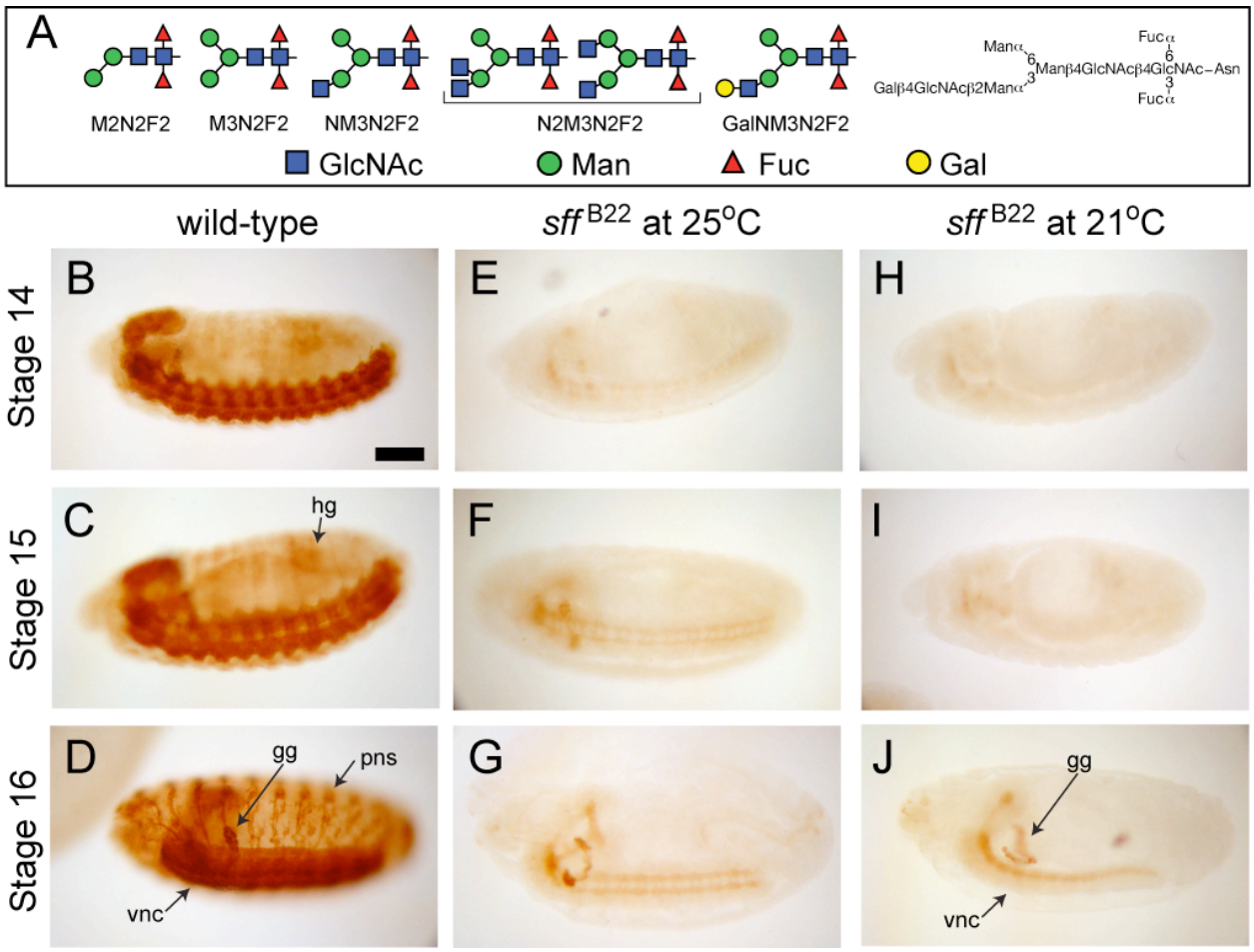

Figure 2.2. HRP-epitope expression is decreased in *sff*^{B22} embryos.
(**A**) HRP-epitopes identified in the *Drosophila* embryo include paucimannose, hybrid, and complex N-linked glycans that all share the same antigenic determinant, Fuc linked a3 to the internal GlcNAc of the chitobiose core. Graphical representations of monosaccharides and glycan structures in all figures are in accordance with the recommendations of the Consortium for Functional Glycomics.
(**B-D**) Anti-HRP staining of wild-type *Drosophila* embryos is shown at progressively later stages, anterior to the left. HRP-epitope is visible along the ventral nerve cord (**vnc**), the hindgut (**hg**), and the garland gland (**gg**). Peripheral nervous system (**pns**) staining is first apparent at Stage 14, but clearly detectable at stage 16. Scale bar corresponds to 60 mm in panels B-J.
(**E-G**) In *sff*^{B22} embryos at 25°C, staining is only detected at the dorsal surface of the nerve cord, along the axon scaffold and in the garland gland. Hindgut staining is not detected. Core glycosylation is not affected by the mutation.
(**H-J**) At 21°C the appearance of residual HRP-epitope in the *sff* mutant is delayed in comparison to 25°C.

glycan profile of wild-type *Drosophila* by converting a major portion of the NM3N2 glycan to M3N2, thereby eliminating the precursor necessary for elaboration of hybrid or complex structures (Leonard et al., 2006). Limited expression levels of branching and terminal glycosyltransferases, such as GlcNAcT2, GlcNAcT4, GalT, or SiaT, also restrict the capacity for generating complex structures in insects (Koles et al., 2004; Sarkar et al., 2006). HRP-epitopes represent less than 1% of all N-linked glycans in the *Drosophila* embryo (Aoki et al., 2007). Therefore, anti-HRP antibody staining reports the status of a limited set of N-glycan processing pathways.

To comprehensively identify glycan expression changes induced by the *sff* mutation, total N-linked glycan profiles of *sff* and wild-type embryos were analyzed by mass spectrometry (NSI-MS^n). High mannose and paucimannose glycans together account for almost 90**%** of the total profile in both wild-type (89.5%) and *sff* mutant (85.5%) embryos, indicating that the dominant glycan processing pathways are largely unaffected by the *sff* mutation (**Table 2.2**, structures 1-13). However, the prevalence of the M5N2 structure, an essential precursor for paucimannose, hybrid, and complex glycan production, is reduced in the *sff* mutant (**Fig. 2.3B**). The decrease in M5N2 is mirrored by an increase in M3N2, a paucimannose glycan whose production requires Fdl, indicating robust activity of the processing hexosaminidase in *sff* embryos. Hybrid and complex glycans together comprise approximately 10% of the total profile in wild-type (9.6%) and *sff* (11.1%) embryos (**Table 2.2**, structures 14-25 and 31-42). This modest increase in the prevalence of the total population of highly processed glycans in the *sff* mutant is more dramatic for a subset of complex structures (**Fig. 2.3C**). For example, the N2M3N2 glycan, a biantennary, non-fucosylated structure, is increased by 30% and the N3M3N2F glycan, a triantennary, core-fucosylated structure, is increased by 385% in the *sff*

mutant. As expected from antibody staining, glycans bearing a3-linked Fuc are significantly reduced in *sff* embryos (**Fig. 2.3D**). However, one HRP-epitope, the complex biantennary N2M3N2F2 glycan, is more prevalent in *sff* than wild-type embryos. This difucosylated structure, like the non-HRP complex structures that are also increased in *sff*, requires the activity of either GlcNAcT2 or GlcNAcT4 (**Fig. 2.3A**), indicating that the *sff* mutation increases the flux of glycan processing toward these terminal branching enzymes, despite apparently normal levels of Fdl activity.

The *Sugar-Free Frosting* Mutation Maps to the *Drosophila* Homologue of *SAD* Kinase

Recombination mapping placed *sff* distal to *scarlet* (*st*) on the left arm of the third chromosome. Deletion non-complementation analysis with overlapping deletion lines that map to the interval between *st* and the left end of the chromosome identified a single deletion (Δbrm^{11}) that failed to complement the *sff* mutation. Embryos of the genotype $sff^{B22}/\Delta brm^{11}$ display a more severe HRP phenotype than *sff* homozygotes and Δbrm^{11} deletion homozygous embryos lack all HRP-epitope, indicating that the sff^{B22} allele is hypomorphic with regard to the induction of HRP-epitope expression (**Fig. 2.4**). The Δbrm^{11} deletion breakpoints have been assigned as 71F1-4;72D1-10. An overlapping deletion line (th^{102}) rescues the sff^{B22} phenotype and has breakpoints assigned as 71F3-72B1;72D12-E12. To resolve the exact overlap between these two deletion lines, we mapped the molecular boundaries of each deficiency chromosome by genomic PCR, assessing the presence or absence of genes that map across the breakpoints (**Fig. 2.5**). The only gene that maps to the interval between the molecularly defined breakpoints of the complementing th^{102} deficiency and the non-complementing brm^{11} deficiency is *CG6114* (**Fig. 2.5A**). Genomic sequencing of the *CG6114* locus in the sff^{B22} mutation identified a single nucleotide change (G to A) in a consensus AP-1 binding site 261 bp upstream

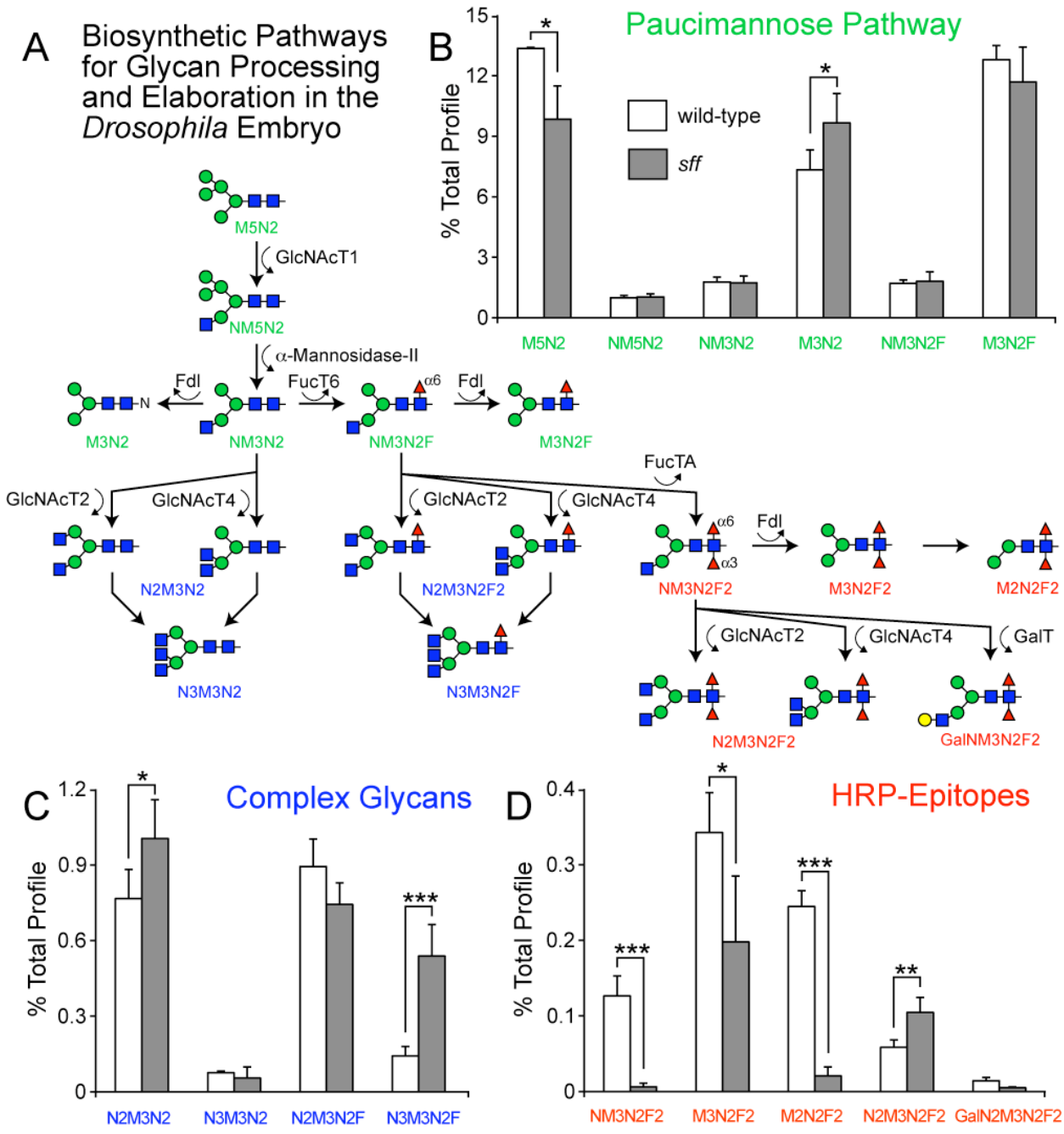
A
Biosynthetic Pathways for Glycan Processing and Elaboration in the *Drosophila* Embryo
M5N2
GlcNAcT1
NM5N2
α-Mannosidase-II
Fdl
FucT6
α6
Fdl
M3N2
NM3N2
NM3N2F
M3N2F
FucTA
GlcNAcT2
GlcNAcT4
GlcNAcT2
GlcNAcT4
α6
α3
Fdl
N2M3N2
N2M3N2F2
NM3N2F2
M3N2F2
M2N2F2
GlcNAcT2
GlcNAcT4
GalT
N3M3N2
N3M3N2F
N2M3N2F2
GalNM3N2F2
B
Paucimannose Pathway
% Total Profile
wild-type
sff
M5N2
NM5N2
NM3N2
M3N2
NM3N2F
M3N2F
C
Complex Glycans
% Total Profile
N2M3N2
N3M3N2
N2M3N2F
N3M3N2F
D
HRP-Epitopes
% Total Profile
NM3N2F2
M3N2F2
M2N2F2
N2M3N2F2
GalN2M3N2F2

Figure 2.3. N-linked glycan profiles are deficient in HRP-epitopes and shifted toward greater complexity in the *sff* mutant.
(**A**) N-linked glycan processing in *Drosophila* proceeds through steps that are well-conserved across animal species. In the cis-Golgi, GlcNAcTransferase-1 (GlcNAcT1, mgat1) transfers a GlcNAc residue to the trimmed high-mannose structure M5N2. Subsequent removal of Man residues by Golgi mannosidases produces NM3N2, a structural node that feeds into three separate pathways. The Fused Lobes hexosaminidase (Fdl) can remove the GlcNAc added by GlcNacT1 to generate the paucimannose glycan M3N2. Alternatively, NM3N2 can be branched by the action of another GlcNAcTransferase (GlcNAcT2 or 4, mgat2 or mgat4) to produce a complex glycan which is resistant to degradation by Fdl. The NM3N2 glycan is also a substrate for a6-fucosylation (FucT6) and subsequent branching by GlcNAcT2/4. Addition of an a3-Fuc residue (FucTA) results in generation of the HRP-epitopes.
(**B-D**) Key N-glycan structures are compared for wild-type and *sff* embryos. The prevalences of the indicated glycans are given as the percent that they contribute to the total profile of N-linked glycans. Values are the mean ± standard deviation for three independent analyses (n=3, biological replicates). Paucimannose glycans are unchanged except for decreased M5N2 and increased M3N2 in the *sff* mutant. Two complex glycans are increased in sff^{B22}, N2M3N2 and N3M3N2F, indicating increased access of substrates to extension by GlcNAcT2 or 4. As expected, HRP-epitopes are decreased in the mutant except for an increase in the GlcNAcT2/4 product, N2M3N2F2. Taken together, the shift in glycan processing indicates that the *sff* mutation drives N-linked processing toward greater complexity, but a change in a single processing step cannot account for the full range of glycan alterations. (* indicates $p<0.05$, ** indicates $p<0.02$, *** indicates $p<0.01$)

Table 2.2. N-linked Glycan Profiles of wild-type and *sff* embryos

	Structure	% of Total Profile: wild-type embryos	% of Total Profile: *sff*^{B22} embryos
1	M2N2 	2.7±0.6	3.8±0.4
2	M3N2 	7.3±1.0	9.6±1.4
3	M4N2 	3.0±0.3	3.0±0.6
4	M5N2 	13.4±0.1	9.8±1.6
5	M6N2 	10.4±0.3	10.4±1.5
6	M7N2 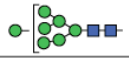	8.0±0.8	8.8±1.2
7	M8N2 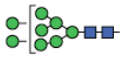	7.6±0.6	7.7±1.4
8	M9N2 	12.6±1.1	11.4±3.4
9	GlcM9N2 	2.4±0.2	2.2±0.7
10	M2N2F$^{3 \text{ or } 6}$ 	8.0±0.4	9.1±1.2
11	M3N2F$^{3 \text{ or } 6}$ 	12.8±0.7	11.7±1.7
12	M4N2F^{6} 	1.0±0.1	0.64±0.05
13	M5N2F^{6} 	0.26±0.07	0.26±0.09
14	NM2N2F^{6} 	0.16±0.03	0.15±0.03
15	NM3N2F^{6} 	1.7±0.2	1.8±0.5
16	NM4N2F^{6} 	0.26±0.07	0.5±0.1
17	NM5N2F^{6} 	0.26±0.06	0.54±0.08
18	GalNM3N2F^{6} 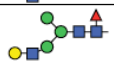	0.08±0.01	0.07±0.06
19	Hex-GalNM3N2F^{6} 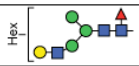	0.02±0.00	0.02±0.01
20	N2M2N2F^{6} 	0.20±0.02	0.31±0.09
21	N2M3N2F^{6} 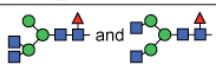	0.89±0.11	0.74±0.08

	Structure	% of Total Profile: wild-type embryos	% of Total Profile: *sff*^{B22} embryos
22	N2M4N2F^{6} 	0.24±0.06	0.37±0.10
23	N2M5N2F^{6} 	0.06±0.02	0.28±0.04
24	N3M3N2F^{6} 	0.14±0.04	0.54±0.12
25	GalN2M3N2F^{6} 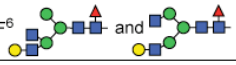	0.04±0.02	0.03±0.01
26	M2N2F2^{3,6} 	0.24±0.02	0.02±0.01
27	M3N2F2^{3,6} 	0.34±0.05	0.20±0.09
28	NM3N2F2^{3,6} 	0.13±0.03	0.01±0.00
29	GalNM3N2F2^{3,6} 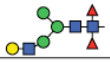	0.01±0.00	<0.01
30	N2M3N2F2^{3,6} 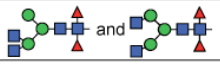	0.06±0.01	0.10±0.2
31	NM2N2 	0.08±0.02	0.02±0.01
32	NM3N2 	1.8±0.2	1.7±0.3
33	NM4N2 	0.74±0.06	1.0±0.1
34	NM5N2 	0.99±0.12	1.0±0.2
35	GalNM3N2 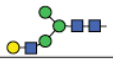	0.31±0.02	0.07±0.02
36	N2M3N2 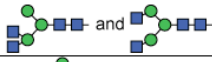	0.77±0.12	1.0±0.2
37	N2M4N2 	0.41±0.02	0.48±0.20
38	N2M5N2 	0.22±0.04	0.32±0.08
39	N3M3N2 	0.08±0.01	0.05±0.04
40	GalN2M3N2 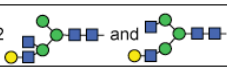	0.10±0.04	0.01±0.01
41	SA-GalNM3N2	0.02±0.01	0.01±0.01
42	SA-GalN2M3N2	0.01±0.00	0.03±0.01

The prevalence of each glycan structure is given as "% Total Profile," where the MS signal intensity for each individual glycan is normalized to the total signal for all quantified glycans. Values are the mean ± standard deviation for 3 independent determinations (biological replicates).

Structures linked by "and" indicate that both isomers were detected. Structures linked by "or" indicate that the isomers were not resolved.

Graphical representations of glycan structures are consistent with the conventions proposed by the Consortium for Functional Glycomics and are as follows:

of the predicted transcript start (**Fig. 2.5B**). The detected nucleotide change causes the sequence to no longer be assigned as an AP-1 binding site above threshold (85% confidence) by the TFSearch prediction algorithm (v 1.3) utilizing the TRANSFAC database (Heinemeyer et al., 1998). No nucleotide changes were detected that altered amino acid sequence or mRNA splicing in sff^{B22}. Therefore, the mutation is predicted to result in decreased levels of wild-type protein, not to impart gain-of-function or neomorphic phenotypes based on altered protein structure, protein stability, or protein-protein interactions.

The CG6114 sequence is highly homologous to a Ser/Thr Protein kinase previously identified as Synapses of the Amphid Defective (SAD Kinase) in *C. elegans* and mammals (SAD-1/2). The kinase domain of the Sff protein encoded by CG6114 exhibits 85% amino acid identity to *C. elegans* SAD-1, 87% identity to mammalian SAD-1, and 86% identity to SAD-2, including complete conservation of the residues required for catalytic activity (**Fig. 2.6**). Unlike mouse, a second *Sff/SAD* kinase gene is not detected in *Drosophila*. The *Drosophila* genes with the next closest homology to Sff/SAD are the Par-1 and SNF1A/AMP Kinases, which possess 52% and 50% identity, respectively, to Sff/SAD in their catalytic domains.

Sff/SAD Expression is Detected in Embryonic Neurons and Decreased in the Sugar-Free Frosting Mutant

By *in situ* hybridization, mRNA for *sff/SAD* is detected in the embryonic ventral nerve cord and peripheral sensory clusters in the ventral and lateral ectoderm (**Fig. 2.7A-E**). Consistent with our genetic characterization of the sff^{B22} allele as a hypomorph, mRNA for *sff/SAD* is reduced but not eliminated in the mutant (**Fig. 2.7B,E**). The cells expressing *sff/SAD* mRNA are neuronal since hybridization signal is detected within cells that are also positive for the neuron-specific mAb 22C10 (**Fig. 2.7F,G**). Expression of *sff/SAD* mRNA is first visible along the midline of the

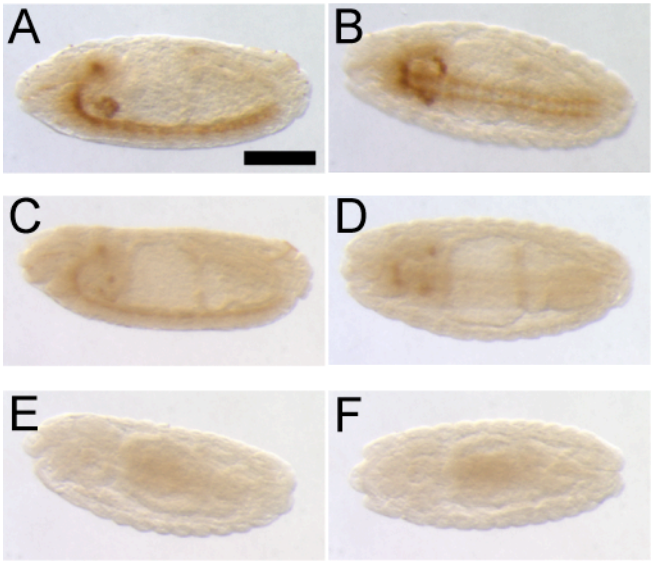

Figure 2.4. The *sff* mutation is uncovered by the Δ*brm*^{11} deficiency and *sff*^{B22} is an hypomorphic allele.
(**A** lateral, **B** ventral) Late stage 14 *sff*^{B22} embryo (anterior to the left) stained with anti-HRP antibody (peroxidase-conjugated secondary antibody with DAB precipitate) exhibit epitope distribution characteristic for the mutant, restricted to the garland gland and the dorsal aspect of the nerve cord. Scale bar corresponds to 120 mm in all panels.
(**C** lateral, **D** ventral) Late stage 14 embryos of the genotype *sff*^{B22}/Δ*brm*^{11} shows reduced staining compared to the *sff*^{B22} homozygote. Embryos in A-D were processed in parallel. Loss of HRP-staining in *sff*^{B22} is more severe over the deletion, consistent with partial loss-of-function. Mapping of the mutation relative to the D*brm*^{11} deletion is described in **Fig. 2.5**.
(**E** lateral, **F** ventral) Late stage embryos homozygous for the D*brm*^{11} deletion show complete loss of HRP-epitope. Older deletion homozygotes were not obtained.

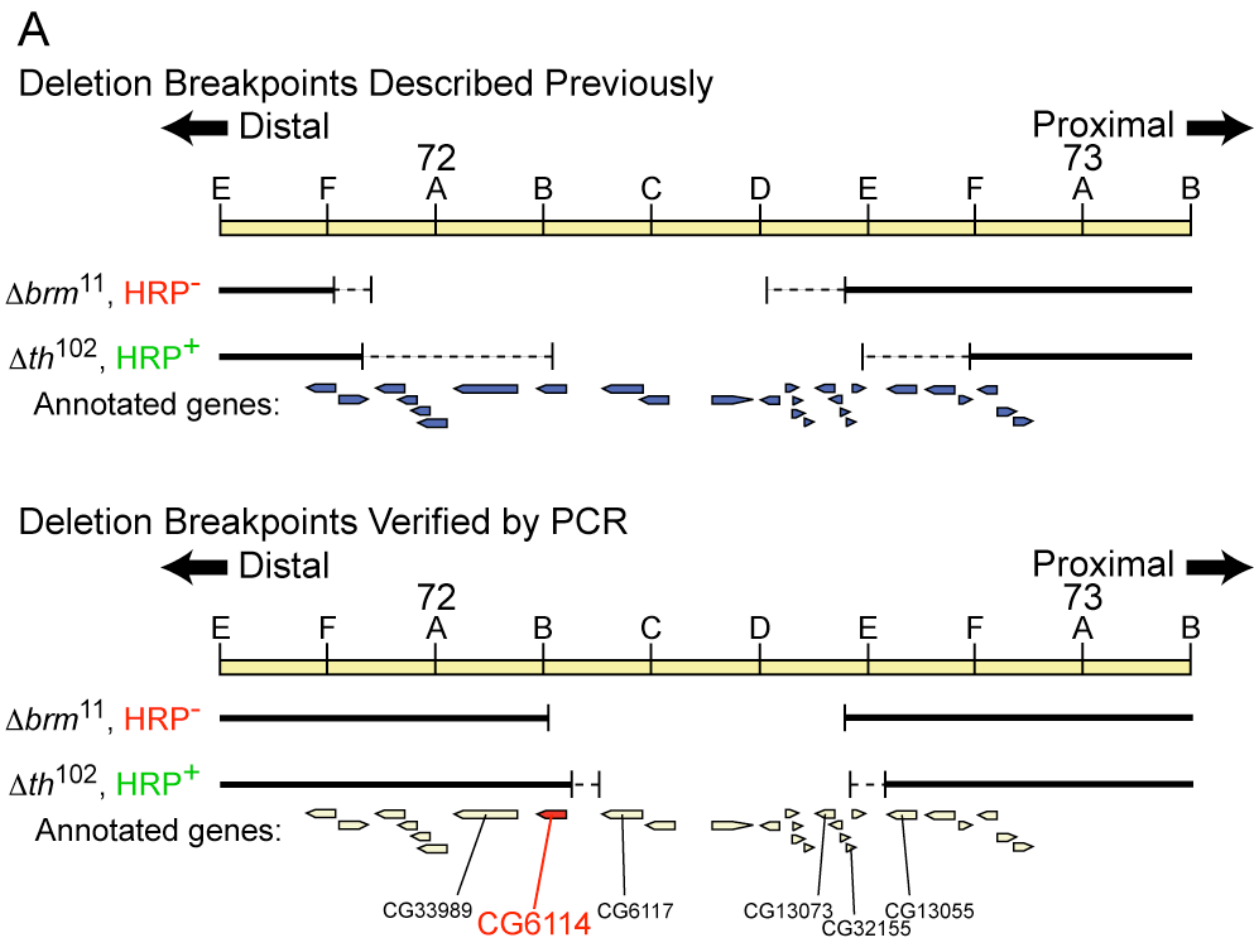
A
Deletion Breakpoints Described Previously
Distal
Proximal
72
73
E F A B C D E F A B
Δbrm11, HRP-
Δth102, HRP+
Annotated genes:
Deletion Breakpoints Verified by PCR
Distal
Proximal
72
73
E F A B C D E F A B
Δbrm11, HRP-
Δth102, HRP+
Annotated genes:
CG33989
CG6114
CG6117
CG13073
CG32155
CG13055

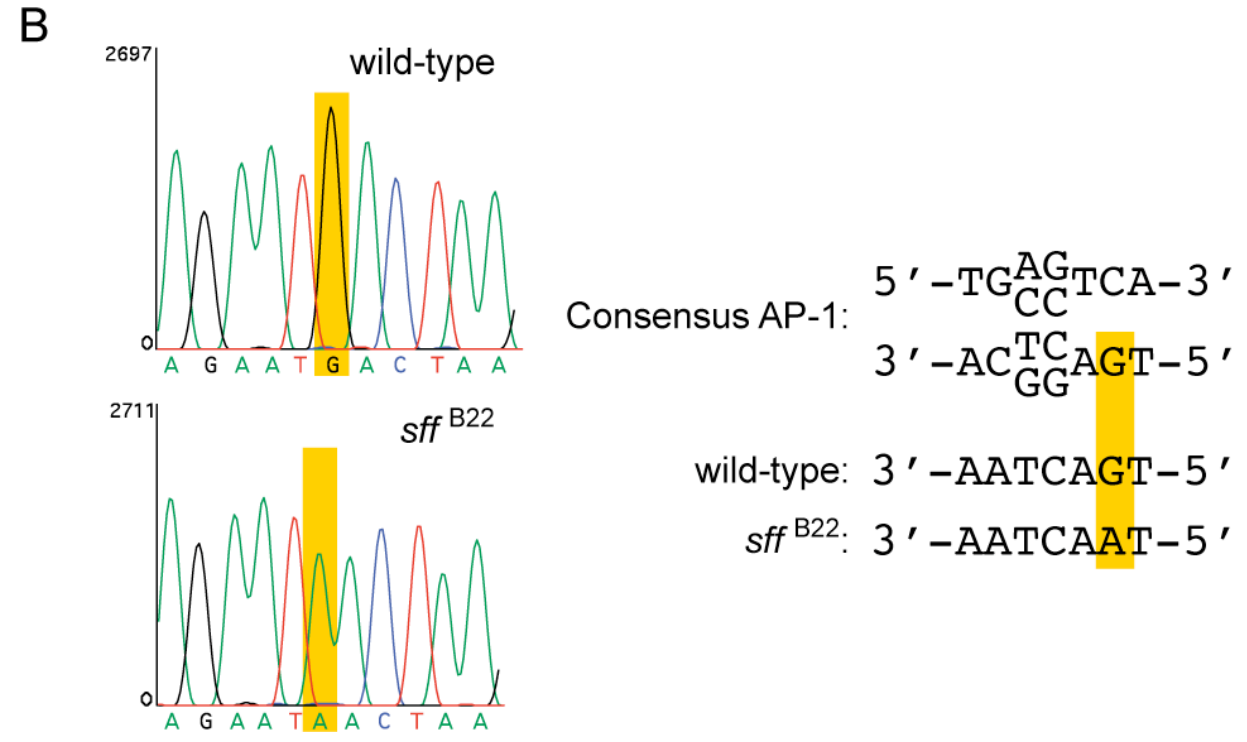
B
2697
wild-type
A G A A T G A C T A A
2711
sff B22
A G A A T A A C T A A
Consensus AP-1:
5′-TGAGCCTCA-3′
3′-ACTCGGAGT-5′
wild-type: 3′-AATCAGT-5′
sff B22: 3′-AATCAAT-5′

Figure 2. 5. The *sff*^{B22} mutation maps to a single nucleotide change in *CG6114*.
(**A**) The breakpoints for two overlapping deletions, one that complements *sff*^{B22} (D*brm*^{11}) and one that does not (D*th*^{102}), were mapped by genomic PCR. Genes predicted to span previously assigned breakpoints were targeted for analysis. The depiction of annotated genes mapped to chromosomal cytological divisions is approximate in the figure, but does reflect their relative order and distribution compared to molecularly mapped breakpoints. We find the proximal breakpoints to be within 72D10 for both deficiencies, with D*th*^{102} breaking between *CG32155 and CG13055*, proximal to D*brm*^{11}, which breaks between *CG32155* and *CG13073*. Thus, the complementing D*th*^{102} deficiency interval encompasses the proximal breakpoint of the non-complementing D*brm*^{11} deficiency. However, we place the distal breakpoint of D*brm*^{11} at 72B1, within the 3' end of *CG6114*, while D*th*^{102} breaks proximal to D*brm*^{11}, leaving *CG6114* intact. The next annotated gene proximal to *CG6114*, designated *CG6117*, was missing in both the D*th*^{102} and D*brm*^{11} deletion intervals, mapping the *sff* mutation to *CG6114*.
(**B**) Genomic sequence analysis in wild-type and *sff*^{B22} revealed a single nucleotide change consistent with ethyl methanesulfonate chemistry (G to A at -256) in an AP-1 binding site that lies 261 bp upstream of the predicted mRNA start.

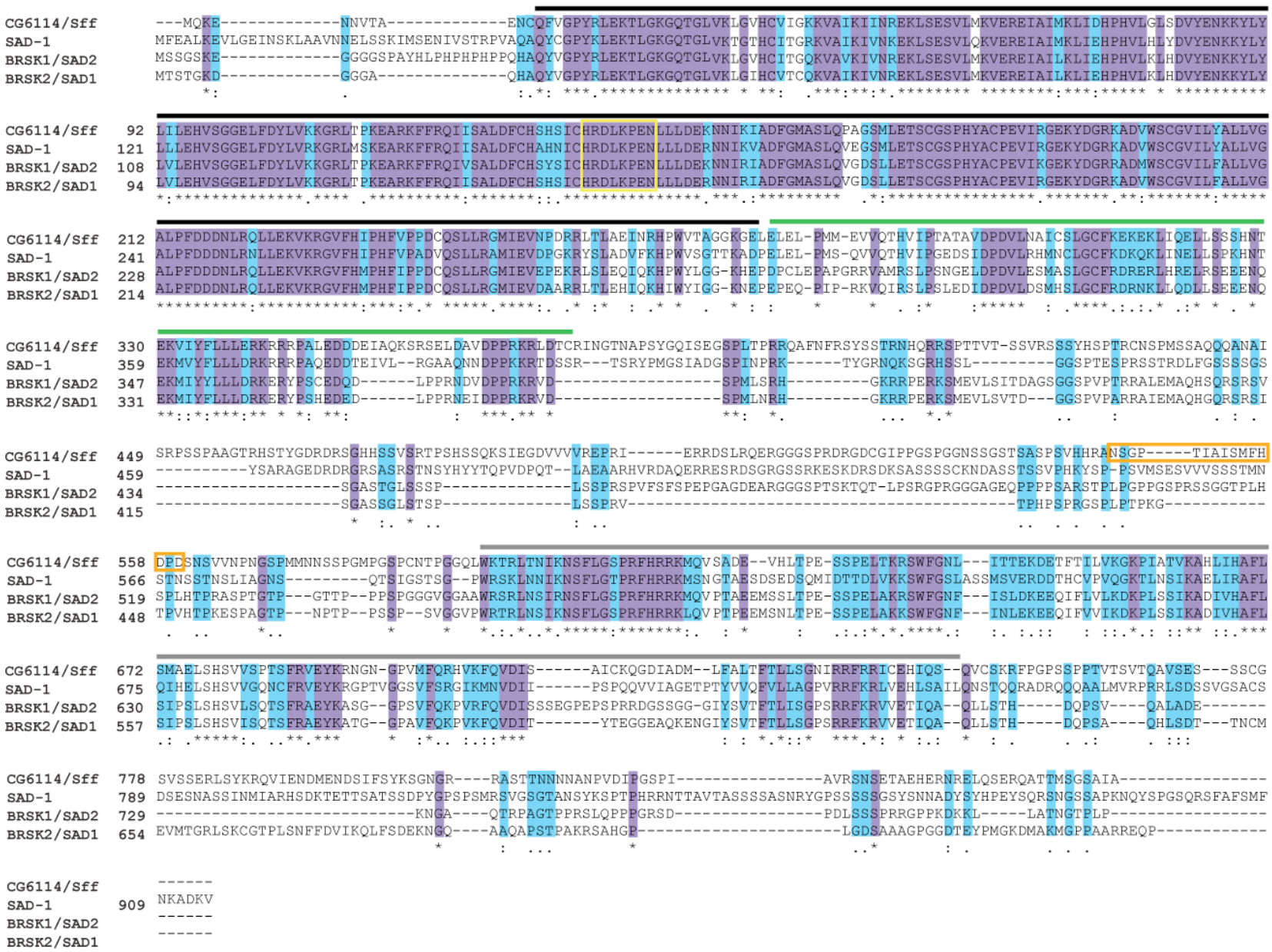
CG6114/Sff
SAD-1
BRSK1/SAD2
BRSK2/SAD1

Figure 2.6. *Drosophila* CG6114/Sff is homologous to *C. elegans* SAD-1, and mouse BRSK1/SAD2 and BRSK2/SAD1.
Identical amino acid residues are highlighted in purple and conservative changes are in blue. Black bars denote the Ser/Thr Kinase catalytic domain (aa 13-276 in Sff). Green (aa 278-394 in Sff) and grey (aa 582-739 in Sff) bars denote other regions conserved in the SAD enzymes. Residues essential for catalysis are boxed in yellow (aa 138-145 in Sff). The sequence highlighted in orange (aa 547-561 in Sff), although predicted to be translated by gene annotation, is absent from the sequence of the major transcript detected in the *Drosophila* embryo.

embryo at stage 11, prior to the initiation of any synapse formation in the embryo and roughly coincident with the initial appearance of the HRP-epitope and transcripts for FucTA, the a3-fucosyltransferase that synthesizes the HRP-epitope (**Fig. 2.8**) (Rendic et al., 2006). As neurons continue to differentiate and extend axons, *sff/SAD* mRNA levels increase across the maturing nerve cord. In peripheral sensory clusters, mRNA is detected as early as stage 13, prior to significant accumulation of the HRP-epitope and before synaptic contact has been made between sensory afferents and their targets in the ventral nerve cord, which generally begins during stage 16 (**Fig. 2.8**) (Martin et al., 2008; Merritt and Whitington, 1995).

Deletion mapping, genomic sequence, and *in situ* hybridization demonstrate that the mutation in sff^{B22} affects expression of the *Drosophila sff/SAD* kinase. Since altered transcription does not always predict altered translation, we directly assessed the impact of the sff^{B22} mutation on Sff/SAD protein levels by LC-MS/MS in wild-type and mutant tissue. To enhance detection of the protein, we harvested adult heads for proteomic analysis to take advantage of the enrichment in neural tissue in this body part. Glycan analysis verified that HRP-epitopes are decreased in sff^{B22} adult heads. Within the total profile of detected peptides, 22 Sff/SAD peptides were identified in wild-type heads but only 8 were identified in sff^{B22} heads (**Table 2.3**). This disparity in detected Sff/SAD peptides is consistent with decreased protein expression in the *sff* mutant. However, many of the peptides identified in wild-type and sff^{B22} material were assigned to the Sff/SAD kinase with relatively low confidence (Xcorr < 2.0, doubly-charged). An alternative proteomic approach for characterizing expression levels is to assess the relative prevalence of individual peptides by LC-MS/MS. In our LC-MSMS analysis, a single peptide was identified and assigned to Sff/SAD with reasonable confidence (Xcorr = 2.2, doubly-charged) in wild-type tissue. This peptide is entirely unique to the Sff/SAD kinase and

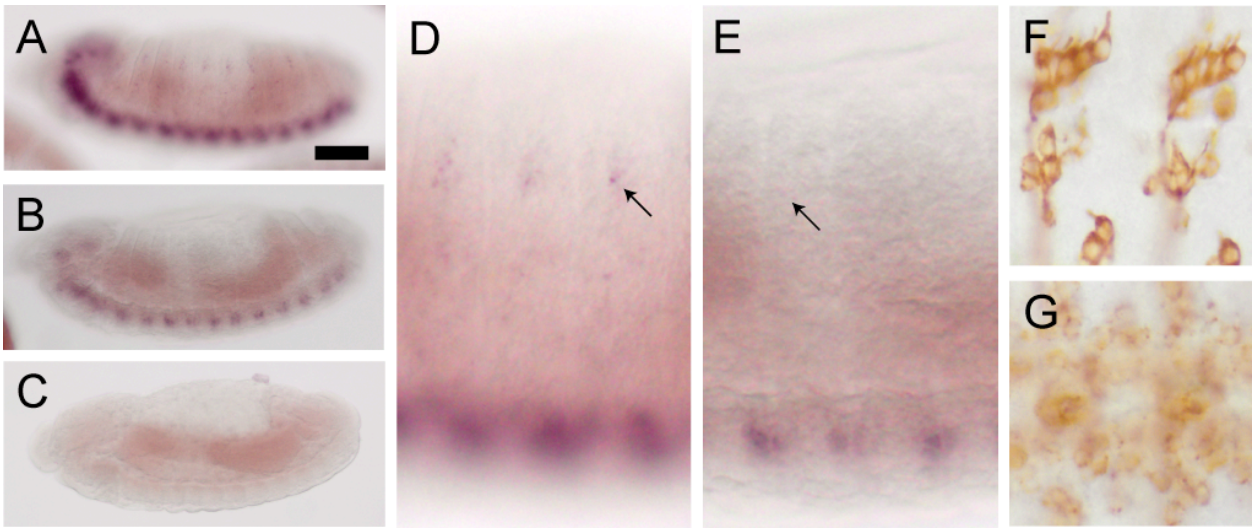

Figure 2.7. *Drosophila sff/SAD* mRNA is expressed in the embryonic nervous system and is reduced in *sff*^{B22}.
(**A,D**) *In situ* hybridization with anti-sense probe for *CG6114* (*sff/SAD*) to late stage 13 wild-type embryo reveals prominent message expression in the ventral nerve cord (**A**) and in sensory neurons in the PNS (**D**). Anterior is to the left. Scale bar corresponds to 60 mm in A-C and 15 mm in D-E, and 10 mm in F-G. The developmental time course of *sff/SAD* message expression is presented in **Fig. 2.8**.
(**B,E**) *In situ* hybridization with anti-sense probe to late stage 13 *sff*^{B22} embryos shows decreased mRNA levels in the ventral nerve cord and PNS of the mutant. Embryos presented in panels A-E were processed in parallel to facilitate quantitative comparisons.
(**C**) *In situ* hybridization with sense probe to late stage 13 wild-type embryo.
(**F-G**) Wild-type embryos double stained with anti-sense probe (purple) and neuron-specific mAb 22C10 (brown) places expression of *sff/SAD* in neurons of the PNS (**F**) and ventral nerve cord (**G**).

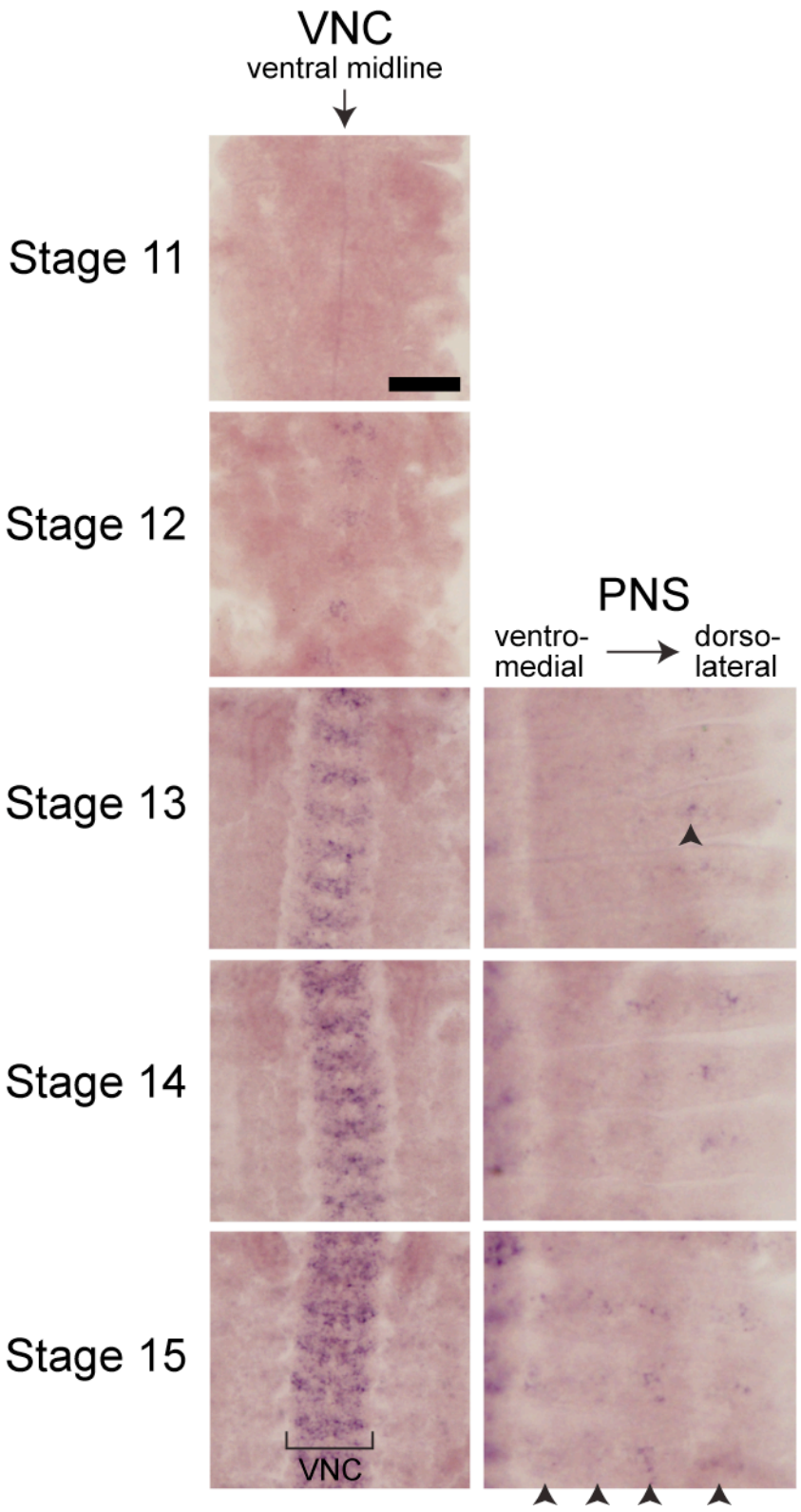
VNC
ventral midline
Stage 11
Stage 12
PNS
ventro-
medial
dorso-
lateral
Stage 13
Stage 14
Stage 15
VNC

Figure 2.8. Developmental appearance of *sff/SAD* mRNA in the *Drosophila* embryo.
In situ hybridization of anti-sense probes to wild-type embryos detects the earliest expression of *sff/SAD* along the ventral midline at stage 11. Expression in the ventral nerve cord (**VNC**) intensifies in parallel with appearance of the HRP-epitope through the later stages of embryogenesis. In the peripheral nervous system (**PNS**), expression is first detected during stage 13 and eventually is found within all clusters of peripheral sensory neurons (arrowheads). Embryos were dissected to reveal the VNC and to expose the PNS within the lateral ectoderm. Scale bar corresponds to 60 mm for the VNC and 35 mm for the PNS.

was not detected in sff^{B22} tissue, although peptides assigned to other proteins were detected at comparable expression levels and consistent relative elution positions (flanking the diagnostic Sff/SAD peptide) in wild-type and mutant (**Fig. 2.9**). Therefore, we have detected alterations in Sff/SAD kinase at the genome, transcript, and protein level in sff^{B22}, and all are consistent with our genetic and biochemical evidence for reduced function.

Sff/SAD Interacts with Tollo/Toll-8

HRP-epitope loss in sff^{B22} suggested that the Sff/SAD kinase may act in the transcellular signaling pathway defined by Tollo/Toll-8 (Seppo et al., 2003). As heterozygous embryos, sff^{B22} or *tollo* mutations (placed individually over a wild-type chromosome) exhibit completely normal HRP-epitope expression. As homozygous embryos, the *sff* phenotype is not identical to the *tollo* phenotype. Hindgut staining is absent and garland gland staining is reduced in sff^{B22} but not in the *tollo* mutant, while nerve cord staining is completely absent in *tollo* mutants but still faintly present in sff^{B22}. Transheterozygous embryos, that are of the genotype sff^{B22}, $tollo^{+}$ /sff^{+}, $tollo^{-}$, possess aspects of both phenotypes; faint residual nerve cord staining is seen along with rescue of hindgut HRP-epitopes (**Fig. 2.10A-D**). This composite phenotype is consistent with an interaction in which reduction of either gene dose results in sensitization for both phenotypes. Thus, sff^{B22} enhances partial loss of *tollo*, and vice versa, indicating functional interactions between the two genes. Furthermore, our previous structural characterization of the glycans expressed in the tollo mutant embryo demonstrated increased prevalence of complex, non-fucosylated glycans in addition to reduced HRP-epitopes, similar to the impact of the sff mutation and consistent with both genes acting within intersecting pathways (Aoki et al., 2007). Finally, interaction between *tollo/toll-8* and *sff* is further supported by significant reduction in *sff* transcripts in embryos that lack *tollo/toll-8* (**Fig. 2.10E,F**). Therefore, ectodermal Tollo/Toll-8

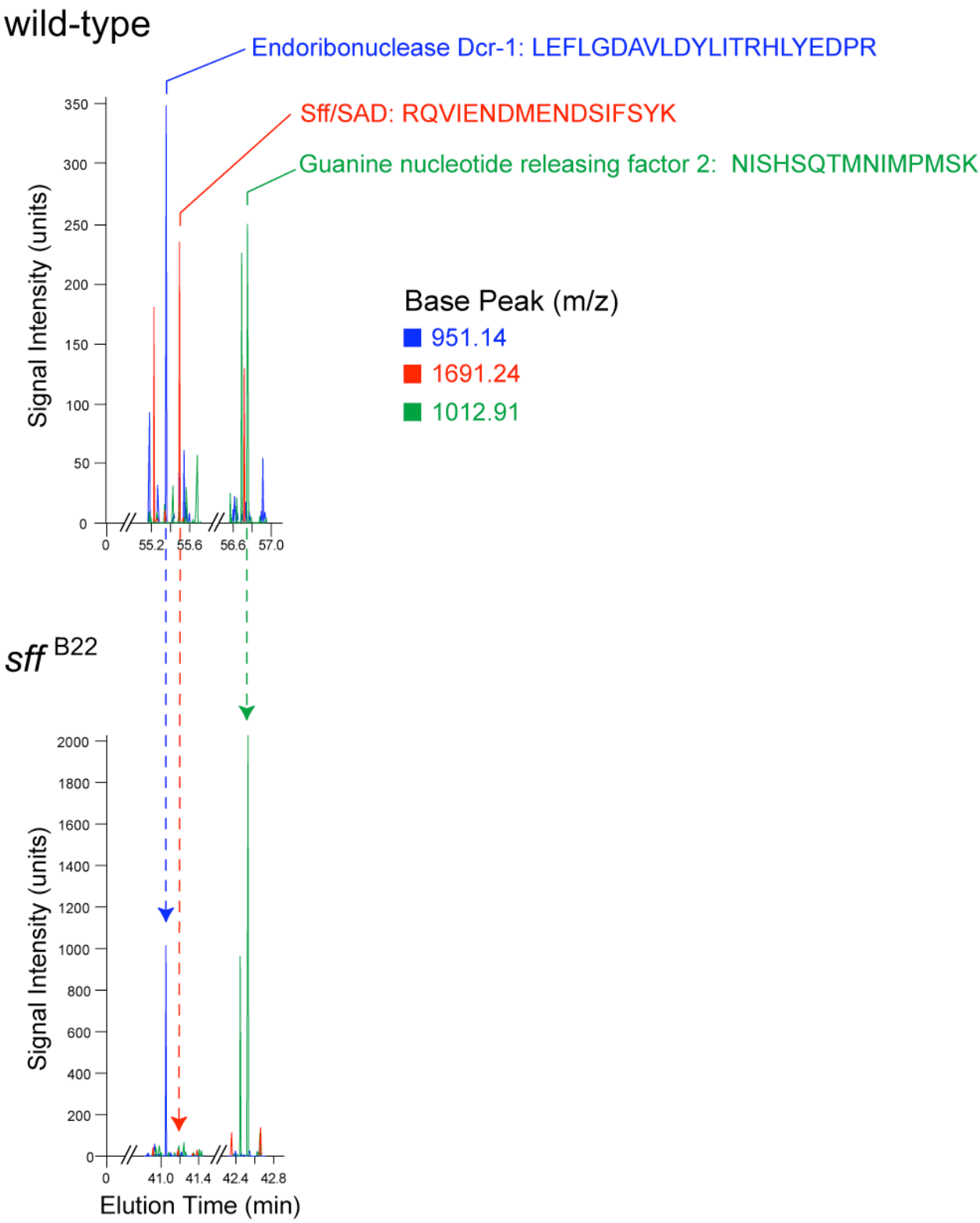
wild-type
Endoribonuclease Dcr-1: LEFLGDAVLDYLITRHLYEDPR
Sff/SAD: RQVIENDMENDSIFSYK
Guanine nucleotide releasing factor 2: NISHSQTMNIMPMSK
Signal Intensity (units)
350
300
250
200
150
100
50
0
0
55.2
55.6
56.6
57.0
Base Peak (m/z)
951.14
1691.24
1012.91
sff B22
Signal Intensity (units)
2000
1800
1600
1400
1200
1000
800
600
400
200
0
0
41.0
41.4
42.4
42.8
Elution Time (min)

Figure 2.9. Proteomic detection of Sff in wild-type and mutant tissue by LC-MS/MS. Proteins from adult head lysates were reduced, alkylated, digested with trypsin and subjected to proteomic analysis by LC-MS/MS. A total of 28 peptides were detected with m/z values and fragmentation profiles appropriate for Sff/SAD. Wild-type heads yielded 22 of these peptides and sff^{B22} heads yielded only 8; 5 peptides were found in both preparations. Of the 5 best peptides found in wild-type heads only 3 were detected in sff^{B22}. See **Supplement Table 4** for specific peptides and Xcorr scores. A single peptide of sequence entirely unique to Sff/SAD was detected in wild-type heads with a reasonable Xcorr value (2.2), yielding a confident assignment. This peptide, m/z=1691.24 (doubly-charged), corresponds to R788-K804, and was not detected in the sff^{B22} mutant. LC-MS/MS chromatograms are shown for the characterization of this peptide from wild-type (**top panel**) and sff^{B22} (**bottom panel**). The elution positions of peptides with one of three different m/z values (Base Peaks) are shown. The red Base Peak (1691.24), corresponding to Sff R708-K804, elutes between two control peptides in wild-type (Endoribonuclease Dcr-1, Base Peak = 951.14, shown in blue; Guanine nucleotide releasing factor 2, Base Peak = 1012.91, shown in green). These two non-Sff proteins were chosen as controls because of their comparable signal intensity and neighboring elution position in comparison to the Sff R708-K804 peptide. In sff^{B22}, both of the control peptides are detected but Base Peak signal for the Sff R708-K804 peptide falls below the detection threshold at the expected elution position.

Table 2.3. Proteomic analysis of wild-type and *sff* adult heads

Protein	Peptides	Genotype	Charge	XCorr
Endoribonuclease Dcr-1 (control)	LEFLGDAVLDYLITRHLYEDPR	wild-type	2	2.0
		sff^{B22}	2	1.5
Guanine nucleotide releasing factor 2 (control)	NISHSQTMNIMPMSK	wild-type	2	1.0
		sff^{B22}	2	1.6
sff/SAD peptides with Xcorr ≥ 1.2 in wild-type or *sff*	RQVIENDMENDSIFSYK[1]	wild-type	2	2.2
		sff^{B22}	nd	
	IERRDSLR	wild-type	2	1.6
		sff^{B22}	nd	
	LGVHVIGK[2]	wild-type	2	1.2
		sff^{B22}	2	0.5
	VEREIAIMK[3]	wild-type	2	0.8
		sff^{B22}	2	1.6
	LEKTLGKGQTGLVK	wild-type	2	0.7
		sff^{B22}	2	1.3
Sff/SAD peptides with Xcorr < 1.2	17 additional peptides	wild-type	1-5	<1.2
	6 additional peptides[4]	*sff*^{B22}	1-2	<1.2

"nd" denotes that the peptide was not detected in *sff* mutant.

[1]See Supplement Figure 5 for LC-MS/MS Base Peak chromatograms.

[2]Detected as its carbamidomethylated form in wild-type and as a missed cleavage (LGVHVIGKKVAIK) in *sff* mutant.

[3]Oxidized in wild-type.

[4]Two of the 6 additional peptides detected in *sff* mutant heads were also detected in wild-type.

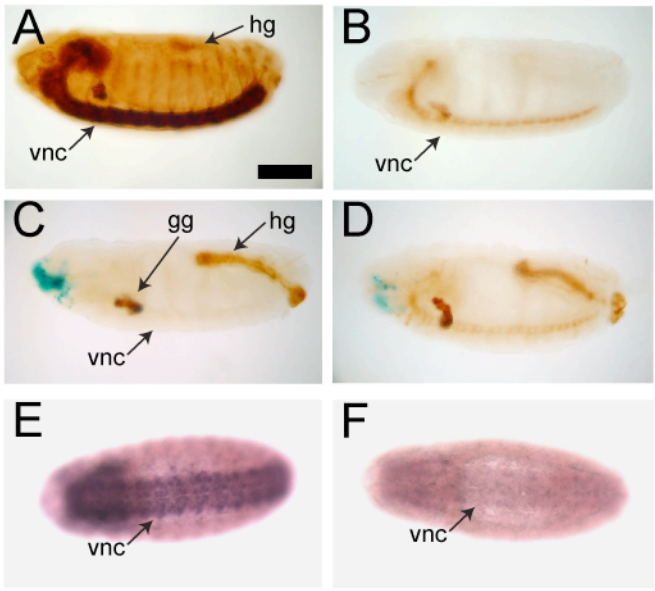

Figure 2.10. *sff* interacts with *tollo/toll-8* and expression of *sff/SAD* mRNA is dependent on *tollo/toll-8*.
(**A**) Wild-type embryos and embryos heterozygous for either *tollo* or sff^{B22} are identical in appearance, with strong staining of the ventral nerve cord (vnc), garland gland (gg), and hindgut (hg). Scale bar corresponds to 90 mm in A-F.
(**B**) Embryos homozygous for the sff^{B22} mutation exhibit reduced vnc and hg staining.
(**C**) Embryos homozygous for loss of *tollo/toll-8* lack vnc staining but retain gg and hg expression of the HRP-epitope.
(**D**) Embryos that are transheterozygous for both sff^{B22} and *tollo* have a composite staining phenotype, indicating functional interactions between the two genes. Reduction of either gene dose results in sensitization for both phenotypes.
(**E-F**) In situ hybridization of antisense probe for *sff* mRNA in wild-type (**E**) and *tollo/toll-8* mutant (**F**) indicates that Tollo signaling induces neuronal expression of *sff* mRNA.

signaling influences neural glycosylation, at least in part, by driving expression of Sff/SAD in differentiating neurons.

Behavioral and Neuromuscular Deficits in the *Sugar-Free Frosting* Mutant

Homozygous sff^{B22} adults are reluctant to move away from the bottom of their culture vials, a phenotype previously described for *tollo/toll-8* mutants (Seppo et al., 2003). We quantified this negative geotaxis defect by measuring the time required for individual adults to climb to a pre-designated height (**Fig. 2.11A**). Wild-type adults quickly reached the target height; 81% succeeded within 15 seconds at 25°C. However, *sff* mutants tarried and often never reached the designated height before the trial was ended at 2 minutes; only 36% succeeded within 15 seconds at 25°C. As with anti-HRP antibody staining, the geotaxis phenotype was more pronounced at reduced temperature. At 18°C, only 21% of sff^{B22} flies succeeded within 15 seconds and 60% took longer than 2 minutes.

Although sff^{B22} adults are able to right themselves when knocked onto their backs at the bottom of an empty culture vial and although sff^{B22} adults exhibit reasonable locomotion once movement is initiated, the geotaxis phenotype could reflect altered function or structure at the neuromuscular junction (NMJ). Therefore, we investigated the status of the larval NMJ at muscles 6 and 7 in the abdominal wall of 3rd instar larvae. In *sff* mutants, the NMJ is considerably less complex (**Fig. 2.11B-E**), with a significant reduction in both bouton and primary branch number. NMJ morphology is also disrupted in the *C. elegans SAD* mutant, indicating that Sff/SAD kinase fulfills similar synaptic functions in both organisms.

In the *C. elegans SAD-1* mutant, synaptic vesicles are poorly aligned at the active zone complex. Despite deficient vesicle tethering, the presynaptic specializations that comprise the active zone are well structured in the *C. elegans* mutant (Crump et al., 2001). To similarly assess

the integrity of the active zone scaffold in our *Drosophila sff* mutant, we examined the distribution of the Bruchpilot protein (Brp) at the NMJ (**Fig. 2.11F,G**). Brp has homology to the vertebrate ELKS/CAST proteins and to Bassoon, which together complex with RIM and Munc13 at the active zone; Brp participates in the formation of T bars, electron-dense projections upon which vesicles are tethered (Wagh et al., 2006). The distribution of Brp within individual boutons was unaltered in *sff* mutant NMJs compared to wild-type. Therefore, reduced Sff in *Drosophila*, similar to reduced SAD in *C. elegans*, does not affect the structural integrity of the presynaptic scaffold required for vesicle release.

Sff/SAD Kinase Modulates Golgi Compartmentation in Neurons

Based on the function of SAD kinases at the synapse, where it facilitates tethering of vesicles to membrane-associated protein complexes, and on the narrowly distributed changes in the N-linked glycan profile of *sff* mutant embryos, we hypothesized that Sff/SAD Kinase activity modulates Golgi vesicle interactions with a subset of cisternal membranes, leading to disrupted Golgi compartmentation in *sff* mutant neurons. Since the major change in *sff* N-glycans is a shift in the profile toward greater complexity, we focused our analysis on late Golgi compartments, using markers previously described to delineate the medial/trans and trans-Golgi in *Drosophila* (LaJeunesse et al., 2004; Yano et al., 2005). We assessed the relative distributions of Golgi-YFP (a medial/trans marker, YFP fused to the transmembrane localization domain of human b4GalT), PNA (a trans marker, Galb3GalNAc specific plant lectin), and a neuronal protein that is known to bear the HRP-epitope (Fasciclin 2) (Desai et al., 1995).

The *Drosophila* Golgi apparatus is striking for its lack of morphologic similarity to classic conceptualizations of the ribbon-like, stacked cisternae evident in many cell types of vertebrate organisms. Rather, the *Drosophila* Golgi exists as distributed puncta, forming

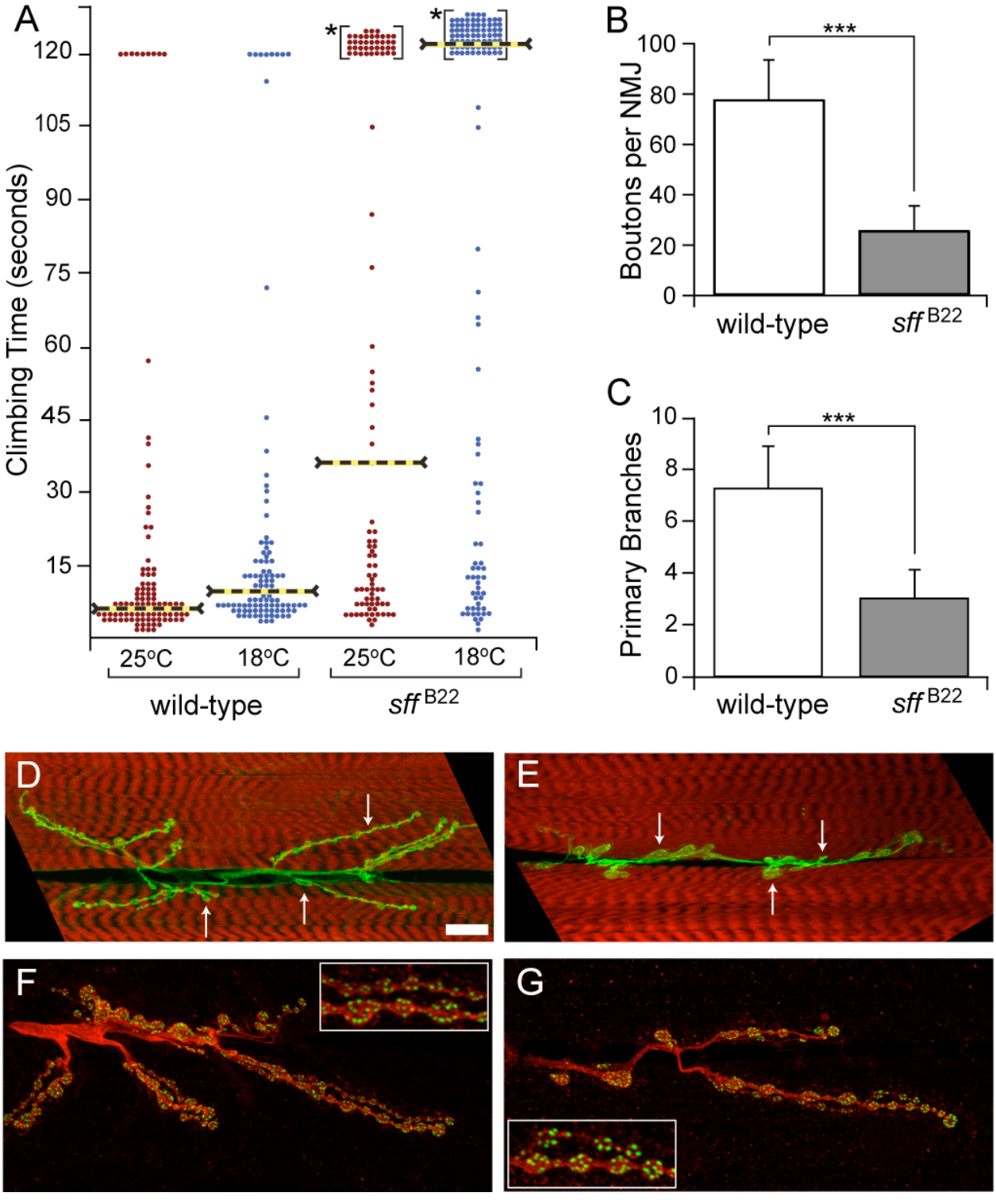
A
Climbing Time (seconds)
120
105
90
75
60
45
30
15
*
*
25°C
18°C
25°C
18°C
wild-type
sff B22
B
Boutons per NMJ
100
80
60
40
20
0
***
wild-type
sff B22
C
Primary Branches
10
8
6
4
2
0
***
wild-type
sff B22
D
E
F
G

Figure 2.11. *Sff* mutants exhibit behavioral and neuromuscular junction phenotypes.
(**A**) *Sff* mutants are deficient in negative geotaxis. Each dot in the histogram plots the climbing time for a single adult male to reach a pre-specified height. Dashed lines indicate the median climbing time for the indicated population. Trials were terminated at 120 seconds. Individuals that did not reach the threshold height within 120 seconds are binned together (*****). The behavioral phenotype of the sff^{B22} mutant is temperature sensitive, with performance decreasing at lower temperatures. For wild-type, n=105 and 103 at 25°C and 18°C, respectively. For sff^{B22}, n=100 and 122 at 25°C and 18°C, respectively.
(**B-C**) The number of boutons and the number of primary nerve branches are significantly decreased at the neuromuscular junction (NMJ) located at larval muscles 6/7 in the sff^{B22} mutant. (*** indicates $p<0.001$; n=25 wild-type, 7 sff^{B22} for panel B and 23 wild-type, 22 sff^{B22} for panel C).
(**D-E**) Compressed Z-stacks from confocal images acquired at the NMJ of muscles 6/7 in wild-type (**D**) and sff^{B22} (**E**) larvae present the gross change in morphology resulting from decreased sff/SAD function. Arrows indicate representative small and large synapses, which were quantified together to determine the number of boutons per NMJ in panel B (red, phalloidin; green, anti-HRP). Scale bar corresponds to 20 mm in D-E.
(**F-G**) The distribution of active zone complexes is not altered by the *sff* mutation. Wild-type (**F**) and sff^{B22} (**G**) larval NMJs were stained with anti-Bruchpilot (green) and anti-HRP (red). Neither the size of Bruchpilot complexes nor the number of complexes per bouton were significantly altered (insets). Scale bar corresponds to 15 mm in F-G and 4 mm for both insets. In panels D-G anti-HRP staining was used to delineate the full extent of the axonal arborization. Despite embryonic reduction of the glycan recognized by the anti-HRP antibody, larval anti-HRP antibody staining is co-extensive with mAb 1D4 staining, another well-established NMJ marker (**Fig. 2.12**).

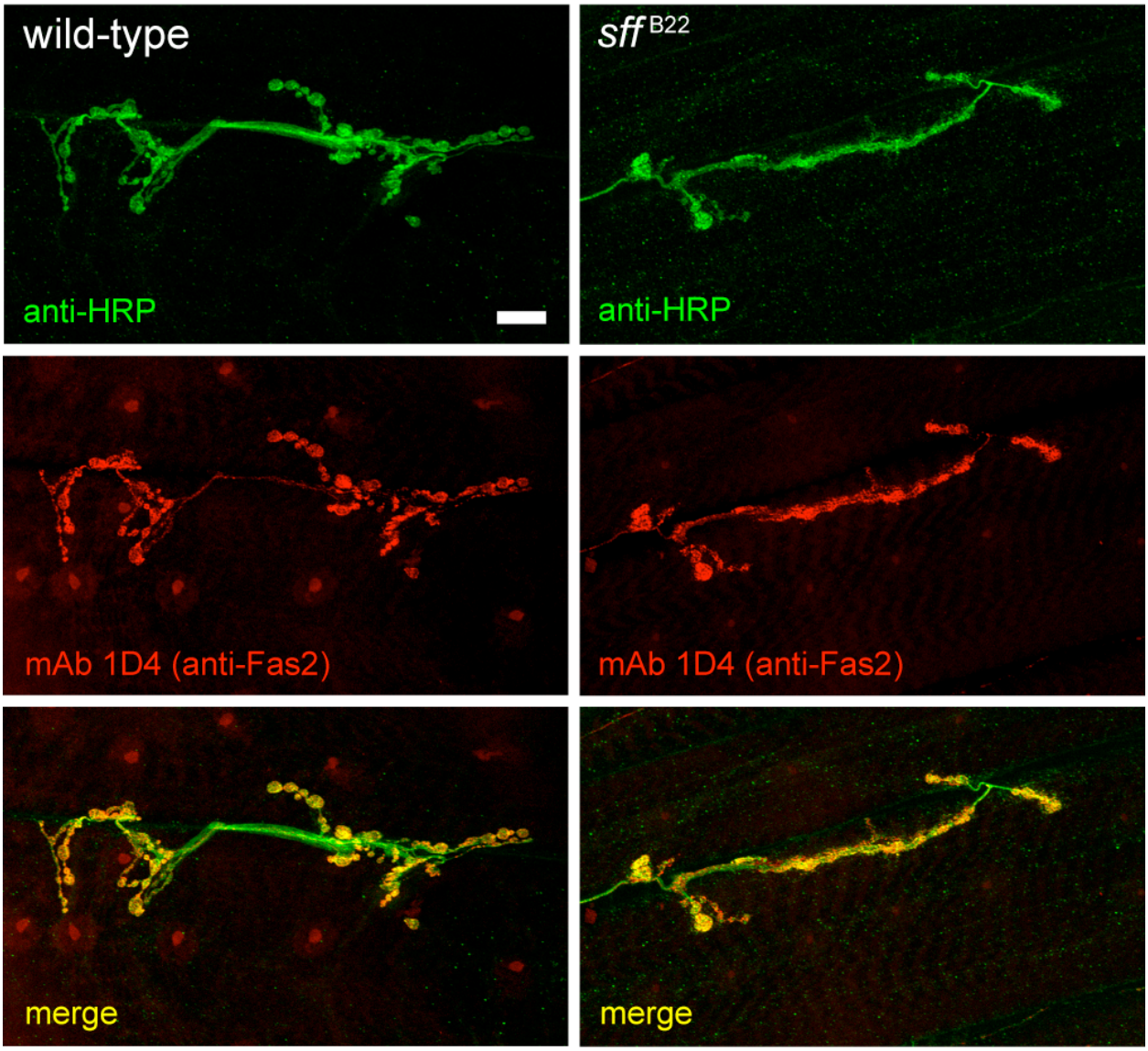

Figure 2.12. Anti-HRP antibody decorates the full axon arborization pattern at the NMJ of wild-type and *sff*^{B22} larvae.
The larval NMJ at muscles 6/7 were double-stained with anti-HRP (green) and mAb 1D4 (anti-Fas2, red) in wild-type and *sff*^{B22}. Merge of anti-HRP and 1D4 staining shows that the entire NMJ is represented by anti-HRP staining in both genotypes. Scale bar corresponds to 15 mm.

multiple organelles within a cell (Kondylis and Rabouille, 2009; Stanley et al., 1997). In triple-stained preparations (Golgi-YFP, PNA, Fas2), these puncta are distributed throughout the nerve cord (**Fig. 2.14A,B**). Strong PNA and Fas2 staining is also associated with axon bundles and specific cell bodies in both wild-type and *sff* embryos. To quantify fluorescence intensity associated with Golgi puncta, independent of axonal staining, we chose regions of interest within the nerve cord that lie ventral to the major exiting nerves and lateral to the longitudinal axon bundles (**Fig. 2.13**). The co-localized fluorescence intensity of each marker was quantified across all of the objects imaged within each region (**Fig. 2.14C-K**). The *sff* mutation causes greater segregation of trans and medial/trans markers; a smaller percent of each marker colocalizes with the other in *sff* than in wild-type (compare **Fig. 2.14D** with **H**, quantified in **K**). Colocalization of Fas2 with medial/trans and trans markers demonstrates a striking change in the association of the glycoprotein with these two overlapping compartments of the Golgi (compare **Fig. 2.14E,F** with **I,J**, quantified in **K**). Essentially all of the quantified Fas2 fluorescence intensity co-localizes with the trans marker, compared to 85% in the wild-type. The differential co-localization of Fas2 in *sff* indicates that the cisternal association of this glycoprotein has shifted toward a later compartment, away from the earlier localization expected for enzymes that generate paucimannose-type glycans (including simple HRP-epitopes) and toward the localization expected for later processing enzymes involved in complex branching (GlcNAcT2,4).

Tissue-specific Protein Glycosylation Requires Coordinated Trafficking of Substrates and Modifying Enzymes Through Golgi Compartments

The expression of HRP-epitopes is not only tissue-restricted, it is also protein-restricted; only a subset of neuronal proteins bears α3-fucosylated glycans (Desai et al., 1995). In general, the

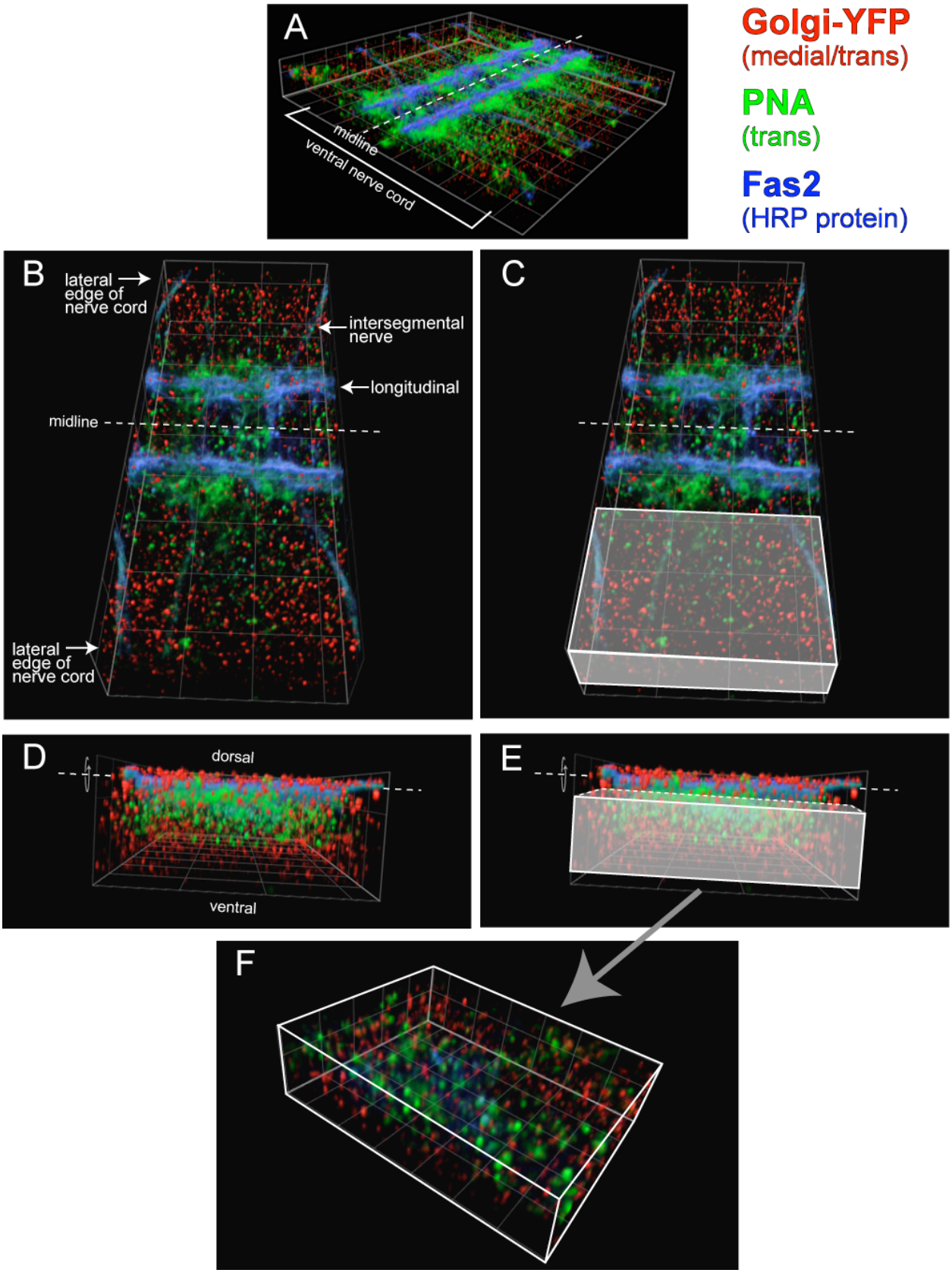
A
midline
ventral nerve cord
Golgi-YFP
(medial/trans)
PNA
(trans)
Fas2
(HRP protein)
B
lateral edge of nerve cord
intersegmental nerve
longitudinal
midline
lateral edge of nerve cord
C
D
dorsal
ventral
E
F

Figure 2.13. Selection of regions of interest for confocal analysis of Golgi marker co-localization in the ventral nerve cord.
(**A**) Three-dimensional reconstruction of multiple segments of the ventral nerve cord from a stage 14 embryo stained with the three indicated markers. The reconstruction is oriented with dorsal toward the top of the panel and anterior at the front. The lateral limits of the nerve cord and the midline are indicated.
(**B,C**) A single segment from the nerve cord is shown, anterior is to the left and the view is from a dorsal vantage point. Regions of interest for the quantification of co-localization were selected to exclude the strong fluorescence signals from axon bundles and from some medially located cell bodies that might otherwise overwhelm the signal associated with Golgi puncta. In the antero-posterior direction, regions of interest extended between the intersegmental nerves in consecutive segments. The white box in panel C indicates the medio-lateral and antero-posterior extent that defines such a region in this representative reconstruction.
(**D,E**) The segment presented in panels B,C is rotated about the midline axis to provide a lateral view. The region of interest is selected so that the dorsally-located nerve roots are excluded.
(**F**) The collection of puncta within a representative region of interest is shown. Note the absence of axonal profiles and cell bodies.

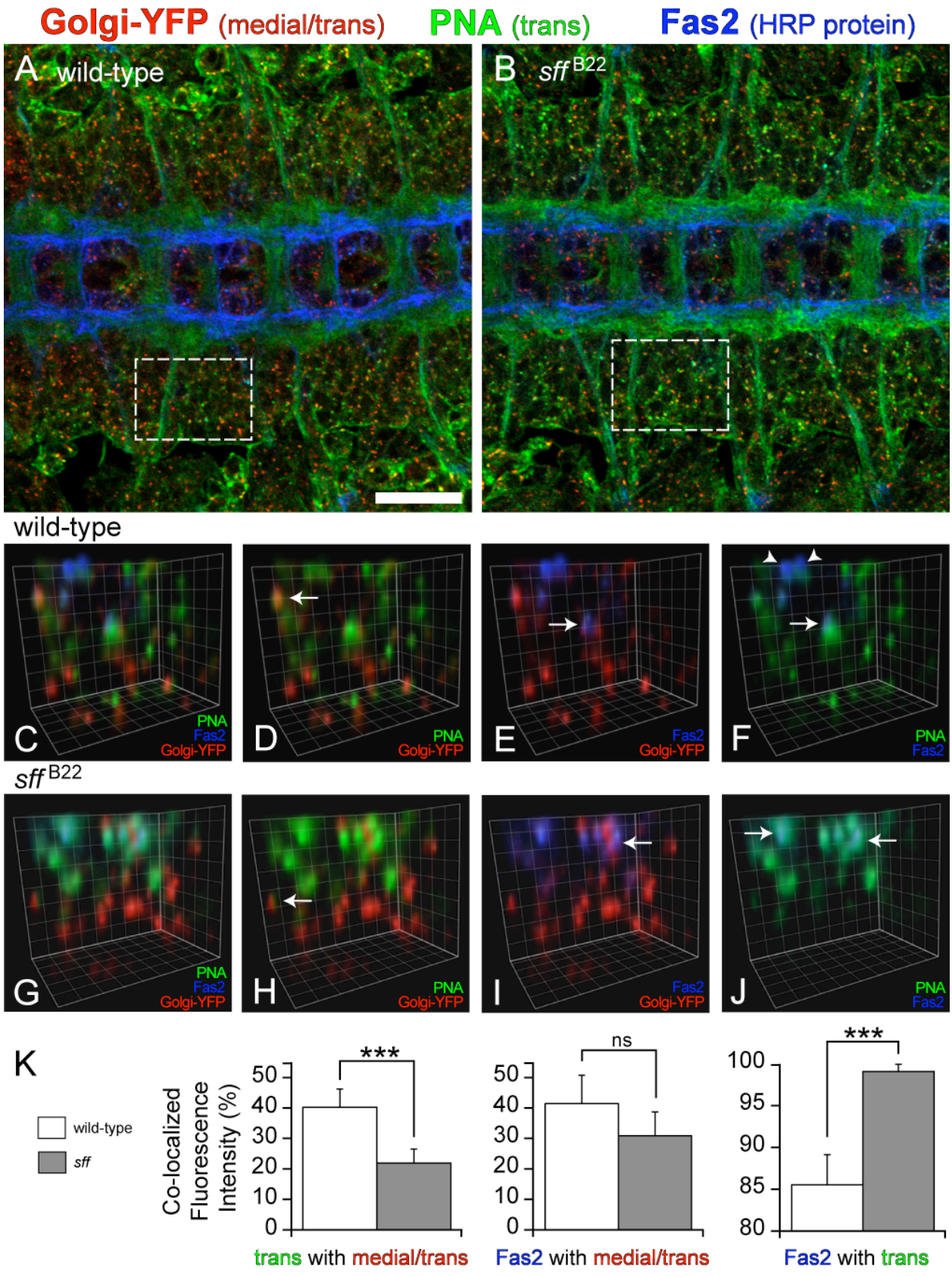
Golgi-YFP (medial/trans)
PNA (trans)
Fas2 (HRP protein)
A wild-type
B sff B22
wild-type
C PNA Fas2 Golgi-YFP
D PNA Golgi-YFP
E Fas2 Golgi-YFP
F PNA Fas2
sff B22
G PNA Fas2 Golgi-YFP
H PNA Golgi-YFP
I Fas2 Golgi-YFP
J PNA Fas2
K
wild-type
sff
Co-localized Fluorescence Intensity (%)
***
ns
***
trans with medial/trans
Fas2 with medial/trans
Fas2 with trans

Figure 2.14. Neuronal Golgi compartmentation is altered in *sff*^{B22}
(**A-B**) Representative single z-slices from approximately the same dorsal-ventral level of the ventral nerve cord of an early stage 14 wild-type (**A**) and *sff* mutant (**B**) embryo demonstrate that gross tissue organization, axonal bundling, and neural architecture are not disrupted in *sff*^{B22}. Preparations were triple stained with anti-YFP (red, marker for media/trans Golgi), PNA lectin (green, marker for trans Golgi), and mAb 1D4 (blue, Fas2, an HRP-bearing protein). Boxes delineated by white dashed lines indicate representative regions of interest used to quantify co-localization. These regions were chosen to exclude the contribution of major axon bundles and nerves to the total fluorescence intensity (described in **Fig. 2.13**). Scale bar corresponds to 20 mm in A-B.
(**C**) Three-dimensional reconstruction of a portion of a region of interest from a wild-type embryo presents objects with varying degrees of overlap for all three markers. Gridlines correspond to 1 mm in C-J.
(**D-F**) Pairwise marker combinations for image presented in panel C reveals objects with overlapping fluorescence intensity (arrows). Objects with well-circumscribed areas of very little co-localized intensity for Fas2 and the trans marker are detected in the wild-type nerve cord (arrowheads in F).
(**G**) Three dimensional reconstruction of a portion of a region of interest from an *sff*^{B22} embryo exhibits greater overlap between Fas2 and the trans Golgi marker (PNA) than is evident in the wild-type (compare to panels C and F).
(**H-J**) Pairwise marker combinations for image presented in G reveal marker overlaps (arrows) and significantly increased co-localization between Fas2 and the trans marker (arrows in J, compare to panel F).
(**K**) Fluorescence intensity co-localization was quantified for medial/trans Golgi, trans Golgi, and Fas2 markers in objects contained within regions of interest for wild-type and *sff*^{B22} mutant embryos. Values are mean ± standard deviation for n=4 wild-type or *sff*^{B22} embryos (total of 24 segments quantified for each genotype). The statistically significant difference in co-localization for the trans and medial/trans markers indicates an increased polarization between these late Golgi compartments; less trans marker overlaps with medial/trans marker in the *sff*^{B22} mutant (mean Pearson's Correlation Coefficient, PCC=0.19±0.03 and 0.31±0.05 in *sff*^{B22} and wild-type, respectively). Consistent with this increased polarization, the Fas2 signal is tightly associated with the trans marker in *sff*^{B22} (PCC=0.62±0.14), a statistically significant increase over the co-localization of these markers in wild-type (PCC=0.45±0.12). (*** indicates $p<0.003$, ns denotes not significant at $p<0.1$)

regulation of glycosylation, and particularly of glycan diversity on specific proteins, is multi-dimensional. The coordinated expression of appropriate glycosyltransferases and target proteins is only a minimum requirement for achieving specific glycosylation. Target and enzyme must be brought together within a permissive Golgi domain, which must also contain the relevant nucleotide sugars and nucleotide sugar transporters for full function. Extremely little is known regarding the coordinated Golgi dynamics that produce the confluence of components necessary for specific glycan expression (Gerardy-Schahn et al., 2001; Nilsson et al., 2009).

A specific role for protein phosphorylation in controlling Golgi function is not without precedent. The cyclin-dependent kinase Cdk1-cyclin B initiates the process of Golgi disassembly during mitosis by phosphorylating Rab1 and Golgin GM130, which together recruit an ER-derived vesicle tethering factor (p115) to cis-Golgi membranes (Misteli and Warren, 1995). Other kinases, including Plks, ERKs, and MEKs, function along with Cdk1-cyclin B to dismantle the Golgi during mitosis, and additional kinases contribute to bulk Golgi trafficking during interphase or modulate vesicle coat assembly (Dirac-Svejstrup et al., 2000; Doray et al., 2002; Preisinger and Barr, 2005). In these examples of full collapse, partition during mitosis, and vesicule coat disruption, kinase activities initiate dramatic Golgi remodeling events. The Sff/SAD function that we have described is more restricted, impacting only a subset of relatively minor glycan structures within a subcompartment of the late Golgi. Thus, the relative dosage of specific kinases, within a larger ensemble of enzymes, may sculpt glycan expression profiles in specific cell types through targeted modulation of Golgi compartmentation.

We propose that Sff/SAD kinase regulates interactions between cistern-specific tethering factors and subsets of Golgi transport vesicles in the embryonic nervous system. Therefore, we draw a parallel between the function of Sff/SAD at the nerve terminal, where it facilitates

tethering of synaptic vesicles to the active zone complex, and at the neuronal Golgi apparatus, where we propose that it facilitates the tethering of transport vesicles to cisternal targets that are competent for production of the HRP-epitope (**Fig. 2.15**). Our glycan characterization indicates that appropriate targeting of these vesicles normally limits the expansion of N-linked glycan complexity and facilitates the generation of HRP-epitopes in neural tissue. When *sff* activity is reduced, some glycoprotein substrates gain access to alternative Golgi processing enzymes (GlcNAcT2,4); the loss in tethering specificity generates a shift in Golgi target selection. At the presynaptic active zone in SAD mutants, synaptic vesicles are not presented with an alternative site for tethering at the nerve terminal; the only available fate for untethered synaptic vesicles is misalignment with respect to the active zone.

Molecular Targets for Sff/SAD Kinase at the Golgi Apparatus

Vesicular capture at presynaptic membranes and at Golgi cisternae requires the interaction of specific Rab GTPase proteins with scaffolding components that share structural and functional similarities (Schoch et al., 2002; Sinka et al., 2008). At the presynaptic membrane, these proteins act upstream of the membrane fusion machinery to facilitate the tethering, maturation, and orientation of synaptic vesicles for rapid release at the active zone. At the core of this presynaptic scaffold lies the first demonstrated substrate for SAD Kinase, the multi-domain RIM protein (Inoue et al., 2006).

Vesicular transport through the Golgi apparatus is also modulated by interactions between Rab proteins and tethering factors that possess multiple protein-protein interaction domains (Ren et al., 2009; Sztul and Lupashin, 2009). The Golgins, which exhibit compartment-specific distributions across the Golgi, are a component of the upstream mechanism that imparts specificity in vesicle-target recognition (Short et al., 2005). Similar to RIM, Bassoon/Piccolo,

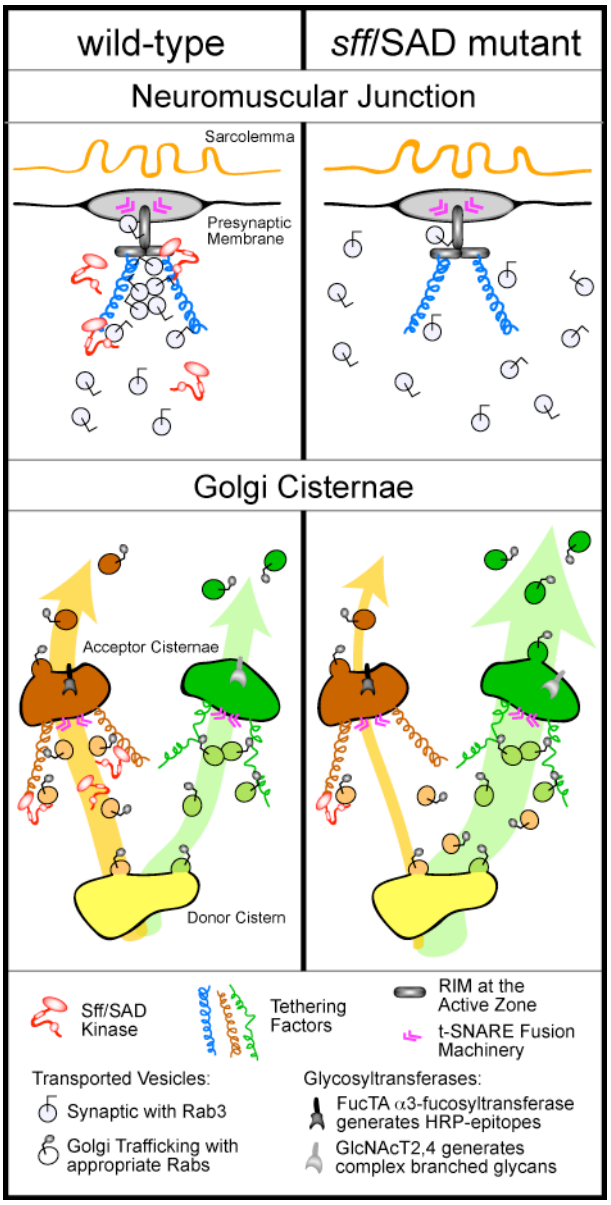
wild-type
sff/SAD mutant
Neuromuscular Junction
Sarcolemma
Presynaptic Membrane
Golgi Cisternae
Acceptor Cisternae
Donor Cistern
Sff/SAD Kinase
Tethering Factors
RIM at the Active Zone
t-SNARE Fusion Machinery
Transported Vesicles:
Synaptic with Rab3
Golgi Trafficking with appropriate Rabs
Glycosyltransferases:
FucTA α3-fucosyltransferase generates HRP-epitopes
GlcNAcT2,4 generates complex branched glycans

Figure 2.15. Parallels between known functions for sff/SAD at the presynaptic membrane of the neuromuscular junction and proposed functions for sff/SAD at cisternal membranes of the Golgi apparatus.
At the neuromuscular junction, SAD kinase facilitates the tethering of synaptic vesicles at presynaptic active zones. The tethering complex brings together molecular components necessary for maturation, priming, and fusion of synaptic vesicles. Presynaptic tethering complexes are comprised of spatially extended tethering factors such as Bruchpilot (a *Drosophila* protein that combines the signature domains of the vertebrate Bassoon/Piccolo and ERKs/CAST family members) and scaffold components such as RIM. In the absence of SAD kinase, synaptic vesicles are inefficiently associated with the active zone. Altered glycan expression in the *Drosophila sff* mutant indicates that the Sff/SAD kinase serves an analogous function at Golgi cisternal membranes, ensuring that specific Golgi transport vesicles associate with appropriate stack-specific tethering factors. In the *sff* mutant, Golgi vesicular transport is not halted since secondary cisternal targets are available and competent for fusion. But, the resulting aberrant trafficking shifts glycan profiles by allowing access of glycoprotein substrates to alternative ensembles of processing enzymes (Golgi glycosyltransferases). In the case of the sff^{B22} mutant, decreased activity reduces HRP-epitope expression and increases complex glycan production.

and the ERC proteins at the synaptic active zone, Golgin family members are large proteins with multiple protein-protein interaction motifs. Structural analysis predicts that the Golgins are extended molecules that reach into the surrounding cytoplasm from the Golgi membranes to which they are attached. The resulting matrix provides a scaffold for interaction and tethering of transport vesicles and other bridging molecules. The glycosylation phenotype that we have quantified in our *Drosophila sff/SAD* mutant indicates that the stability or functional integrity of Golgin/Rab/vesicle complexes might be differentially influenced by the activity of specific kinases. Therefore, Golgins, Rabs, and, possibly, components of the retrograde transport machinery (COGs, GARP complexes), are prime candidate substrates for phosphorylation by Sff/SAD.

Signaling Pathways That Impinge Upon Tissue-Specific Glycosylation

SAD Kinases belong to the AMPK/SNF1 family of Ser/Thr kinases, many of which convey signals that regulate cell polarity and energy utilization (Carling et al., 1994). Mice lacking both SAD-1 and SAD-2 are immobile, die within 2 hours of birth, and exhibit neuronal polarity defects (Kishi et al., 2005). While SAD Kinase is normally present throughout the neuron, its activation is enhanced in axons. In this context, neurite-initiating factors signal through Protein Kinase A (PKA) to activate the LKB1 polarity kinase (Barnes et al., 2007). In turn, LKB1 activates SAD within the growing neurite, which phosphorylates Tau, stabilizing nascent neuronal polarity in embryos or mature axonal structure in developed nervous systems.

Neuronal polarization defects are not apparent in our *sff* mutant embryo. Neurons in the ventral nerve cord and in the peripheral nervous system are born on time and migrate to appropriate positions. Pioneering axon extension is unaltered and the full axon scaffold is well formed in the late embryo. The lack of gross polarity defects in *sff* likely reflects the

hypomorphic nature of our sff^{B22} allele, indicating that neuronal polarization requires less Sff/SAD protein than is necessary for establishing neuron-specific glycan expression. However, it is well appreciated that the sorting function of the Golgi apparatus is intimately associated with cell polarity. In some cases, the glycans on sorted proteins influence their sorting, linking the Golgi function that we have detected for Sff/SAD to cell polarity (Potter et al., 2006).

While activation of SAD through PKA/LKB1 allows the kinase to influence neuronal polarity and may contribute to its Golgi function, it is not likely to constitute the signaling pathway through which tollo/toll-8 in *Drosophila* embryonic ectodermal cells drives HRP-epitope expression in neighboring neurons. The significant loss of *sff/SAD* mRNA in the *tollo/toll-8* mutant background (**Fig. 5**) implicates transcriptional control or message stability as a major mechanism underlying the neuron-specific glycan expression mediated by Sff/SAD. Vertebrate SAD kinase expression is regulated through metabolic sensing pathways involving AKT inhibition of TSC1-TSC2 and activation of TORC1 (Wildonger et al., 2008). This paradigm nominates a range of survival/growth factors, hormones, neurotransmitters, and other effectors of AKT or PI3K activation as molecules capable of propagating the transcellular signal initiated by tollo/toll-8 in *Drosophila*. Our ongoing screen for mutants that affect glycosylation should allow us to capture informative alleles of genes that fall into these control pathways. In a broader context, our results provide a new mechanism for reinterpreting many years of empiric observations describing the impact of endocrine factors, tissue microenvironments, and culture conditions on cellular protein glycosylation (Knezevic et al., 2009; Varki, 2006).

Concluding Remarks

We have demonstrated that Sff/SAD Kinase modulates neural-specific glycosylation in the *Drosophila* embryo and have presented data supporting our hypothesis that altered Golgi compartmentation is the underlying mechanism responsible for the observed shift in glycan expression. The magnitude of the shift in global glycan expression is subtle (affecting the elaboration of minor complex and a3-fucosylated structures), but commensurate with the degree of altered Golgi compartmentation detected in the *sff* mutant. Therefore, we have proposed a parallel between Sff/SAD kinase function in vesicle tethering at the synapse and at Golgi cisternal membranes, allowing the enzyme to influence flux through specific Golgi processing pathways. When considered in the context of the full range of kinases that have access to Golgi membrane or matrix proteins, our results suggest that cellular glycan processing may be tailored by the integrated balance of all relevant kinase activities. Upstream of vesicle capture, kinase activation reflects the propagation of specific extracellular signals, linking cellular glycan expression to the detection of appropriate environmental cues. For Sff/SAD and neural-specific glycosylation, one of these cues is activation of tollo/toll-8 transcellular signaling in the early embryo.

ACKNOWLEDGEMENTS

The authors most gratefully acknowledge valuable consultations with R. Steet (CCRC, UGA), K. Ten Hagen (NIH), V. Panin (Texas A&M), and L. Wells (CCRC, UGA). P. Zhao, M. Ishihara, T. Katoh, and L. Wells provided expert advice and useful discussions related to proteomic analysis and MS-based glycomics. K. Habenicht, C. Hupman, M. Hirsu, and R. Cantu contributed invaluable technical support to the development and implementation of the genetic screen. S. Lee and N. Price contributed to the initial characterization of the *sff* mutant. This work

was supported by a grant from NIH/NIGMS (1-R01-GM072839 to MT), a Cousins Foundation Fellowship (to SB), and a Toyobo Biotechnology Foundation Long-term Research Grant (to KA).

REFERENCES

Acheson, A., Sunshine, J.L., and Rutishauser, U. (1991). NCAM Polysialic acid can regulate both cell-cell and cell-substrate interactions. J Cell Biol *114*, 143-153.

Allendoerfer, K.L., Durairaj, A., Matthews, G.A., and Patterson, P.H. (1999). Morphological domains of Lewis-X/FORSE-1 immunolabeling in the embryonic neural tube are due to developmental regulation of cell surface carbohydrate expression. Dev Biol *211*, 208-219.

Aoki, K., Perlman, M., Lim, J., Cantu, R., Wells, L., and Tiemeyer, M. (2007). Dynamic developmental elaboration of N-linked glycan complexity in the *Drosophila melanogaster* embryo. J Biol Chem *282*, 9127-9142.

Barnes, A., Lilley, B., Pan, Y., Plummer, L., Powell, A., Raines, R., Sanes, J.R., and Polleux, F. (2007). LKB1 and SAD kinases define a pathway required for the polarization of cortical neurons Cell *129*, 549-563.

Carling, D., Aguan, K., Woods, A., Verhoeven, A.J., Beri, R.K., Brennan, C.H., Sidebottom, C., Davison, M.D., and Scott, J. (1994). Mammalian AMP-activated protein kinase is homologous to yeast and plant protein kinases involved in the regulation of carbon metabolism. J Biol Chem *269*, 11442-11448.

Constantine-Paton, M., Blum, A.S., Mendez-Otero, R., and Barnstable, C.J. (1986). A cell surface molecule distributed in a dorso-ventral gradient in the perinatal rat retina. Nature *324*, 459-462.

Crump, J., Zhen, M., Yishi, J., and Bargmann, C. (2001). The SAD-1 kinase regulates presynaptic vesicle clustering and axon termination. Neuron *29*, 115-129.

Dennis, J.W., Nabi, I.R., and Demetriou, M. (2009). Metabolism, cell surface organization, and disease. Cell *139*, 1229-1241.

Desai, C., Popova, E., and Zinn, K. (1995). A *Drosophila* receptor tyrosine phosphatase expressed in the embryonic CNS and larval optic lobes is a member of the set of proteins bearing the "HRP" carbohydrate epitope. J. Neurosci *14*, 7272-7283.

Dirac-Svejstrup, A., Shorter, J., Waters, M., and Warren, G. (2000). Phosphorylation of the vesicle-tethering protein p115 by a casein kinase II-like enzyme is required for Golgi reassembly from isolated mitotic fragments. J Cell Biol *150*, 475-488.

Doray, B., Ghosh, P., Griffith, J., Geuze, H.J., and Kornfeld, S. (2002). Cooperation of GGAs and AP-1 in packaging MPRs at the trans-Golgi network. Science *297*, 1700-1703.

Fabini, G., Freilinger, A., Altmann, F., and Wilson, I.B. (2001). Identification of core alpha 1,3 fucosylated glycans and cloning of the requisite fucosyltransferase cDNA from *Drosophila melanogaster*. Potential basis of the neural anti-horseradish peroxidase epitope. J Biol Chem *276*.

Freeze, H. (2002). Human disorders in N-glycosylation and animal models. Biochim Biophys Acta *1573*, 388-393.

Gerardy-Schahn, R., Oelmann, S., and Bakker, H. (2001). Nucleotide sugar transporters: biological and functional aspects. Biochimie *83*, 775-782.

Heinemeyer, T., Wingender, E., Reuter, I., Hermjakob, H., Kel, A.E., Kel, O.V., Ignatieva, E.V., Ananko, E.A., Podkolodnaya, O.A., Kolpakov, F.A.*, et al.* (1998). Databases on transcriptional regulation: TRANSFAC, TRRD and COMPEL. Nucleic Acids Res *26*, 362-367.

Inoue, E., Mochida, S., Takagi, H., Higa, S., Deguchi-Tawarada, M., Takao-Rikitsu, E., Inoue, M., Yao, I., Takeuchi, K., Kitajima, I.*, et al.* (2006). A presynaptic kinase associated with synaptic vesicles and the active zone cytomatrix that regulates neurotransmitter release. Neuron *50*, 261-275.

Jan, L., and Jan, Y. (1982). Antibodies to horseradish peroxidase as specific neuronal markers in *Drosophila* and grasshopper embryos. Proc Natl Acad Sci USA *79*, 2700-2704.

Kaufmann, N., DeProto, J., Ranjan, R., Wan, H., and Van Vactor, D. (2002). *Drosophila* liprin-alpha and the receptor phosphatase Dlar control synapse morphogenesis. Neuron *28*, 27-38.

Kishi, M., Pan, Y., Crump, J., and Sanes, J. (2005). Mammalian SAD kinases are required for neuronal polarization. Science *307*, 929-932.

Knezevic, A., Polasek, O., Gornik, O., Rudan, I., Campbell, H., Hayward, C., Wright, A., Kolcic, I., O'Donoghue, N., Bones, J.*, et al.* (2009). Variability, heritability and environmental determinants of human plasma N-glycome. J Proteome Res *8*, 694-701.

Koles, K., Irvine, K.D., and Panin, V.M. (2004). Functional characterization of *Drosophila* sialyltransferase. J Biol Chem *279*, 4346-4357.

Kondylis, V., and Rabouille, C. (2009). The Golgi apparatus: lessons from *Drosophila*. FEBS Lett *583*, 3827-3838.

Kopczynski, C., Davis, G., and Goodman, C. (1996). A Neural Tetraspanin, Encoded by late bloomer, That Facilitates Synapse Formation. Science *271*, 1867-1870.

Kruse, J., Mailhammer, R., Wernecke, H., Faissner, A., Sommer, I., Goridis, C., and Schachner, M. (1984). Neural cell adhesion molecules and myelin-associated glycoprotein share a common carbohydrate moiety recognized by monoclonal antibodies L2 and HNK-1. Nature *311*, 153-155.

Kurosaka, A., Yano, A., Itoh, N., Kuroda, Y., Nakagawa, T., and Kawasaki, T. (1991). The structure of a neural specific carbohydrate epitope of horseradish peroxidase recognized by anti-horseradish peroxidase antiserum. J Biol Chem *266*, 4168-4172.

LaJeunesse, D.R., Buckner, S.M., Lake, J., Na, C., Pirt, A., and Fromson, K. (2004). Three new *Drosophila* markers of intracellular membranes. Biotechniques *36*, 784-788, 790.

Lee, S., Grigorian, A., Pawling, J., Chen, I., Gao, G., Mozaffar, T., McKerlie, C., and Demetriou, M. (2007). N-glycan processing deficiency promotes spontaneous inflammatory demyelination and neurodegeneration. J Biol Chem *282*, 33725-33734.

Leonard, R., Rendic, D., Rabouille, C., Wilson, I.B., Preat, T., and Altmann, F. (2006). The *Drosophila fused lobes* gene encodes an N-acetylglucosaminidase involved in N-glycan processing. J Biol Chem *281*, 4867-4875.

Lim, J., Sherling, D., Teo, C., Hausman, D., Lin, D., and Wells, L. (2007). Defining the regulated secreted proteome of rodent adipocytes upon the introduction of insulin resistance. J Proteome Res *7*, 1251-1263.

Martin, V., Mrkusich, E., Steinel, M.C., Rice, J., Merritt, D.J., and Whitington, P.M. (2008). The L1-type cell adhesion molecule Neuroglian is necessary for maintenance of sensory axon advance in the *Drosophila* embryo. Neural Dev *3*, 10.

Matani, P., Sharrow, M., and Tiemeyer, M. (2007). Ligand, modulatory, and co-receptor functions of neural glycans. Front Biosci *12*, 3852-3879.

Matthews, R.T., Kelly, G.M., Zerillo, C.A., Tiemeyer, M., and Hockfield, S. (2002). Aggrecan glycoforms contribute to the molecular heterogeneity of perineuronal nets. J Neurosci *22*, 7536-7547.

Merritt, D.J., and Whitington, P.M. (1995). Central projections of sensory neurons in the *Drosophila* embryo correlate with sensory modality, soma position, and proneural gene function. J Neurosci *15*, 1755-1767.

Michele, D., and Campbell, K. (2003). Dystrophin-glycoprotein complex: Post-translational processing and dystroglycan function. J Biol Chem *278*.

Misteli, T., and Warren, G. (1995). A role for tubular networks and a COP I-independent pathway in the mitotic fragmentation of Golgi stacks in a cell-free system. J Cell Biol *130*, 1027-1039.

Nilsson, T., Au, C.E., and Bergeron, J.J. (2009). Sorting out glycosylation enzymes in the Golgi apparatus. FEBS Lett *583*, 3764-3769.

Okajima, T., and Irvine, K.D. (2002). Regulation of notch signaling by o-linked fucose. Cell *111*, 893-904.

Patel, N. (1994). Imaging neuronal subsets and other cell types in whole-mount *Drosophila* embryos and larvae using antibody probes. Methods Cell Biol *44*, 445-487.

Potter, B., Hughey, R., and Weisz, O. (2006). Role of N- and O-glycans in polarized biosynthetic sorting. Am J Physiol Cell Physiol *290*, C1-C10.

Preisinger, C., and Barr, F. (2005). Kinases regulating Golgi apparatus structure and function. Biochem Soc Symp *72*, 15-30.

Ren, Y., Yip, C.K., Tripathi, A., Huie, D., Jeffrey, P.D., Walz, T., and Hughson, F.M. (2009). A structure-based mechanism for vesicle capture by the multisubunit tethering complex Dsl1. Cell *139*, 1119-1129.

Rendic, D., Linder, A., Paschinger, K., Borth, N., Wilson, I.B., and Fabini, G. (2006). Modulation of neural carbohydrate epitope expression in *Drosophila melanogaster* cells. J Biol Chem *281*, 3343-3353.

Sarkar, M., Leventis, P.A., Silvescu, C.I., Reinhold, V.N., Schachter, H., and Boulianne, G.L. (2006). Null mutations in *Drosophila N-acetylglucosaminyltransferase I* produce defects in locomotion and a reduced life span. J Biol Chem *281*, 12776-12785.

Schnitzer, J., and Schachner, M. (1982). Cell type specificity of a neural cell surface antigen recognized by the monoclonal antibody A2B5. Cell Tissue Res *224*, 625-636.

Schoch, S., Castillo, P., Jo, T., Mukherjee, K., Geppert, M., Wang, Y., Schmitz, F., Malenka, R., and Sudhof, T. (2002). RIM1α forms a protein scaffold for regulating neurotransmitter release at the active zone. Nature *415*, 321-326.

Seppo, A., Matani, P., Sharrow, M., and Tiemeyer, M. (2003). Induction of neuron-specific glycosylation by Tollo/Toll-8, a *Drosophila* Toll-like receptor expressed in non-neural cells. Development *130*, 1439-1448.

Short, B., Haas, A., and Baar, F. (2005). Golgins and GTPases, giving identity and structure to the Golgi apparatus. Biochim Biophys Acta *1744*, 383-395.

Sinka, R., Gillingham, A.K., Kondylis, V., and Munro, S. (2008). Golgi coiled-coil proteins contain multiple binding sites for Rab family G proteins. J Cell Biol *183*, 607-615.

Snow, P., Patel, N., Harrelson, A., and Goodman, C. (1987). Neural-specific carbohydrate moiety shared by many surface glycoproteins in *Drosophila* and grasshopper embryos. J Neurosci *7*, 4137-4144.

Stanley, H., Botas, J., and Malhotra, V. (1997). The mechanism of Golgi segregation during mitosis is cell type-specific. Proc Natl Acad Sci U S A *94*, 14467-14470.

Sztul, E., and Lupashin, V. (2009). Role of vesicle tethering factors in the ER-Golgi membrane traffic. FEBS Lett *583*, 3770-3783.

Varki, A. (2006). Nothing in glycobiology makes sense, except in the light of evolution. Cell *126*, 841-845.

Vyas, A.A., Patel, H.V., Fromholt, S.E., Heffer-Lauc, S.E., Vyas, K.A., Dang, J., Schachner, M., and Schnaar, R.L. (2002). Gangliosides are functional nerve cell ligands for myelin-associated glycoprotein (MAG). Proc Natl Acad Sci USA *99*, 8412-8417.

Wagh, D.A., Rasse, T.M., Asan, E., Hofbauer, A., Schwenkert, I., Dürrbeck, H., Buchner, S., Dabauvalle, M.C., Schmidt, M., Qin, G.*, et al.* (2006). Bruchpilot, a protein with homology to ELKS/CAST, is required for structural integrity and function of synaptic active zones in *Drosophila*. Neuron *49*, 833-844.

Wildonger, J., Jan, L., and Jan, Y. (2008). The Tsc1-Tsc2 complex influences neuronal polarity by modulating TORC1 activity and SAD levels. Genes and Dev *22*, 2447-2453.

Yano, H., Yamamoto-Hino, M., Abe, M., Kuwahara, R., Haraguchi, S., Kusaka, I., Awano, W., Kinoshita-Toyoda, A., Toyoda, H., and Goto, S. (2005). Distinct functional units of the Golgi complex in *Drosophila* cells. Proc Natl Acad Sci U S A *102*, 13467-13472.

Zak, G., Crawford, B., and Esko, J. (2002). Hereditary multiple exostoses and heparan sulfate polymerization. Biochim Biophys Acta *1573*, 346-355.

CHAPTER 3

WHITE AND BIOGENIC AMINES INTERACT WITH *SUGAR-FREE FROSTING* TO INFLUENCE NEURAL-SPECIFIC GLYCOSYLATION IN *DROSOPHILA*[1]

[1] Sarah Baas, Emily King, Meg Middleton, and Michael Tiemeyer. To be submitted.

SUMMARY

The *Drosophila* SAD homolog, Sugar-free frosting (Sff), regulates neural-specific glycosylation in the embryo. Tollo, a toll-like receptor expressed in ectodermal cells, signals to Sff in surrounding neural cells to drive glycan expression, particularly a family of difucosylated N-glycans known as HRP-epitopes. Data presented demontrate that *white*, a gene originally identified for its involvement in eye pigment synthesis, interacts with *sff* with regard to glycan expression. A mutation in *white* decreases the severity of the phenotypes associated with the *sff* mutant. A *white* mutation alone also influences the N-glycan expression in the embryo. White has been reported to affect neural function and biogenic amine levels and we find that White influences the neuromuscular junction morphology of *sff* mutants. We also report that *sff* mutants have a reduction in serotonin levels. Pharmacological treatment of *sff* mutant adults with antidepressants rescues their behavioral defect. Interestingly, pharmacological treatment of *sff* and wild-type embryos increases HRP-epitope expression. Therefore we propose that signaling through biogenic amines regulates neural-specific glycosylation.

INTRODUCTION

The *Drosophila* White (w) protein is a member of the ATP-binding cassette (ABC) transporter family. White forms a complex with Brown or Scarlet to transport guanine or tryptophan, respectively (Ewart and Howells, 1998). It has also been suggested that White and Scarlet transport not tryptophan but 3-hydroxykynurenine, an intermediate in the synthesis of ommochrome eye pigment (Mackenzie et al., 2000). Eye pigment is comprised of red drosopterins (from guanine) and brown ommochromes (from tryptophan), and *white* mutants lack both (Phillips and Forrest, 1980). *White* is not only expressed in cells producing eye

pigment. Abundant levels of transcript for *white* have been detected in heads missing eyes and ocelli (simple visual organ that also contains eye pigment), indicating White may serve other functions (Campbell and Nash, 2001). Several groups have reported neurobiological roles for White, as well as other genes involved in pigment biosynthesis. For example, over-expression of *white* triggers male-male courtship, while reduction in *white* results in defects in spatial learning (Diegelmann et al., 2006; Zhang and Odenwald, 1995). Mutations in genes involved in ommochrome pigment synthesis- *cardinal*, *vermillion* and *cinnabar*, have an alteration of mushroom body volume (Savvateeva et al., 2000; Savvateeva et al., 1999). These mutants, as well as *white*, *brown*, and *scarlet* mutants, also have decreased immunoreactivity to cysteine string protein (CSP), which functions in Ca^{2+}-regulated synaptic vesicle exocytosis (Borycz et al., 2008). *White*, *brown*, and *scarlet* mutants also have decreased levels of the biogenic amines histamine, dopamine and serotonin in the adult head, as well as a reduction in the number of photoreceptor synaptic vesicles (Borycz et al., 2008).

Biogenic amines are generated by metabolism of amino acids. In vertebrates the biogenic amines are dopamine, norepinepherine, epinephrine, serotonin, and histamine. In invertebrates, tyramine and octopamine replace norepinepherine and epinephrine, respectively (Blenau and Baumann, 2001). Tyramine, octopamine, and dopamine are derived from the amino acid tyrosine (**Fig. 3.1A**). Serotonin / 5-hydroxy tryptamine (5-HT) is synthesized from tryptophan by tryptophan hydroxylase (**Fig. 3.1B**). Biogenic amines can serve as neurotransmitters, neuromodulators, and paracrine activators. In invertebrates, they are released in the hemolymph and can act as neurohormones. Some biogenic amines (dopamine) are involved in sclerotization, or hardening, of the cuticle (Monastirioti, 1999). Melatonin, a derivative of serotonin, is also present in the fly and plays a role in female receptivity and egg-laying (Finocchiaro et al., 1988).

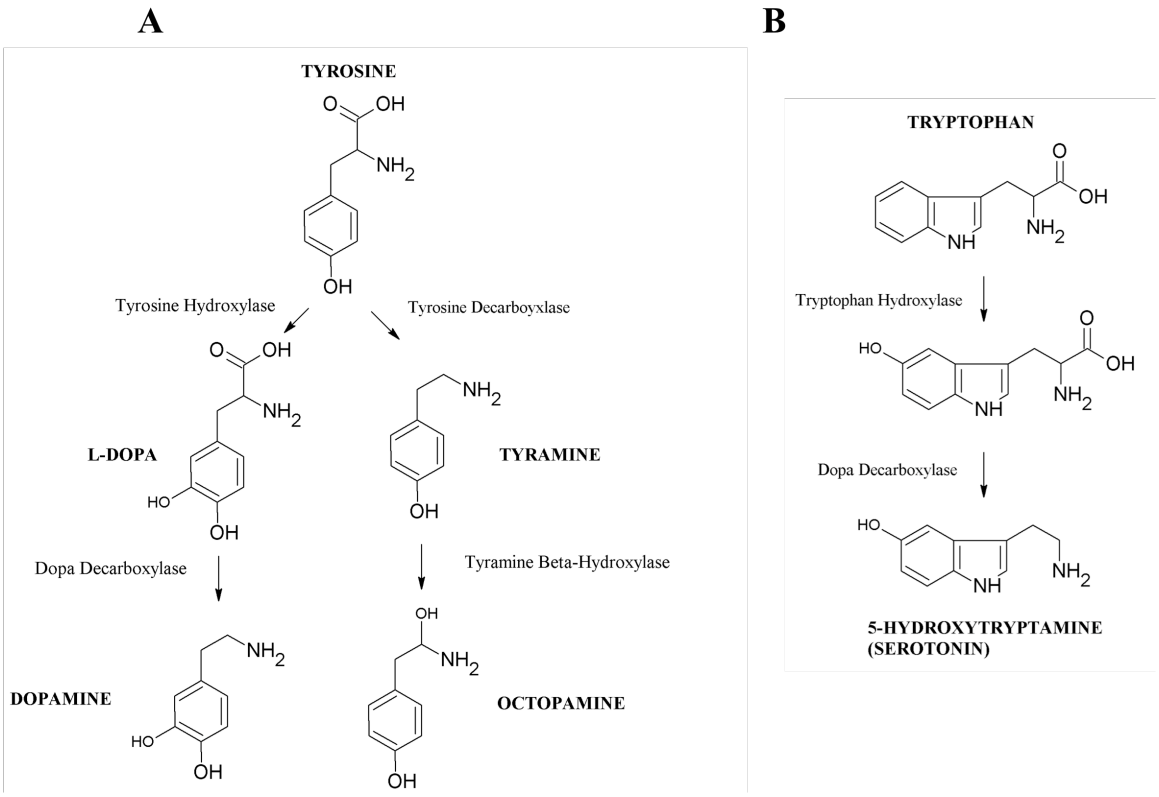

Figure 3.1. Biosynthesis of the biogenic amines in *Drosophila*
(**A**) Tyrosine is modified to yield dopamine, through the intermediate L-DOPA. Tyrosine can also be decarboxylated to produce tyramine, which can then be hydroxlated to form octopamine. (**B**) Serotonin is derived from the amino acid tryptophan, and Tryptophan hydroxylase catalyzes the rate-limiting step.

Serotonin has also been shown to play roles in the regulation of locomotion and in learning and memory in *Drosophila*. Serotonergic neurons are a small population of neurons. In larvae they are bilaterally symmetrical neurons that innervate the midgut, pharyngeal muscles, and the ring gland (the larval endocrine organ). Serotonergic neurons also innervate the feeding apparatus, suggesting that serotonin may help modulate feeding behavior as wells as neuroendrocrine activity (Monastirioti, 1999).

We previously reported the characterization of a mutation in the *Drosophila SAD* kinase, *sugar-free frosting* (*sff*) (see chapter 2). Isolated from a screen for mutations that affect neural-specific glycosylation, we proposed that Sff/SAD modulates glycosylation by regulating vesicular traffic through the Golgi. We report here a genetic interaction between *sff* and *white*, in which a mutation in *white* lessens the severity of phenotypes associated with the *sff* mutant. We also report that, like *white*, *sff* mutants have a decreased level of serotonin. Intriguingly, altering biogenic amine levels influences tissue-specific glycan expression, suggesting that signaling through biogenic amines can regulate glycosylation.

EXPERIMENTAL PROCEDURES

Drosophila Culture

Flies were reared on standard molasses media at 25° or 18°C, as indicated. *OreR* and w^{1118} strains were obtained from the Bloomington Stock Center at Indiana University. Sff^{B22} arose from the EMS-induced mutagenesis of w^{1118}, followed by scrubbing against *OreR*. The flies were then recombined against the *rucuca* chromosome. A strain resulting from the recombination carrying *ebony (e)*, *claret (ca)*, and *roughoid (ru)* mutations (*ru*, sff^{B22}, *e*, *ca*) was used for all experiments, either in a w^- or w^+ background where indicated.

Viability experiment

An overnight collection of embryos at 25°C were counted and placed in a vial of standard media and allowed to mature. The number of males and females that hatched were counted, as well as the number of pupal cases.

N-glycan Analysis

For embryos, total N-glycans were prepared from an overnight collection of embryos at 25°C as previously described (Aoki et al., 2007). For larval brains, the brain lobes and CNS from 3rd instar larvae raised at 18°C were dissected in 1X PBS and frozen in heptane until enough brains (several hundred) were collected. Briefly, samples were homogenized and delipidated by chloroform:methanol:water::4:8:3 (v/v/v) extraction. Proteins were then precipitated to generate a powder, which was digested with trypsin and chymotrypsin (both from Sigma). C18 Sep-Pak chromatography was used to enrich the glycopeptides, which were then digested by PNGaseA. N-glycans were enriched by C18 and then permethylated. Glycans were analyzed by nanospray ionization interfaced to a linear ion trap (NSI-MS^n on an LTQ Ion Trap, Thermo/Fisher). Total Ion Mapping (TIM) was used to acquire full profiles. MS and MS/MS spectra were interpreted manually to assign glycan structures; quantification was based on relative glycan prevalence.

Immunohistochemistry

Embryos from overnight collections were dechorionated, fixed, devitellinized, and stained with antibodies according to standard procedures (Patel, 1994). Antibody dilutions were 1:2000 in embryos and 1:1000 in larvae for rabbit-anti-HRP (Jackson Labs), 1:100 for TRITC phalloidin (Invitrogen), 1:1000 for goat-anti-rabbit-HRP (Jackson Labs), 1:500 for Alexa-conjugated goat-anti-rabbit (Molecular Probes). HRP-conjugated secondary antibodies were detected with 3,3-diaminobenzidine precipitation in the presence of H_20_2 as substrate. Fluorescently-stained

preparations were mounted in glycerol with 4% DABCO. Nomarski (DIC) and light micrographs were obtained on a Zeiss Axioskope microsope fitted with a Retiga 2000R CCD camera (Q Imaging).

Analysis of the larval NMJ

Wandering third instar larvae raised at 18°C were dissected according to (Kaufmann N et al., 2002). Briefly, larvae were pinned dorsal side up onto sylgard plates in a solution of 128mM NaCl, 2mM KCl, 4mM $MgCl_2$, 35.5mM sucrose, 5mM HEPES, 1mM EDTA. A mid longitudinal incision was made and internal organs were removed. The pelts were secured by pins and fixed. After fixation the pins were removed and the pelts were stained. The 6/7 NMJ was imaged by confocal microscopy (Olympus FV100) and maximum Z-stacks were analyzed using NIH Image J. For consistency, only the junction in abdominal segments 3 and 4 were used for the quantification of bouton number and bouton size.

***In situ* hybridization**

OreR genomic sequence corresponding to the 3' UTR of *CG6114* was amplified by PCR (sense: CGCTGCTCATTGCACAGTGC, antisense: GCTGAGCACGAACGCAACC) and cloned into PCR 2.1 TOPO vector (Invitrogen) and clones were obtained in both directions. Digoxigenin-11-UTP-labeled RNA was prepared by in-vitro transcription using the DIG RNA Labeling Kit (Roche) and detected in embryos from an overnight collection at 25°C according to (Kopczynski et al., 1996).

Geotaxis testing and drug administration

8 day old males raised at 25° or 18°C were placed in individual empty vials and dark- adapted for one hour at 18°C. Under red light, the vials were gently tapped to the bottom, and the flies

were given up to 2 minutes to climb to a height of 3 cm. The test was terminated if the fly failed to reach the designated height in 2 minutes.

For drug administration, 8 day old males raised at 25° or 18°C were starved in individual vials for six hours in the dark at 18°C. The flies were then fed a 5mM drug solution, imipramine or phenelzine (both from Sigma) in 10% sucrose, prepared by pipetting 50µl onto a small disk of Whatman paper at the bottom of the vial. Flies were repeatedly tapped to the bottom of the vial to ensure sufficient presentation for ingestion of the drug. After 15 minutes the flies were transferred back to empty vials and tested for their geotaxis ability. The drug administration protocol was adapted from (Nichols et al., 2002).

HPLC measurement of biogenic amine levels

Adapted from Hardie and Hirsh, 2006, brains from 8 day old males raised at 18°C were dissected in 1X PBS, being careful to remove all traces of eye pigment. A minimum of 10 brains was obtained per genotype. The brains were homogenized on ice in 50mM citrate/acetate, pH 4.5 in a ratio of 5µl per brain. Insoluble material was removed by centrifuging the sample in a 0.22µm spin column (Millipore) and the flow through was analyzed immediately. The injection volume was the equivalent of 2 brains. The HPLC system consisted of a Dionex GS50 gradient pump and an AD25 absorbance detector. A glassy carbon electrode with an Ag/AgCl reference electrode was used for electrochemical detection of the biogenic amines. Reverse phase chromatography was performed using a Hypersil 100 C_{18} column, 100mm x 4.6mm i.d., with a 5µm particle size and 100 angstrom pore size (Thermo Electron). The guard column was a Brownlee Validated C_{18} Newguard column, 15mm x 3.2mm (Perkin-Elmer). Buffer conditions for HPLC was 52% buffer B (A=50mM citrate/acetate, pH 4.5, 11mM decanesulfonic acid; B= 50mM citrate/acetate, pH 4.5, 11mM decanesulfonic acid, 40% acetonitrile) at a rate of

1mL/min. The cell potential was 0.85V and the run time was 10 minutes. Standard mixes of octopamine, dopamine, serotonin, and tyramine (Sigma) were used to generate a standard curve based on injections of 10, 25, 50, 100, and 200pg. Biogenic amines were analyzed and quantified using Chromeleon software (Dionex).

Pharmacological treatment of embryos

Treatment was performed as previously described (Hsouna et al., 2007). Briefly, wild-type and *sff*^{B22} flies were allowed to lay ninety minutes at 25°C. Embryos were collected and dechorionated with bleach. Following a brief rinse in deionized water, embryos were nutated in 500µl 1mM phenelzine in 1X phosphate buffered saline (PBS) for 15 minutes. After treatment, three five-minute washes with 1X PBS and 0.3% Triton-X 100 were performed. The final wash solution was removed and replaced with 1X PBS and embryos were aged approximately 12 hours at 25°C. Embryos were then fixed and stained with anti-HRP antibody as described above.

RESULTS

A mutation in white suppresses the partial lethality of *sff*^{B22}

We previously determined that *sff*^{B22}, a hypomorph, is only 40% viable. We noticed that *sff* mutant flies with a null mutation of *white* (w^-) seemed to be more robust than their wild-type counterparts (w^+) so we assessed viability in both backgrounds. *sff*^{B22} and w^-;*sff*^{B22} embryos were collected, counted, and placed in a food vial. The number of individuals that pupated was counted, and the flies that eclosed were also counted and genotyped. *sff*^{B22} have a much lower survival rate (37%) than w^-;*sff*^{B22} (74.6%), whose survival is comparable to *OreR* and w^{1118} (**Table 3.1**). The lethal period is during late embryonic or larval stages. Therefore a mutation in *white* suppresses the lethality of *sff*^{B22}.

A mutation in *white* alters the N-linked glycan profile of sff^{B22} embryos

The *sff* mutation was first characterized by a reduction in anti-HRP staining (see chapter 2). The epitopes recognized by anti-HRP antibody constitute a family of difucosylated N-glycans. Wild-type embryos exhibit staining of the ventral nerve cord, peripheral nervous system, and a few non-neural tissues- the garland gland, posterior hindgut, and anal pads (**Figure 3.2A**). In sff^{B22} embryos, only faint staining of the axon scaffold of the nerve cord and garland gland is visible. By antibody staining, the expression of HRP-epitopes in sff^{B22} is not significantly affected by the absence of *white* (**Fig. 3.2B-C**). As HRP-epitopes account for less than 1% of the N-linked glycans in the embryo (Aoki et al., 2007) the full N-glycan profile of embryos was characterized by mass spectrometry.

Both sff^{B22} and $w^{-};sff^{B22}$ do not dramatically alter the most prevalent glycans- the high mannose, paucimannose, or structures extended only by GlcNAcT1 (GnT1). However, M5N2 and M4N2F are slightly decreased and M3N2 is slightly increased (**Fig. 3.3A,B**). Previous characterization of the total N-glycan profile of sff^{B22} embryos revealed a severe reduction in all but one of the HRP-epitope (difucosylated) structures. Also, minor complex structures, such as N2M3N2F, were significantly increased. Analysis of $w^{-};sff^{B22}$ revealed a rescue of the prevalence of M2N2F2 and NM3N2F2 (**Fig. 3.3C**). The only HRP-epitope structure to be slightly increased by sff^{B22}, N2M3N2F2, is actually significantly decreased in $w^{-};sff^{B22}$, compared to both w^{1118} and sff^{B22}. Interestingly, the *white* mutation alone increases N2M3N2F, N2M5N2, and N3M3N2F, just as is the case of the *sff* mutation alone (**Fig. 3.3D**). In both cases, w^{1118} and sff^{B22} independently increase the prevalence, but together the effect is mitigated. The results suggest that for some structures (like N3M3N2F), *white* can independently influence N-glycosylation, similarly to *sff*. Also, some glycan structures are Sff dependent but are influenced

Table 3.1 A mutation in *white* rescues the lethality associated with *sff*^{B22}

The number of pupal cases and adults arising from a defined number of embryos of *OreR*, w^{1118}, *sff*^{B22} and w^{-};*sff*^{B22} were determined. Percent expected for each genotype at each stage is calculated relative to the total number of initial embryos. Viabilities of *OreR*, w^{1118} and w^{-};*sff*^{B22} are comparable, while *sff*^{B22} results in significant lethality.

Parental Genotype	Embryos	Pupae	% of expected	Adult Males	Adult Females	Total Adults	% of Expected
OreR (w^{+})	457	373	82	181	183	364	80
w^{1118} (w^{-})	585	484	82	222	223	445	76
sff^{B22}	560	219	39	108	99	207	40
w^{-}; *sff*^{B22}	548	434	80	203	206	409	75

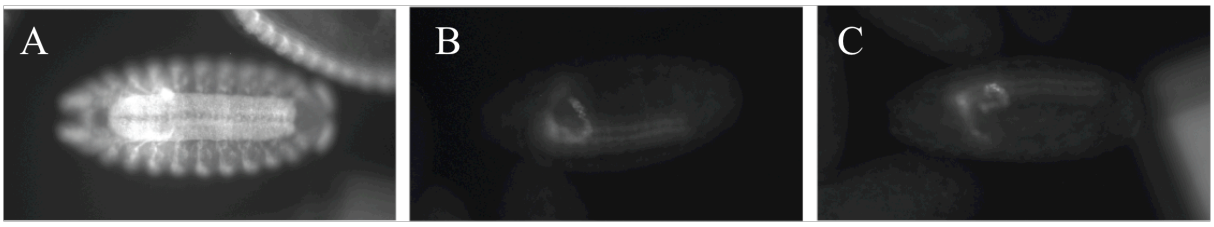

Figure 3.2 Anti-HRP staining of *sff*^{B22} embryos is not significantly affected by a mutation in *white*

A-C. Anti-HRP antibody staining of stage 16 *Drosophila* embryos. (**A**) Staining of *OreR* embryos reveals the full ventral nerve cord and peripheral nervous system, while *sff*^{B22} (**B**) and *w*$^{-}$;*sff*^{B22} (**C**) only exhibit garland gland staining and faint staining of the axon scaffold. Embryos were processed and stained together, and images were taken at the same exposure.

by White (such as NM3N2F2). For other structures, like N2M5N2F, White and Sff act independently, but also interact together.

When specific types of glycans are grouped together, the effects of *white* and *sff* mutations on the N-glycan profiles of embryos and larval brains become more apparent (**Table 3.4**). The *white* mutation alone reduces the prevalence of high mannose structures, while HRP-epitopes and complex glycans are increased, suggesting White's impact on the N-glycan profiles is a general shift towards more complex structures. The effects of the *sff* mutation are more specific, with a drastic decrease in HRP-epitopes and an increase in complex glycans. The double mutant has a decrease in high mannose and an increase in paucimannose, GlcNAcT1 products, and complex structures; HRP-epitopes are higher than the *sff* mutant alone. Therefore mutations in *white* and *sff* affect the N-glycan profile more than either of single mutations alone.

N-glycan analysis was also performed on 3rd instar larval brains, as Sff acts exclusively in neural cells (**Fig. 3.4**). Also, White has some neural-specific functions (Borycz et al., 2008; Campbell and Nash, 2001; Zhang and Odenwald, 1995). Complex glycans gain more prominence in larval brains, as high mannose structures as a group decrease (from 52.91% in embryos to 34.6% in larval brain) and M3N2F emerges as the most abundant glycan structure (**Fig. 3.4A, Table 3.4**). HRP-epitope structures are enriched ten fold in w^{1118} larval brains (9.42% of the total profile) compared to w^{1118} embryos (0.96%). HRP-epitopes are vastly reduced in the larval brains of $w^{-};sff^{B22}$ (3.67%), which is a sharper decrease than was seen in embryos (**Fig. 3.4C**). The reduction in HRP-epitopes in $w^{-};sff^{B22}$ causes an increase in the precursor stuctures M2N2F, M3N2F and NM3N2F. Complex structures, such as GalN2M3N2 and N2M3N2, are increased in w^{1118} larvae but the levels in $w^{-};sff^{B22}$ remain similar to those in the embryo (**Fig. 3.4D**). However as a group complex glycans are increased in $w^{-};sff^{B22}$ (4.28%)

A

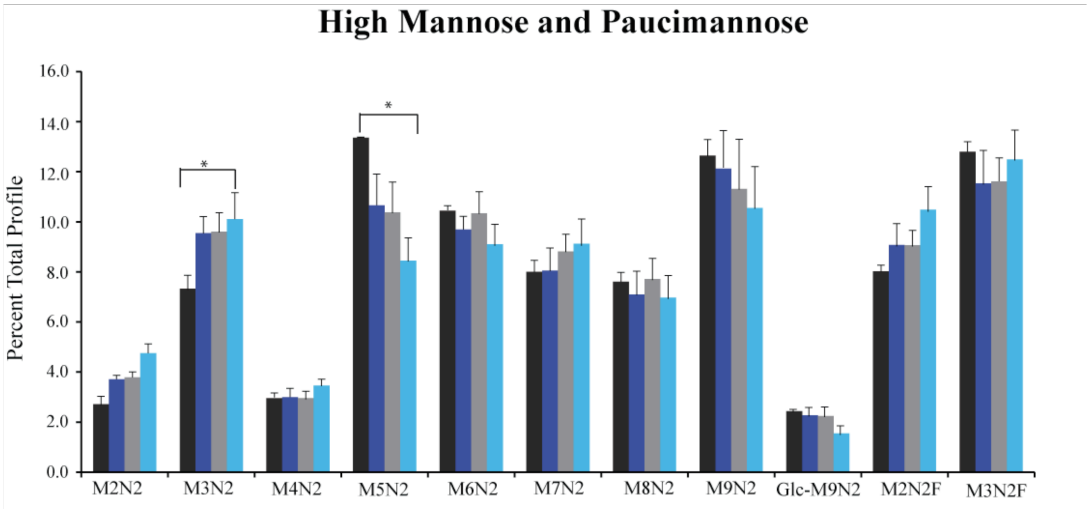
High Mannose and Paucimannose
Percent Total Profile
16.0
14.0
12.0
10.0
8.0
6.0
4.0
2.0
0.0
*
*
M2N2
M3N2
M4N2
M5N2
M6N2
M7N2
M8N2
M9N2
Glc-M9N2
M2N2F
M3N2F

B

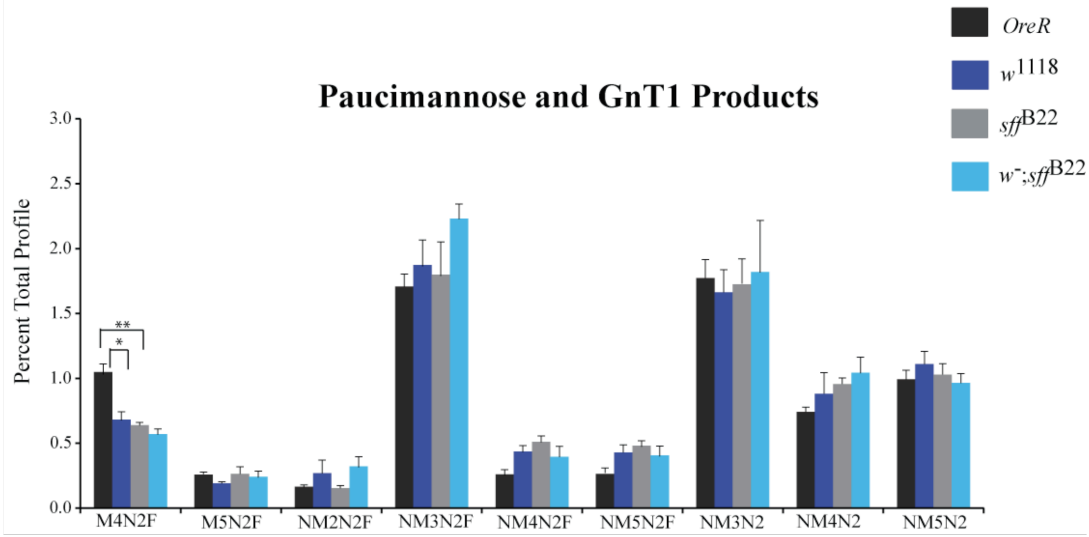
OreR
w1118
sffB22
w-;sffB22
Paucimannose and GnT1 Products
Percent Total Profile
3.0
2.5
2.0
1.5
1.0
0.5
0.0
**
*
M4N2F
M5N2F
NM2N2F
NM3N2F
NM4N2F
NM5N2F
NM3N2
NM4N2
NM5N2

C

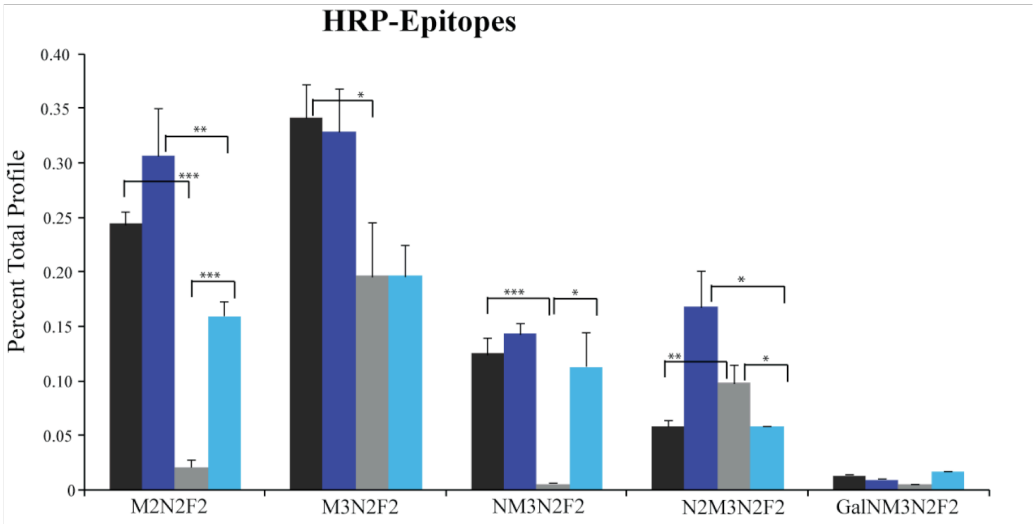
HRP-Epitopes
Percent Total Profile
0.40
0.35
0.30
0.25
0.20
0.15
0.10
0.05
0
M2N2F2
M3N2F2
NM3N2F2
N2M3N2F2
GalNM3N2F2

D

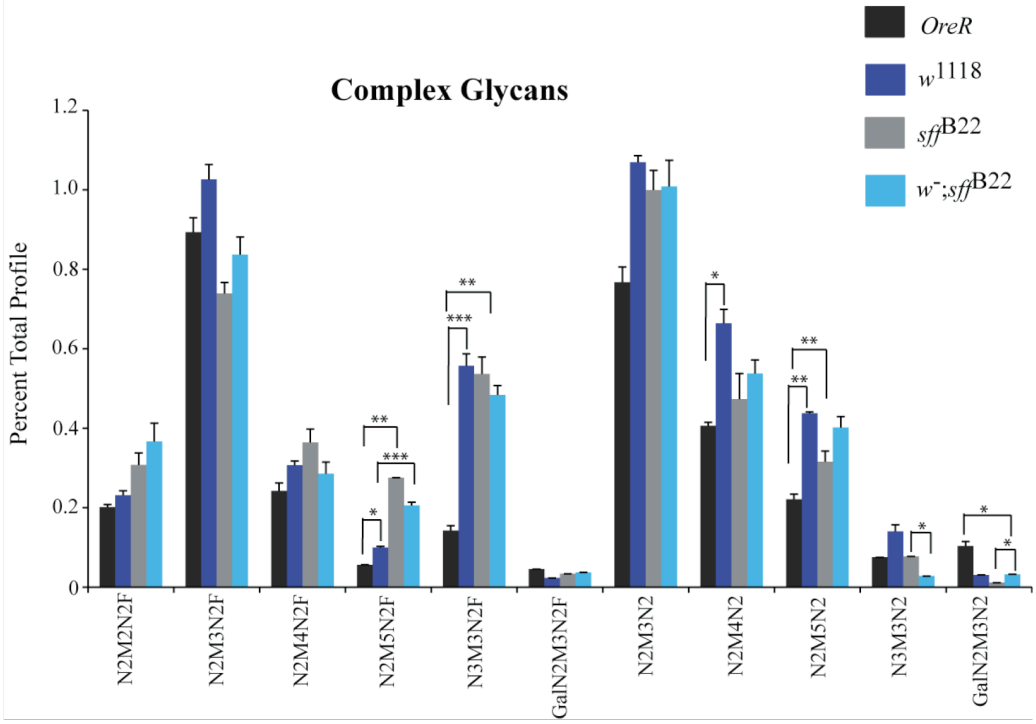
Complex Glycans
OreR
w1118
sff B22
w-;sff B22
Percent Total Profile
1.2
1.0
0.8
0.6
0.4
0.2
0
N2M2N2F
N2M3N2F
N2M4N2F
N2M5N2F
N3M3N2F
GalN2M3N2F
N2M3N2
N2M4N2
N2M5N2
N3M3N2
GalN2M3N2

Figure 3.3. A mutation in *white* influences N-glycan profiles alone and in conjunction with the *sff* mutation

Analysis of N-glycans obtained from embryos. Each glycan is expressed as the percent of the total profile and represents the mean ± standard deviation of three independent analyses (n=3, biological replicates). (**A**) High mannose and paucimannose structures are not significantly affected by the *white* mutation, although M3N2 is increased and M5N2 is decreased. (**B**) Paucimannose and glycans extended only by GlcNAcT1 are also not greatly affected by the *white* and *sff* mutations, except M4N2F. (**C**) HRP-epitope structures (difucosylated N-glycans) are significantly decreased in sff^{B22} embryos, save N2M3N2F2. Adding a mutation in *white* partially rescues the prevalence of M2N2F2, NM3N2F2, and N2M3N2F2 to levels comparable to wild-type (*OreR*). (**D**) The *white* mutation alone (w^{1118}) increases the prevalences of N2M3N2F, N2M4N2, and N2M5N2; the *sff* mutation alone also increases these structures. For some structures (GalN2M3N2, N3M3N2), the *white* mutant interacts with the *sff* mutant to affect prevalences. As with the *sff* mutation, the *white* mutation also influences the glycan processing steps occurring later (trans) Golgi compartments. (* $p < 0.05$, ** $p < 0.01$, *** $p < 0.005$).

Table 3.2. N-glycan profiles of *OreR*, w^{1118}, sff^{B22} and $w^{-};sff^{B22}$ embryos

Prevalences of the 42 N-glycans detected in the *Drosophila* embryo. Values represent the mean ± standard deviation of independent samples (n=3, biological replicates). Pictoral representations of each structure are colored based on the standard set by Consortium for Function Glycomics.

N-linked Glycan Profiles by NSI-LTQ/MS^n													
	Structure	Percent of Total Profile					Structure	Percent of Total Profile			
		OreR embryos	w^{1118}	sff^{B22}	$w^{-};sff^{B22}$			OreR embryos	w^{1118}	sff^{B22}	$w^{-};sff^{B22}$
1	M2N2	2.7±0.6	3.7±0.3	3.8±0.4	4.8±0.7	22	N2M4N2F^6	0.24±0.06	0.31±0.03	0.37±0.10	0.29±0.09
2	M3N2	7.3±1.0	9.6±1.2	9.6±1.4	10.1±1.8	23	N2M5N2F^6	0.06±0.02	0.10±0.01	0.28±0.04	0.21±0.02
3	M4N2	3.0±0.3	3.0±0.6	3.0±0.6	3.5±0.5	24	N3M3N2F^6	0.14±0.04	0.56±0.09	0.54±0.12	0.48±0.07
4	M5N2	13.4±0.5	10.7±2.1	9.8±1.6	8.5±1.6	25	GalN2M3N2F^6 and	0.04±0.02	0.02±0.00	0.03±0.01	0.04±0.00
5	M6N2	10.4±0.3	9.7±0.9	10.4±1.5	9.1±1.5	26	M2N2F2^{3,6}	0.24±0.02	0.31±0.08	0.02±0.01	0.16±0.02
6	M7N2	8.0±0.8	8.1±1.6	8.8±1.2	9.1±1.8	27	M3N2F2^{3,6}	0.34±0.05	0.33±0.07	0.20±0.09	0.20±0.05
7	M8N2	7.6±0.6	7.1±1.6	7.7±1.4	7.0±1.6	28	NM3N2F2^{3,6}	0.13±0.03	0.14±0.02	0.01±0.00	0.11±0.05
8	M9N2	12.6±1.1	12.6±2.6	11.4±3.4	10.6±2.9	29	GalNM3N2F2^{3,6}	0.01±0.00	0.01±0.00	<0.1	0.02±0.00
9	GlcM9N2	2.4±0.2	2.3±0.6	2.2±0.7	1.6±0.6	30	N2M3N2F2^{3,6} and	0.06±0.01	0.17±0.06	0.10±0.02	0.06±0.00
10	M2N2F$^{3 \text{ or } 6}$	8.0±0.4	9.8±1.6	9.1±1.2	10.5±1.7	31	NM2N2	0.08±0.02	0.04±0.00	0.02±0.01	0.05±0.00
11	M3N2F$^{3 \text{ or } 6}$	12.8±0.7	11.6±2.4	11.7±1.7	12.5±2.0	32	NM3N2	1.8±0.2	1.7±0.3	1.7±0.3	1.8±0.7
12	M4N2F^6	1.0±0.1	0.68±0.11	0.64±0.05	0.57±0.08	33	NM4N2	0.74±0.06	0.88±0.28	1.0±0.1	1.0±0.2
13	M5N2F^6	0.26±0.07	0.19±0.02	0.26±0.09	0.24±0.08	34	NM5N2	0.99±0.12	1.1±0.2	1.0±0.2	0.97±0.13
14	NM2N2F^6	0.16±0.03	0.27±0.18	0.15±0.03	0.32±0.14	35	GalNM3N2	0.31±0.02	0.04±0.00	0.07±0.02	0.07±0.00
15	NM3N2F^6	1.7±0.2	1.9±0.4	1.8±0.5	2.2±0.2	36	N2M3N2 and	0.77±0.12	1.1±0.1	1.0±0.2	1.0±0.2
16	NM4N2F^6	0.26±0.07	0.44±0.09	0.5±0.1	0.40±0.14	37	N2M4N2	0.41±0.02	0.66±0.10	0.48±0.20	0.54±0.10
17	NM5N2F^6	0.26±0.06	0.43±0.10	0.54±0.08	0.41±0.13	38	N2M5N2	0.22±0.04	0.44±0.01	0.32±0.08	0.40±0.08
18	GalNM3N2F^6	0.08±0.01	0.04±0.00	0.07±0.06	0.01±0.00	39	N3M3N2	0.08±0.01	0.14±0.05	0.05±0.04	0.03±0.00
19	Hex-GalNM3N2F^6 Hex	0.02±0.00	0.02±0.00	0.02±0.01	0.01±0.00	40	GalN2M3N2 and	0.10±0.04	0.03±0.00	0.01±0.01	0.03±0.00
20	N2M2N2F^6	0.20±0.02	0.23±0.03	0.31±0.09	0.37±0.14	41	SA-GalNM3N2	0.02±0.01	0.02±0.00	0.01±0.01	0.02±0.00
21	N2M3N2F^6 and	0.89±0.11	1.0±0.11	0.74±0.08	0.84±0.13	42	SA-GalN2M3N2 or	0.01±0.00	0.01±0.00	0.03±0.01	0.03±0.00

compared to w^{1118} (3.80%) (**Table 3.4**). Other structures, in particular N3M3N2, are dramatically down in w^{1118} larvae, but restored to embryonic levels in the *white;sff* double mutant. Altogether, these results demonstrate the mechanisms that limit greater N-glycan complexity in the embryo are lessened in the brains of 3rd instar larvae. The results also demonstrate that the effect of Sff and White on neural-specific glycosylation extends into later developmental stages.

A mutation in *white* influences the neuromuscular defect of sff^{B22} larvae

The *SAD* gene in *C. elegans*, *SAD-1*, was first identified based on morphological defects in the neuromuscular junction (NMJ) of chemosensory neurons (Crump et al., 2001). The boutons of *SAD-1* NMJs appear more diffuse and less organized than wild-type. Within these boutons, synaptic vesicles are not tethered correctly to the active zone and thus more vesicles are located farther away. Similar to *SAD-1*, the NMJs of *sff* mutants are also disrupted (**Fig. 3.5**). The larval neuromuscular junction in sff^{B22} larvae is extremely simple, with a significant reduction in branch and bouton numbers compared to wild-type. Mutation of *white* in an *sff* mutant background slightly increases the bouton number, but the number is still smaller than wild-type (**Fig. 3.5 A-E**). Interestingly, the boutons of $w^{-};sff^{B22}$ NMJs are significantly larger than wild-type; sff^{B22} boutons are slightly larger but the difference is not significant (**Fig. 3.5F**). Larger boutons, if they have increased synaptic machinery, may be compensation for fewer boutons, so as with viability, a mutation in *white* partially rescues the phenotype seen in sff^{B22}.

White influences the expression of *sugar-free frosting/SAD* kinase

The B22 mutation ablates a binding site for the transcription factor AP1. By *in situ* hybridization, the level of *sff/SAD* mRNA in the embryo is significantly decreased in the mutant,

A

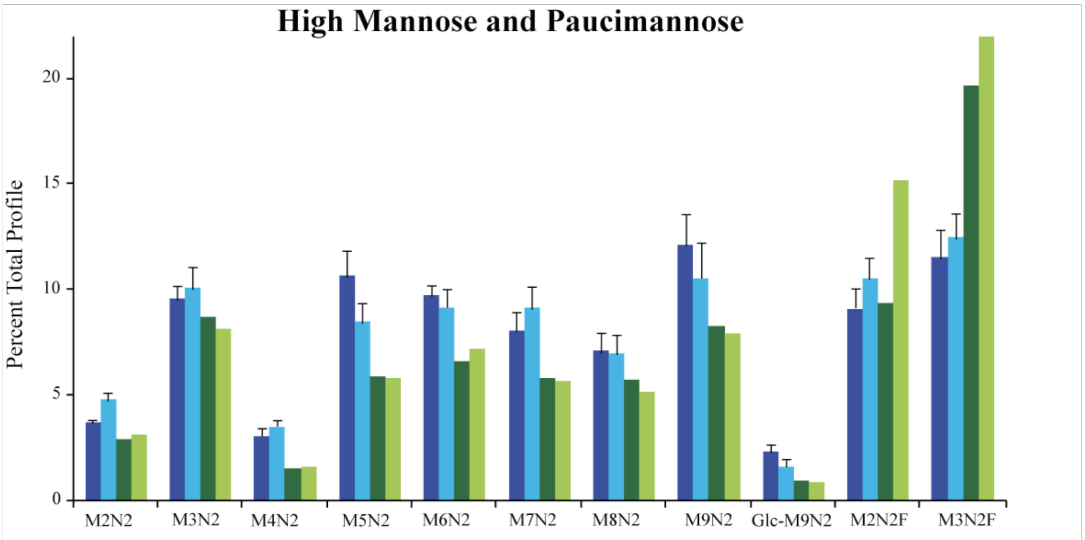
High Mannose and Paucimannose
Percent Total Profile
0
5
10
15
20
M2N2
M3N2
M4N2
M5N2
M6N2
M7N2
M8N2
M9N2
Glc-M9N2
M2N2F
M3N2F

B

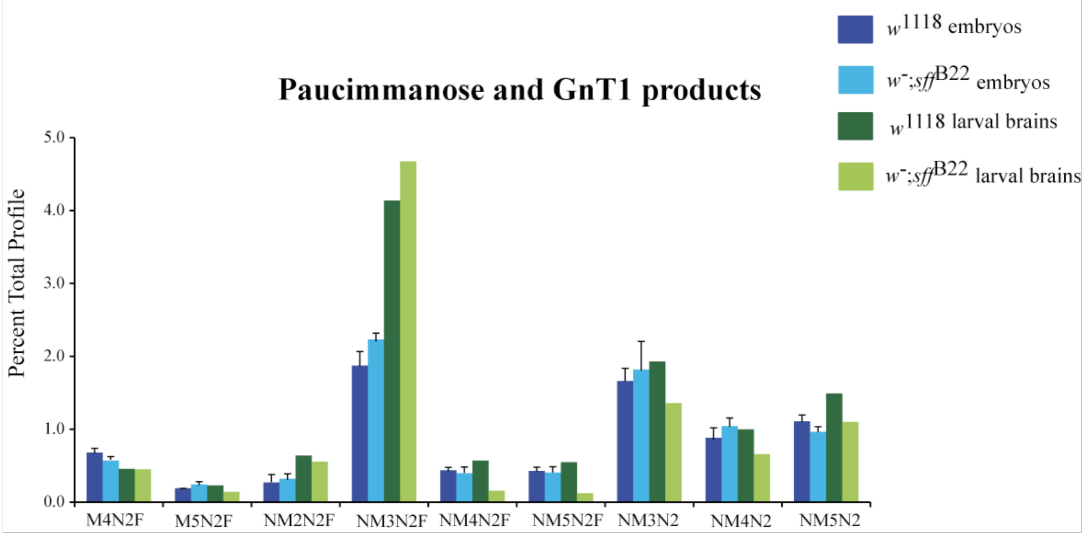
Paucimmanose and GnT1 products
Percent Total Profile
0.0
1.0
2.0
3.0
4.0
5.0
M4N2F
M5N2F
NM2N2F
NM3N2F
NM4N2F
NM5N2F
NM3N2
NM4N2
NM5N2
w1118 embryos
w-;sff B22 embryos
w1118 larval brains
w-;sff B22 larval brains

C

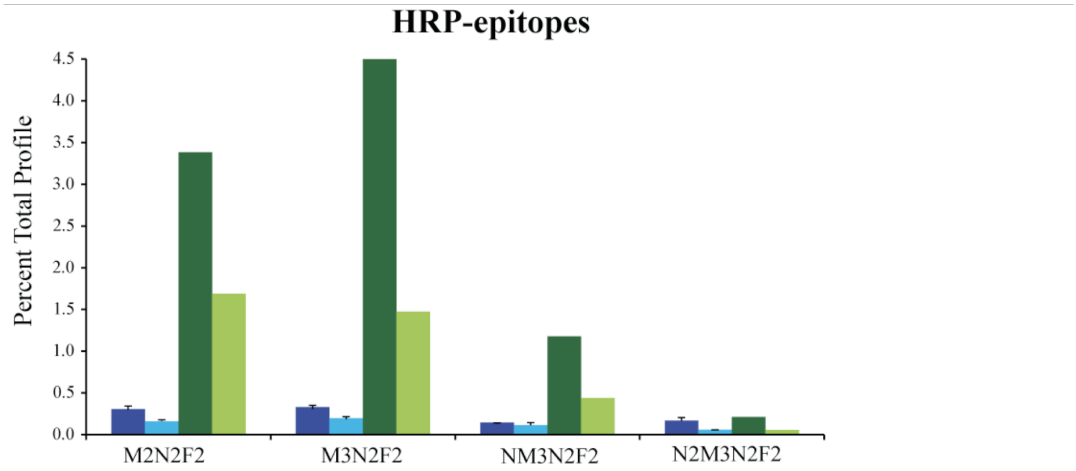
HRP-epitopes
Percent Total Profile
4.5
4.0
3.5
3.0
2.5
2.0
1.5
1.0
0.5
0.0
M2N2F2
M3N2F2
NM3N2F2
N2M3N2F2

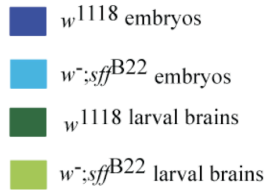
w1118 embryos
w-;sff B22 embryos
w1118 larval brains
w-;sff B22 larval brains

D

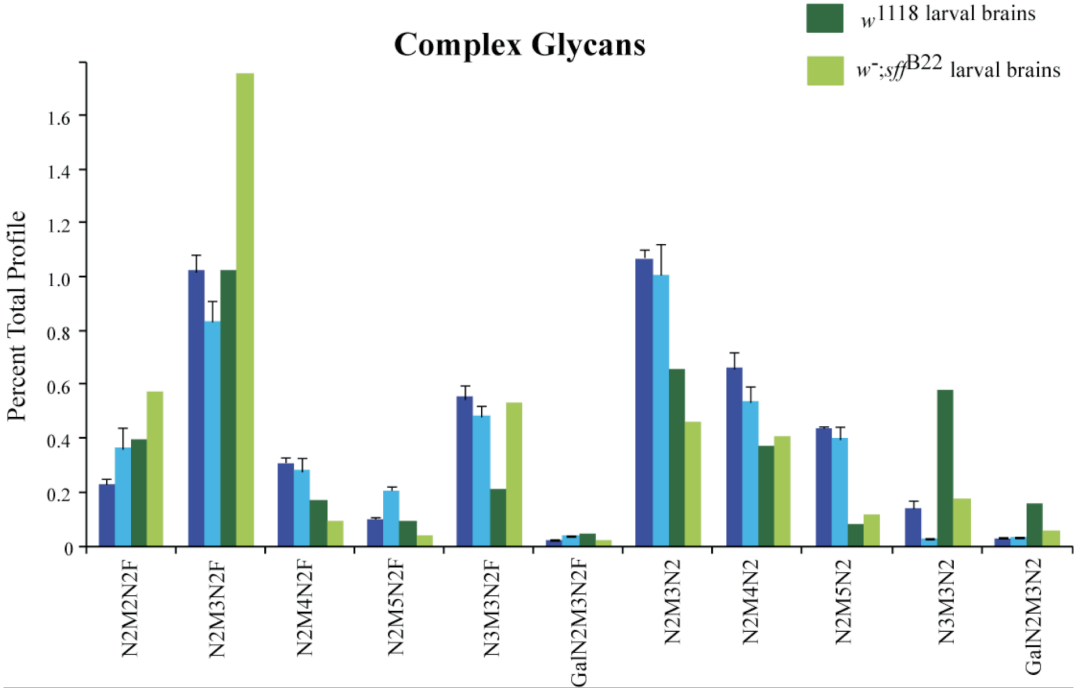
Complex Glycans
Percent Total Profile
1.6
1.4
1.2
1.0
0.8
0.6
0.4
0.2
0
N2M2N2F
N2M3N2F
N2M4N2F
N2M5N2F
N3M3N2F
GalN2M3N2F
N2M3N2
N2M4N2
N2M5N2
N3M3N2
GalN2M3N2

Figure 3.4. The N-glycome of larval brains is more complex and retains influence from Sff and White.
Comparison of the prevalences of N-glycans from embryos and 3rd instar larval brains. Values for embryos represent the mean ± standard deviation for three independent analyses (n=3, biological replicates); values for larval brains are from one analysis. (**A**) As a group, high mannose structures are decreased in larval brains and paucimannose structures (particularly M3N2F) are increased. (**B**) GlcNAcT1 products are similar in embryos and larval brains, except NM3N2F is greatly increased. w^{-};sff^{B22} larval brains have a decrease in NM4N2F and NM5N2F, a trend not seen in embryos. (**C**) Larval brains have an increase in HRP-epitopes and other complex structures compared to embryos. *White;sff* double mutants are more deficient in HRP-epitopes compared to w^{1118} in larval brains than in embryos. (**D**) N2M3N2F is greatly increased in the double mutant but several other complex structures (N3M3N2, N2M3N2) are decreased. The specific trends seen in embryos do not necessarily extend to larval brains but nevertheless it is clear that White and Sff still interact together to influence N-glycosylation beyond the embryonic stages of development.

Table 3.3. N-glycan profiles w^{1118} and $w^{-};sff^{B22}$ embryos and larval brains

Prevalences of the 42 N-glycans detected in the *Drosophila* embryo and larval brain. Values for embryos represent the mean ± standard deviation of independent samples (n=3, biological replicates). Values for larval brains are only one analysis. Pictoral representations of each structure are colored based on the standard set by Consortium for Function Glycomics.

N-linked Glycan Profiles by NSI-LTQ/MS^n											
	Structure	Percent of Total Profile					Structure	Percent of Total Profile			
		w^{1118} embryos	$w^{-};sff^{B22}$ embryos	w^{1118} L. brains	$w^{-};sff^{B22}$ L. brains			w^{1118} embryos	$w^{-};sff^{B22}$ embryos	w^{1118} L. brains	$w^{-};sff^{B22}$ L. brains
1	M2N2	3.7±0.3	4.8±0.7	2.9	3.1	22	N2M4N2F^6	0.31±0.03	0.29±0.09	0.17	0.10
2	M3N2	9.6±1.2	10.1±1.8	8.7	8.2	23	N2M5N2F^6	0.10±0.01	0.21±0.02	0.09	0.04
3	M4N2	3.0±0.6	3.5±0.5	1.5	1.6	24	N3M3N2F^6	0.56±0.09	0.48±0.07	0.21	0.54
4	M5N2	10.7±2.1	8.5±1.6	5.9	5.8	25	GalN2M3N2F^6 and	0.02±0.00	0.04±0.00	0.04	0.02
5	M6N2	9.7±0.9	9.1±1.5	6.6	7.2	26	M2N2F2^{3,6}	0.31±0.08	0.16±0.02	3.38	1.7
6	M7N2	8.1±1.6	9.1±1.5	5.78	5.7	27	M3N2F2^{3,6}	0.33±0.07	0.20±0.05	4.62	1.5
7	M8N2	7.1±1.6	7.0±1.6	5.69	5.1	28	NM3N2F2^{3,6}	0.14±0.02	0.11±0.05	1.2	0.44
8	M9N2	12.6±2.6	10.6±2.9	8.2	7.9	29	GalNM3N2F2^{3,6}	0.01±0.00	0.02±0.0	0.21	0.06
9	GlcM9N2	2.3±0.6	1.6±0.6	0.95	0.88	30	N2M3N2F2^{3,6} and	0.17±0.06	0.06±0.0	0.03	<0.1
10	M2N2F^3 or 6	9.8±1.6	10.5±1.7	9.3	15.2	31	NM2N2	0.04±0.0	0.05±0.00	0.14	<0.1
11	M3N2F^3 or 6	11.6±2.4	12.5±2.0	19.7	22.02	32	NM3N2	1.66±0.30	1.8±0.7	1.9	1.4
12	M4N2F^6	0.68±0.11	0.57±0.08	0.46	0.45	33	NM4N2	0.88±0.28	1.0±0.2	1.0	0.66
13	M5N2F^6	0.19±0.02	0.24±0.08	0.23	0.14	34	NM5N2	1.1±0.2	1.0±0.1	1.5	1.1
14	NM2N2F^6	0.27±0.18	0.32±0.14	0.64	0.55	35	GalNM3N2	0.04±0.00	0.07±0.00	0.11	0.03
15	NM3N2F^6	1.9±0.3	2.2±0.2	4.1	4.7	36	N2M3N2 and	1.1±0.1	1.0±0.2	0.66	0.46
16	NM4N2F^6	0.44±0.09	0.40±0.14	0.57	0.16	37	N2M4N2	0.66±0.10	0.54±0.10	0.37	0.41
17	NM5N2F^6	0.43±0.10	0.41±0.13	0.55	0.12	38	N2M5N2	0.44±0.01	0.40±0.08	0.08	0.12
18	GalNM3N2F^6	0.04±0.0	0.01±0.0	0.21	0.11	39	N3M3N2	0.14±0.05	0.03±0.00	0.58	0.18
19	Hex-GalNM3N2F^6 Hex	0.2±0.0	0.01±0.0	0.03	<0.01	40	GalN2M3N2 and	0.03±0.00	0.03±0.00	0.16	0.06
20	N2M2N2F^6	0.23±0.03	0.37±0.14	0.40	0.58	41	SA-GalNM3N2	0.02±0.0	0.02±0.00	0.02	0.02
21	N2M3N2F^6 and	1.0±0.1	0.84±0.13	1.0	1.8	42	SA-GalN2M3N2 or	0.01±0.0	0.3±0.00	0.02	0.03

Table 3.4 Summary of the effects of *white* and *sff* mutations on N-glycan profiles
Glycans from embryos and larval brains are grouped into classes-high mannose, paucimmanose, glycans that have been extended by GlcNAcT1, HRP-epitopes, and complex (modified by GlcNAcT 2 and/or 4). Values are the combined percent of the total profile for each group. For embryos, the three independent samples were calculated separately and then averaged. The *white* mutation alone affects the prevalences of glycans, shifting the profile to greater structural complexity. *White* and *sff* double mutant alters the N-glycan profile more significantly than either alone, resulting in a further shift towards more complex structures. However, HRP-epitopes remain below the levels of *OreR*, despite an increase over the *sff* mutation alone. w^{1118} larval brain profiles are deficient in the high mannose group and more prevalent in paucimannose, HRP-eptiopes, and GlcNAcT1 structures. w^{-};sff^{B22} larval brains show similar trends as their embryonic counterparts, with an increase in paucimannose and complex groups, but a more significant decrease in HRP-epitopes. Altogether, the balance between simplicity and complexity of N-glycan structures is altered by mutations in *sff* and *white*.

	OreR embryos	w^{1118} embryos	sff^{B22} embryos	w^{-};sff^{B22} embryos	w^{1118} L. brains	w^{-};sff^{B22} L. brains
High mannose	57.45±2.28	52.90±4.28	53.73±5.32	49.20±4.33	34.66	34.23
Paucimannose	32.18±2.48	34.75±5.30	34.95±4.32	38.65±6.11	41.29	49.02
GlcNAcT1	5.99±0.33	6.70±1.18	7.23±1.07	6.69±0.68	10.46	8.63
HRP-epitopes	0.79±0.07	0.96±0.06	0.33±0.12	0.55±0.09	9.42	3.67
Complex	2.98±0.19	4.00±0.22	3.57±0.35	3.73±0.71	3.80	4.28

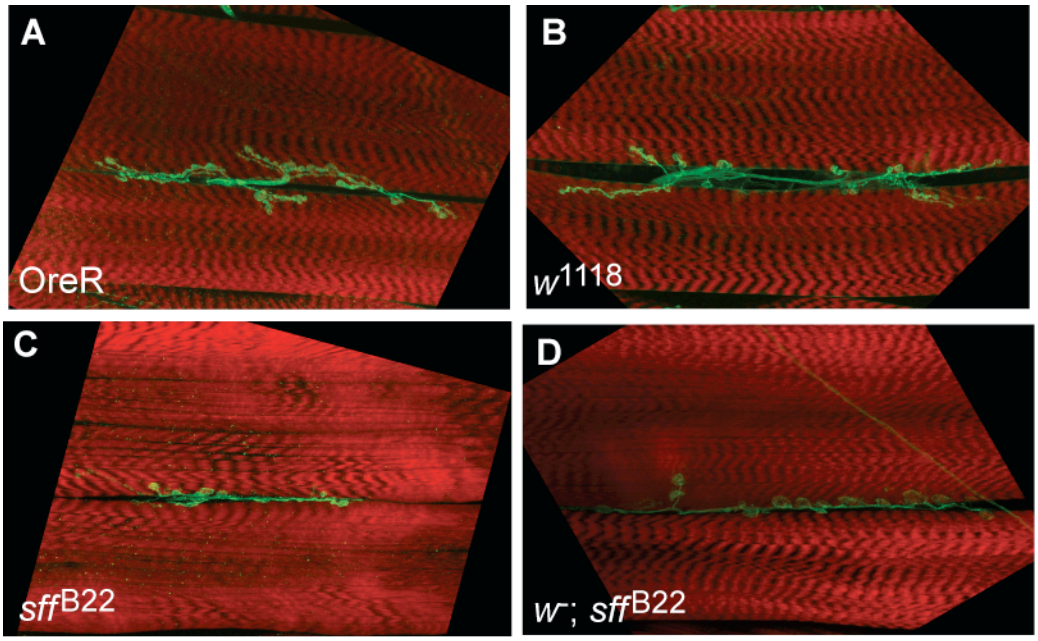
A
OreR
B
w1118
C
sffB22
D
w-; sffB22

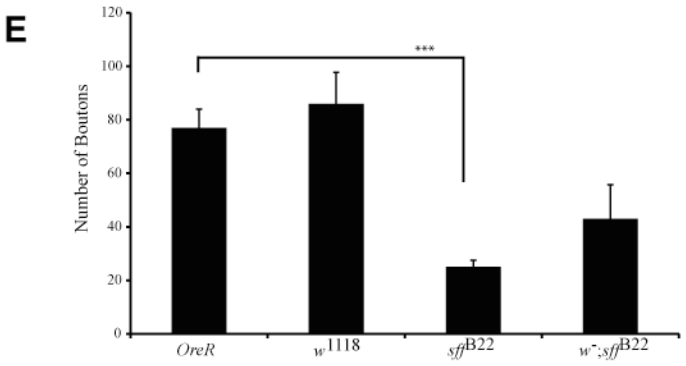
E
Number of Boutons
120
100
80
60
40
20
0
***
OreR
w1118
sffB22
w-;sffB22

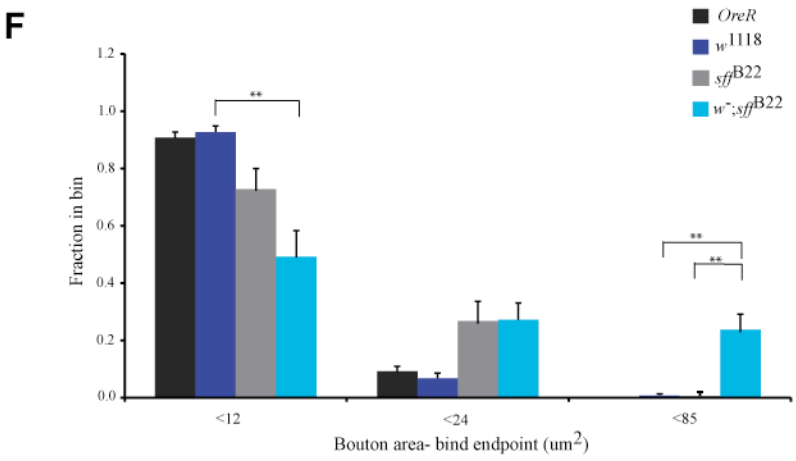
F
OreR
w1118
sffB22
w-;sffB22
Fraction in bin
1.2
1.0
0.8
0.6
0.4
0.2
0.0
**
**
**
<12
<24
<85
Bouton area- bind endpoint (um2)

Figure 3.5. A mutation in *white* increases bouton size of sff^{B22} NMJs
A-D. Confocal images of 3rd instar larval 6/7 NMJs stained with anti-HRP antibody (green and TRITC phalloidin (red). Note the extensive branching and many small boutons seen in *OreR* (**A**) and w^{1118} (**B**). *Sff* mutants (**C**) have fewer branches and boutons. $w^{-};sff^{B22}$ NMJs (**D**) have less branching and the boutons appear larger. (**E)** Quantification of the number of boutons per NMJ. The number of boutons in $w^{-};sff^{B22}$ is not significantly different from wild-type or sff^{B22}. (**F**) Quantification of bouton size. Boutons were grouped into bins based on size. $w^{-};sff^{B22}$ boutons are significantly larger than wild-type and sff^{B22}. For *OreR* and w^{1118} n=4 NMJs, sff^{B22} n=11, $w^{-};sff^{B22}$ n=5 NMJs. (**p <0.01, ***p<0.001).

hybridization of *sff*/SAD mRNA in a double mutant background (**Fig. 3.6**). Compared to sff^{B22}, mRNA expression was significantly higher in $w^{-};sff^{B22}$. Therefore *white* decreases the severity of the sff^{B22} phenotype by increasing *sff* expression.

Acute administration of antidepressants rescues the behavioral defect associated with sff^{B22}

The defect seen in the larval NMJ of sff^{B22} suggests locomotion could be compromised by altered NMJ morphology. *Sff* mutant adults exhibit a deficiency in their geotaxis ability, or the movement away from gravity. When a wild-type fly is tapped to the bottom of its vial it will quickly crawl to the top of the vial. This behavior was quantified in *sff* mutants by timing how long it takes a single fly to reach a designated height after being sent to the bottom of the vial. The median time for wild-type is around 10 seconds and 81% of flies reach the height in 15 seconds (**Fig. 3.7**). Comparatively, 36% of sff^{B22} flies complete the same task in 15 seconds, when raised at 25°C. At 18°C, the number drops to 21%. The locomotor activity of $w^{-};sff^{B22}$ flies is slightly better than sff^{B22} at 25°C, with 42.3% reaching the height within 15 seconds. However at 18°C the opposite is true with $w^{-};sff^{B22}$'s value at 12.3% (compared to 21% for sff^{B22}). Since *sff* activity is more severely affected at the lower temperature, any alleviation by removal of *white* is not enough to rescue the behavioral defect. One of the substrates for transport by white is tryptophan, a precursor for the production of serotonin (5-HT). Mutants in *white*, as well as *scarlet* and *brown*, have been shown to have reduced levels of serotonin, dopamine, and histidine in the adult head (Borycz et al., 2008). To assess whether *sff* mutants are deficient in one or more biogenic amines, we administered a monoamine oxidase inhibitor, phenelzine, and tested geotaxis ability after treatment. sff^{B22} flies were dramatically faster after treatment, at both 25° and 18°C (**Fig. 3.7**). At 18°C, prior to treatment 60.1% of flies had not reached the designated height after 120 seconds. After treatment, 32.5% of flies remained, and

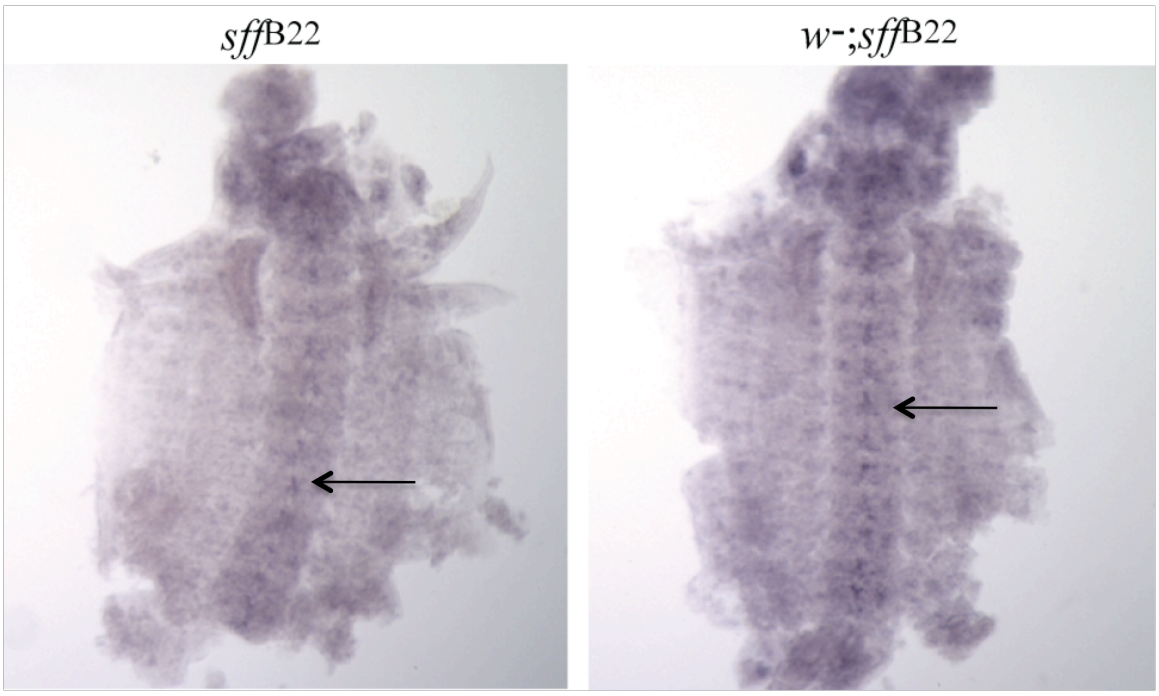

Figure 3.6. A mutation in *white* rescues *sff/SAD* mRNA expression in sff^{B22}
In situ hybridization with antisense probe for *sff/SAD* in stage 13 embryos. Embryos were processed and probed at the same time, and dissected along the midline to reveal the ventral nerve cord. The *sff* mRNA level in the ventral nerve cord is higher in $w^{-};sff^{B22}$ when compared to an age-matched sff^{B22}. Note the increased expression in the midline glial cells (arrows), indicating that *white* can influence the expression of *sff*.

the median climbing time went from 120 seconds to only about 20 seconds. Acute administration of flies with a serotonin reuptake inhibitor, imipramine, gave similar results. However, the administration of imipramine to *w⁻;sff*^{B22} flies did not have any affect on their geotaxis ability, at either temperature. Therefore the locomotor activity of *sff*^{B22} flies is sensitive to the action of biogenic amines, an effect that can be blocked with a white deficiency.

sff^{B22} has a reduction in the level of serotonin in the adult brain

Administration of drugs that raise biogenic amine levels rescued the behavior of *sff*^{B22} adults, suggesting they are deficient in these molecules. To determine the levels of biogenic amines in the *sff* mutant, we performed high performance liquid chromatography (HPLC) with electrochemical detection. The level of serotonin in the adult brains of *sff*^{B22} is only 70.5±3.6% that of wild-type (n=3) (**Fig. 3.8**). Levels of dopamine, tyramine, and octopamine were not altered. A reduction in serotonin levels is consistent with the rescue of adult behavior by administration of a serotonin reuptake inhibitor or monoamine oxidase inhibitor.

Biogenic amines influence neural glycosylation patterns in the embryo

Thus far, the results have demonstrated that a mutant with a defect in neural-specific N-glycan expression also has a deficiency of serotonin, revealing a previously unknown link between glycosylation and biogenic amines. During the course of mapping the *sff*^{B22} mutation, several P-elements in a region predicted by recombination to contain the *sff* locus were screened. With low penetrance, one P-element line, Pbac[PB]Trhc^{01440}, when crossed to *sff*^{B22}, yielded embryos that lacked anti-HRP staining (**Fig. 3.9**). The P-element in Pbac[PB]Trhc^{01440} is inserted into the 5' region of *Tryptophan hydroxlyase* (*Trh*), which catalyzes the rate-limiting reaction in the synthesis of serotonin. Therefore, Trh may be interacting with Sff/SAD through altered biogenic amine levels to influence neural glycosylation.

25°C

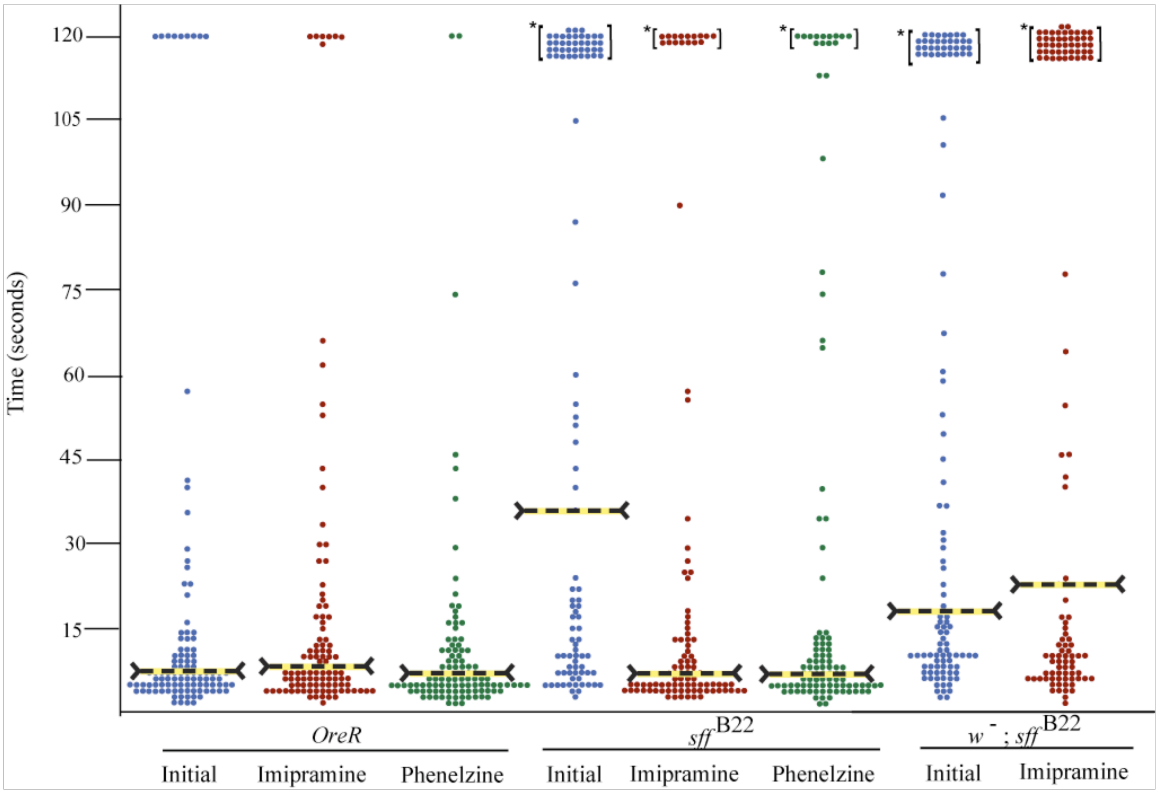
Time (seconds)
120
105
90
75
60
45
30
15
*
*
*
*
*
OreR
sff B22
w - ; sff B22
Initial
Imipramine
Phenelzine
Initial
Imipramine
Phenelzine
Initial
Imipramine

18°C

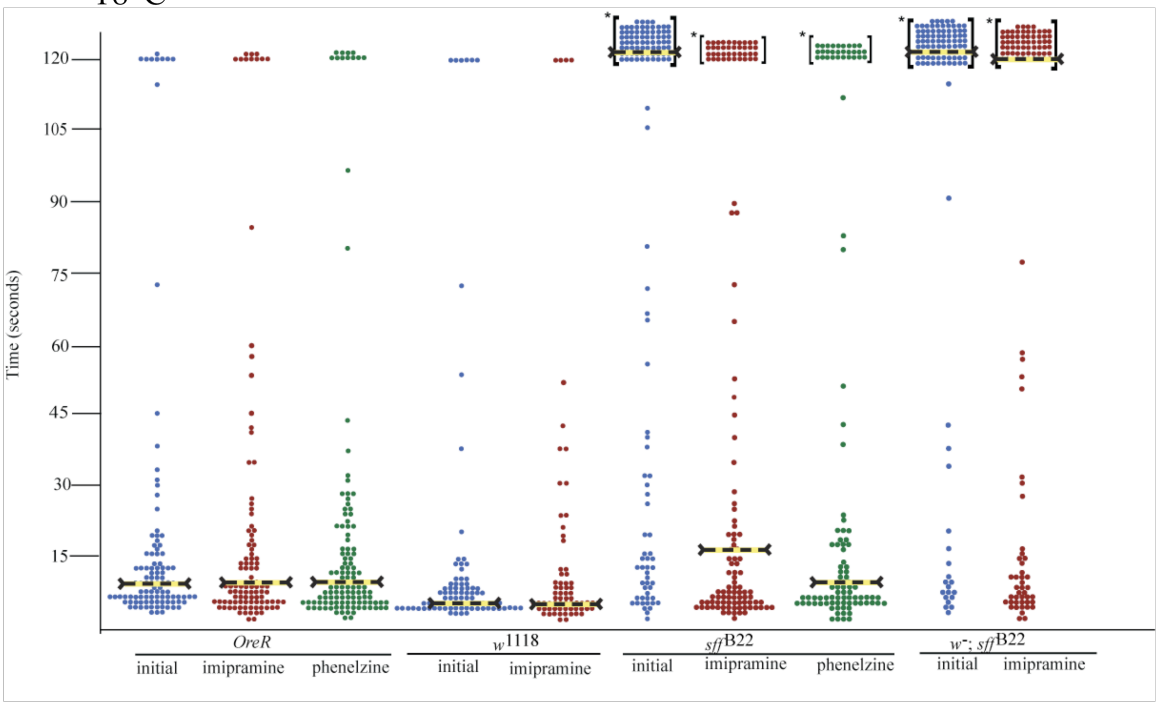
Time (seconds)
120
105
90
75
60
45
30
15
*
*
*
*
*
OreR
w1118
sff B22
w-; sff B22
initial
imipramine
phenelzine
initial
imipramine
initial
imipramine
phenelzine
initial
imipramine

Figure 3.7 Acute administration of antidepressants rescues the behavioral phenotype of *sff*^{B22} but not *w*$^{-}$;*sff*^{B22}

Geotaxis test of flies raised at 25°C or 18°C. Each dot on the graph represents the climbing time of a single adult male. Flies were given up to 120 seconds to climb a height of 3 cm. Those flies that did not finish in 120 seconds are bracketed. The yellow dashed line indicates the median climbing time. Flies were tested before (initial) and after administration of a monoamine oxidase inhibitor, phenelzine, or a serotonin reuptake inhibitor, imipramine. Administration of either drug to *sff*^{B22} rescued their climbing ability at both temperatures. *w*$^{-}$;*sff*^{B22} flies did not respond to imipramine at either temperature. At 25°C *OreR* initial and impramine n=105, phenelzine n=104; *sff*^{B22} initial and impramine n=100, phenelzine n=104; *w*$^{-}$;*sff*^{B22} n=112. At 18°C *OreR* n=103 for initial and imipramine, 120 for phenelzine; *w*^{1118} initial n=87, imipramine n=70; *sff*^{B22} initial and imipramine n=123, phenelzine =106; *w*$^{-}$;*sff*^{B22} initial n=106, imipramine n=116.

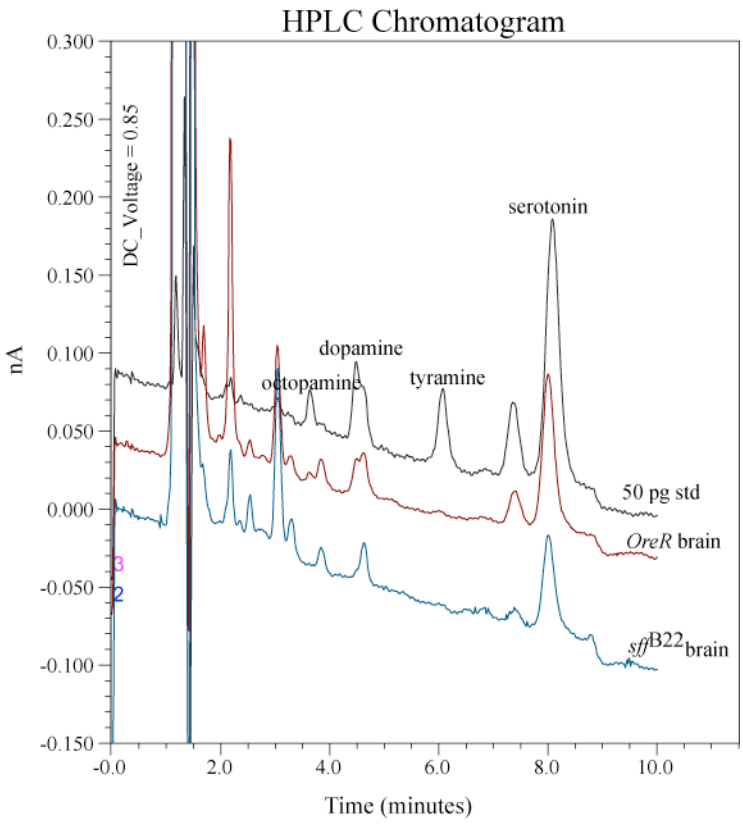

Figure 3.8. *sff*^{B22} has reduced levels of serotonin in the adult brain
Chromatogram from an HPLC analysis of the biogenic amines octopamine, dopamine, tyramine and serotonin from the equivalent of two 8 day old brains of adults raised at 18°C. A standard (black) was run prior to the samples, which included 50pg each of octopamine, dopamine, tyramine and serotonin. *sff*^{B22} (blue) has a reduced level of serotonin compared to *OreR* (red).

Since pharmacological treatment of *sff*^{B22} adults rescued their behavior, we wondered whether treatment of embryos could rescue their glycosylation phenotype, in particular the reduction in HRP-epitope expression. Newly laid embryos were incubated with phenelzine and allowed to mature. Embryos were then stained with anti-HRP antibody. The staining of *sff*^{B22} embryos increased following treatment (**Fig. 3.10**). The staining did not expand beyond the scaffold of the nerve cord but the intensity of the staining was increased. Treatment of wild-type embryos also increased anti-HRP staining levels. Treatment of embryos was for a very short time (15 minutes) very early in embryonic development, before the appearance of HRP-epitope and before expression of *sff*. Therefore an increase in biogenic amines can induce sustained changes in glycosylation patterns. It remains to be determined whether biogenic amine signaling can affect *sff* expression levels.

DISCUSSION

The data presented here introduce a genetic interaction between *sugar-free frosting* and *white* in both glycosylation and neural phenotypes. Also, serotonin levels are deficient in *sff*^{B22} and that raising biogenic amine levels rescues their adult behavior. Moreover, altering biogenic amine levels influences HRP-epitope expression in the embryo.

Also presented here is the first characterization of the N-glycan profile from 3rd instar larval brains. Compared to embryos, the most striking difference is a great enrichment of anti-HRP epitopes in larval neural tissue. Since HRP-epitopes are almost exclusively found on neuronal proteins this enrichment is not surprising. The precursors for HRP-epitope structures like M3N2F and NM3N2F, are also greatly increased. However, the prevalence of HRP-epitopes still remains small compared to the prevalences of precursor structures, indicating that there are

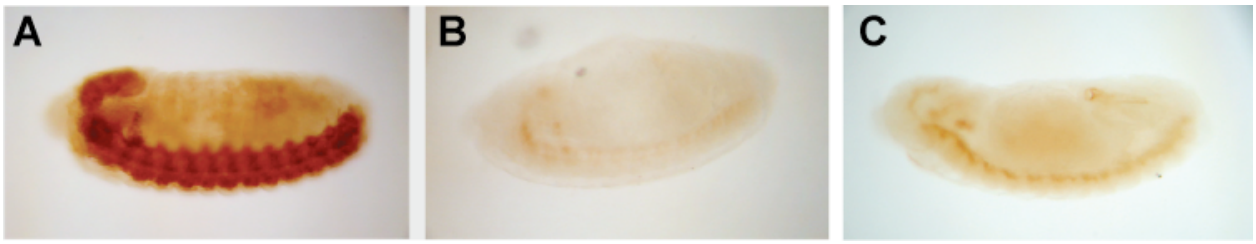

Figure 3.9. *Tryptophan hydroxylase* interacts with *sff*
A-C. Anti-HRP staining (peroxidase-conjugated secondary antibody with DAB precipitate) of stage 13 embryros. Staining of *OreR* (**A**) is strong in the ventral nerve cord. However, staining is barely visible in sff^{B22} (**B**). (**C**) sff^{B22} crossed to Pbac[PB]Trhc^{01440}, a P-insertion in *tryptophan hydroxylase*, gave a small number of embryos (25%) that resemble *sff* homozygotes. Therefore *tryptophan hydroxylase* genetically interacts with *sff*, supporting the hypothesis that serotonin helps modulate neural-specific glycan expression in the embryo.

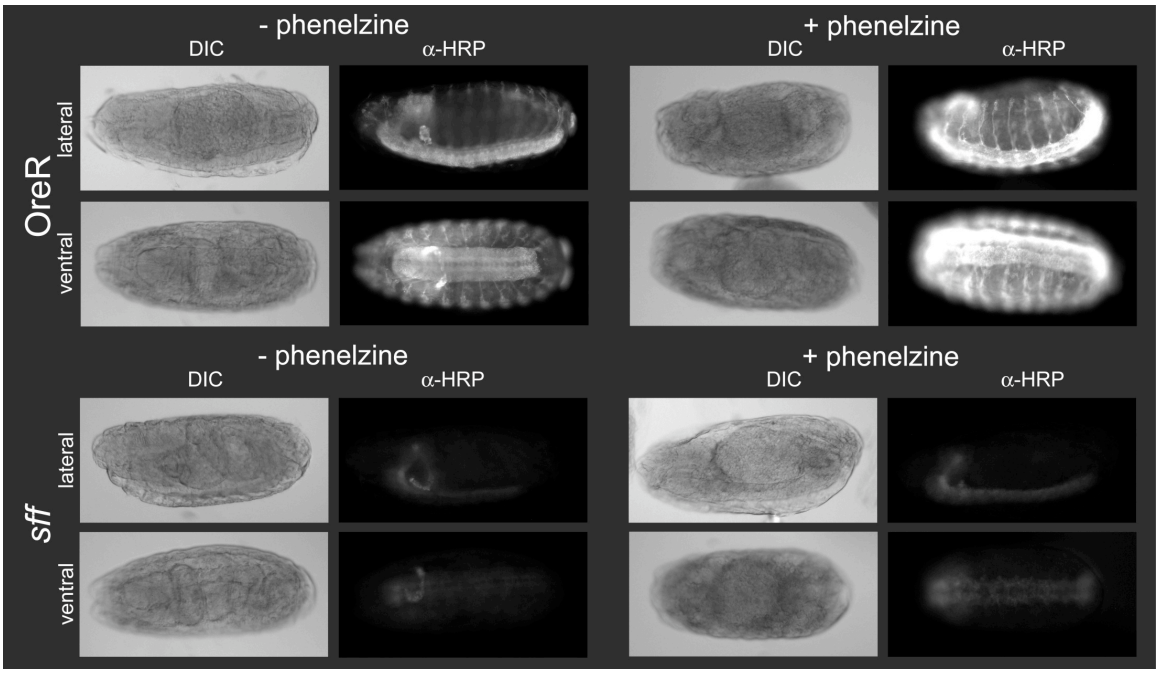

Figure 3.10. Biogenic amines contribute to the regulation of HRP-epitope expression
Nomarski (DIC) and fluorescent images of embryos stained with anti-HRP antibody with and without treatment with a monoamine oxidase inhibitor, phenelzine. Embryos were incubated with drug for a brief time soon after birth. Embryos were then aged 12 hours and stained with antibody. The upper panel illustrates that treatment of *OreR* embryos increases anti-HRP staining (upper right panel) as compared to no treatment (upper left panel). Similarly, treatment of *sff* mutant embryos (bottom panel) increases the staining of the axon scaffold of the ventral nerve cord (bottom right panel).

still constrictions in place in that limit further elaboration (fused lobes or FucTA for example). Complex glycans, although higher than in embryos, still remain the least prevalent, indicating the antagonistic balance between fused lobes and GlcNAcT 2/4 still remains in the larval brain as it does in the embryo.

The relationship between White and Sugar-free frosting is complex

White has emerged as a new regulator of tissue-specific glycan expression, and may interact with Sff to modulate its effects on neural-specific glycan expression in *Drosophila*. The majority of the most abundant N-glycans remain relatively unchanged in *white* or *sff* mutant backgrounds, indicating their influence is on the later processing pathways, those involving FucTA, GlcNAcT 2 and 4. At least one HRP-modified protein, Fasciclin II, is more associated with the trans Golgi in the *sff* mutant than in wild-type (see chapter 2). The effect of White on the N-glycan profile indicates that White's role may be similar to that of Sff. However, White is an ABC transporter, not a traffic-modulating kinase so its impact on glycan processing must be indirect. One possibility is that White, in complex with Brown, transports guanine, a precursor for GTP (Lloyd et al., 2002). GTP serves as the precursor for the sugar donors GDP-mannose and GDP-fucose, providing a direct link to the flux of glycan processing pathways. Nucleotide sugar levels have not yet been characterized in wild-type or mutant tissues of *Drosophila*.

Another intriguing link between glycosylation and White involves the gene *sugarless* (*sgl*). *Sugarless* encodes UDP-glucose dehydrogenase, which catalyzes the formation of UDP-D- glucuronic acid (UDP-GlcA) from UDP-D- glucose. Ablation of *sugarless* expression by P-element insertion affects the expression of *white* (Benevolenskaya et al., 1998). The P-element insertion line, *l(3)05007*, darkens the eye color of a mutant *white* allele, *apricot* (w^a). Sgl regulates *white* at the transcript level, as *l(3)05007* mutant larvae have a reduction in *white*

mRNA. Interestingly, the mutation also affects the transcript levels of *scarlet* and *brown*. It is suggested that Sgl may affect *white* expression through signaling pathways involving Wingless (wg) and/or Hedgehog (hh), both involved in *Drosophila* eye development. UDP-GlcA is a building block of glycosaminoglycans (GAGs) such as heparan sulfate, and a reduction in GAGs has been shown to negatively affect Wg signaling (Binari et al., 1997; Haerry et al., 1997). Therefore Wg and Hh signaling pathways may impact the expression of *white*, and perhaps tissue-specific N-glycan expression.

Both *white* and *sff* mutants have a reduction in serotonin levels and similar affects on N-glycan prevalences, but the phenotypes of the double mutant do not exacerbate the single mutant phenotype of sff^{B22} (Borycz et al., 2008). Instead, the *white* mutation partially rescues the *sff* mutation (summarized in **Table 3.5**). There is an entire class of eye color genes that regulate the trafficking and sub-cellular localization of the proteins involved in pigment synthesis, termed the granule group genes (Lloyd et al., 2002). These genes include *garnet*, *claret*, *carnation*, *purple*, *pink*, *rose*, and *ruby*, among others. Garnet has homology to the δ subunit of AP-3 adaptin complex, which is involved in vesicle transport from the trans-Golgi to lysosomes and other organelles like pigment granules (Ooi et al., 1997; Simpson et al., 1997). Garnet mutants, like *white* over-expression mutants, also exhibit homosexual male courtship, indicating this phenotype results from mis-sorting of White (Lloyd et al., 2002).

Sff drives neural-specific glycosylation in the *Drosophila* embryo by modulating vesicular traffic in Golgi compartments. In the *sff* mutant, there is a shift of at least one substrate to associate more with trans-Golgi compartments (see chapter 2). Sff/SAD kinase also modulates synaptic vesicle tethering at the cytomatrix active zone (Crump et al., 2001; Inoue et al., 2006). These vesicles arise from the trans-Golgi network, as do pigment granules

Table 3.5 Summary of the influence of the *white* mutation on the phenotypes of *sff*^{B22}
The white mutation has the greatest affect on the viability, N-glycan profile, and *sff* mRNA levels of the *sff* mutant. The *white* mutation has a lesser effect on the NMJ morphology and locomotor ability of *sff* mutants, although it does prevent rescue by drug.

Phenotype	OreR	sff^{B22}	w^{-};sff^{B22}	Rescue
viability (%)	80	40	75	yes
HRP-epitopes (% total profile)	0.785	0.33	0.55	partial
bouton number	77±25	16±10	43±33	minimal
boutons <85 um^2	0%	0.50%	23.70%	partial?
Geotaxis 25^{o}C (% under 15s)	81	36	42.3	minimal
Geotaxis 18^{o}C (% under 15s)	72.8	21	12.3	no
rescue by imipramine		yes	no	no
sff mRNA expression	normal	greatly reduced	slightly reduced	partial

(Borycz et al., 2008; Regnier-Vigouroux and Huttner, 1993; Shoup, 1966). Based on the effects of *white* on *sff* mutants, it is conceivable that Sff may also be involved in the trafficking of White. AP-3 coats vesicles that transport White and in neurons AP-3 is also a component of synaptic vesicles (Newell-Litwa et al., 2007). Since sff/SAD is involved in the transport of synaptic vesicles and vesicles at the Golgi, it is also possible that sff/SAD also aids the transport of other vesicles, like those that carry White. It is possible that the *sff* mutant causes White to be trafficked inappropriately, exacerbating the phenotypes. This hypothesis is supported by observations that removing *white* alleviates some of the defects seen in sff^{B22}. Granted, *sff* is only expressed in neural cells, so only neurally-expressed *white* would be affected. The defect is not enough to yield a change in eye color. However, given emerging evidence for a requirement of White in neural cells, mis-sorting of White by Sff could certainly impact White's neural functions.

There are some hypotheses of how White contributes to neural function. For example, a downstream product of White function, GTP, is crucial to the functions of small GTP-ases in vesicle recycling (Lloyd et al., 2000). Also, the precursor for drosopterins, dihydroneopterin triphosphate (derived from guanine), is converted to tetrahydrobiopterin, which serves is an essential cofactor for Tyrosine and Tryptophan hydroxylases (Krishnakumar et al., 2000). Therefore guanine transport by White may affect the synthesis of biogenic amines. *White* and *brown* null mutants are less sensitive to enflurane, which is a volatile general anesthetic (Campbell and Nash, 2001). Independent of light perception, *white* and *brown* mutants are more motile after exposure to enflurane than wild-type flies. The authors posit that White/Brown transport aids in neuromuscular function (Campbell and Nash, 2001). In an *sff* mutant background, a mutation in *white* does not significantly influence locomotor ability. However,

neuromuscular junction morphology is affected. The NMJ is primarily glutamatergic, although biogenic amines have been implicated to also be involved based on phenotypes associated with a mutant vesicular monoamine transporter (Simon et al., 2009). Therefore, it is unclear whether White's role at the NMJ is dependent upon its transporter function. Given that White can affect the transcript levels of *sff/SAD*, White's neural function may be attributed, at least in part, to the modulation of signaling pathways that influence Sff/SAD activity.

Biogenic amine signaling in the HRP-epitope expression pathway

It has been reported that an ectodermally expressed Toll-like receptor, Tollo, regulates anti-HRP epitope expression (Seppo et al., 2003). Sff acts on the other side of the pathway, in the neural cell. Based on the data presented here, we hypothesize that the signal between cells is a biogenic amine (**Fig. 3.11**). Pharmacological rescue of some anti-HRP staining in *sff* mutant embryos indicates action by monoamines lies upstream of *sff*. The close proximity of Tollo-expressing ectodermal cell to the HRP-epitope decorated neural cell does not rule out the paracrine action of a small molecule, such as a monoamine, as the signal of communication.

That a biogenic amine like serotonin would function in direct concert with a Toll-like receptor has already been suggested in vertebrates. Enterochrommafin cells in the intestinal tract, which are one of the major sites of serotonin synthesis, increase their secretion of serotonin during mucosal inflammation (Kidd et al., 2009). IL-1β and lipopolysaccharide (LPS) stimulated serotonin secretion in enterochrommafin cells isolated from patients with Crohn's disease, an effect found to be mediated by TLR4 and IL-1β. Symptoms resulting from bacterial infection, such as loss of appetite, are also thought to be mediated by serotonin (Langhans, 2007). During the acute-phase response to microbial products like LPS, the cytokines produced through the action of TLR4 and CD14 signal across the blood-brain barrier to serotonergic

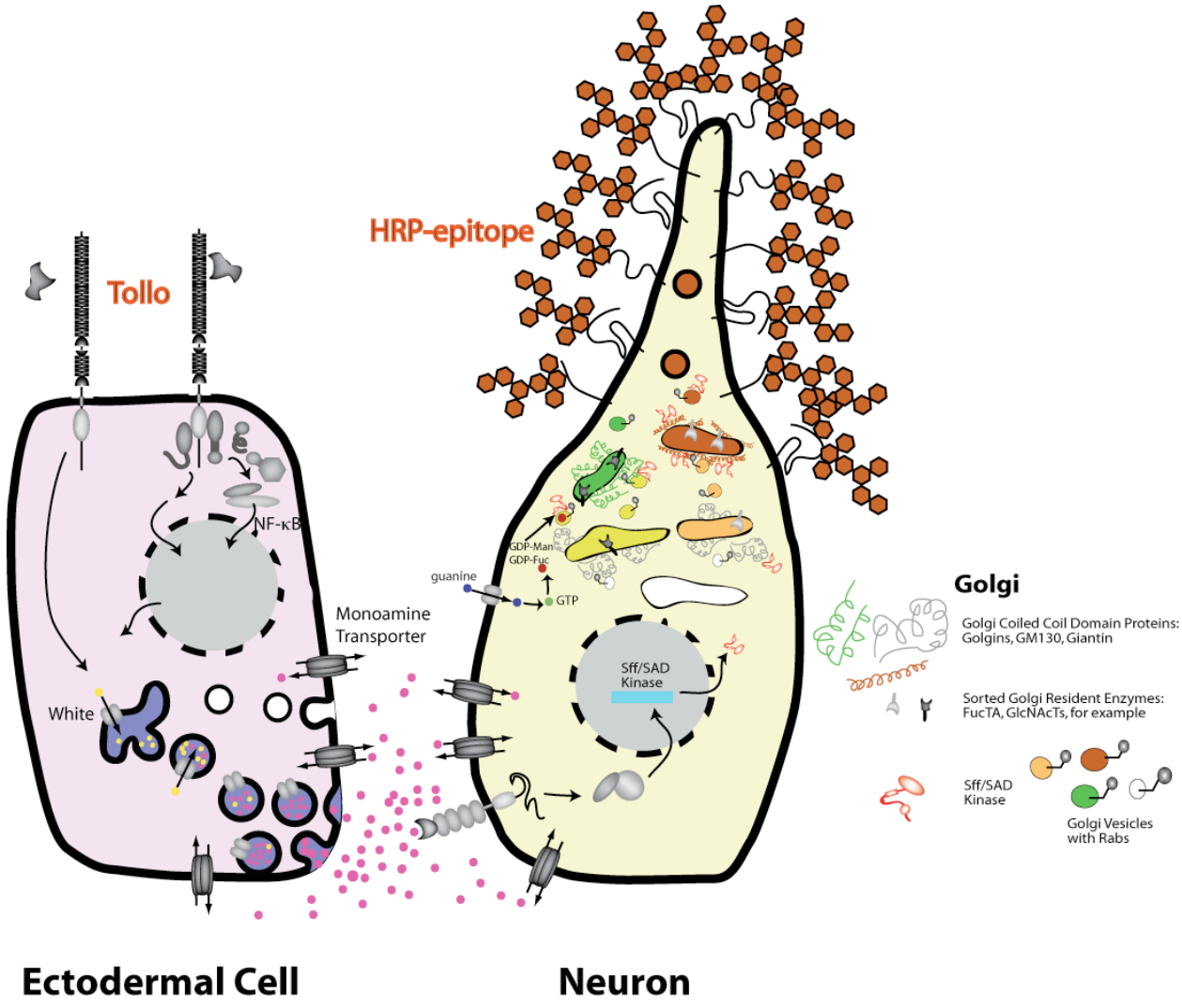

Figure 3.11. Model for HRP-epitope expression pathway
Depicted above is the current understanding about how HRP-epitope expression is regulated in neural cells. In a neighboring ectodermal cell, signaling through Tollo results in the release of a signal that is received by the neural cell, activating *sff/SAD* kinase expression leading to increased Sff/SAD function in the Golgi to facilitate vesicular traffic of newly synthesized proteins to Golgi compartments where glycosyltranferases (like FucTA) add the appropriate glycans. Based on the data that indicates signaling involving biogenic amines can affect embryonic HRP-epitope expression, we hypothesize that the molecule released from the ectodermal cell is a monoamine. Transporters, including White, import precursor molecule (like tryptophan, yellow) into secretory vesicles. Enzymes convert precursors into monoamines (like serotonin, pink). The vesicles fuse with the plasma membrane and release their contents into the extracellular space. The molecules bind to receptors on the neuron, signaling a cascade that triggers events leading to generation of HRP-epitopes. White also has a more direct impact on the regulation of glycosylation, perhaps through the import of guanine leading to the generation of GDP-Man and GDP-Fuc, or GTP, which is crucial for vesicular trafficking events. Through an unknown mechanism, White also influences *sff* mRNA expression, likely independent of signaling through Tollo.

neurons. Serotonin, acting through receptor 5-HT_{2C}, modulates the anorexic response induced by LPS.

Serotonin can also influence immune function. Binding serotonin to either the 5-HT_4 or 5-HT_7 receptor in mature dendritic cells results in the production of cAMP, resulting in an increase of IL-1β, IL-8, and a reduced secretion of IL-12 and TNFα (Meredith et al., 2005). Serotonin receptor antagonists were found to inhibit TNF production induced by LPS (TLR-4) in human monocytes (Fiebich et al., 2004). Another receptor antagonist (of 5-$HT_{2A/C}$), mianserin, blocks signaling of endosomally located TLR 3, 8, and 9 in primary human macrophages; in cultures of human rheumatoid arthritis synovial membranes the drug reduces production of IL-6 and TNF (Sacre et al., 2008).

A developmental function for monoamines, particularly serotonin, is also not without precedent. Serotonin has been detected in early embryogenesis in frog, sea urchin, and chick (Buznikov et al., 1996; Lauder, 1993; Schmucker et al., 2000). Studies using pharmacological agents has suggested that serotonin helps to regulate cell proliferation and morphogenic movements (Lauder, 1988). In mouse, serotonin is involved in craniofacial and cardiac development (Shuey et al., 1993; Yavarone et al., 1993). What is most interesting is the fact that simpler organisms lacking a nervous system possess catecholamines. For example, Tetrahymena (a ciliated protozoan) has noradrenaline and adrenaline and their levels fluctuate during the cell cyle, implicating these molecules in a broader range of biological processes than just neurotransmission (Pendelton et al., 1998).

The importance of serotonin early in development is conserved in *Drosophila*. One of the serotonin receptors, 5-HT_{2Dro}, is expressed early during embryogenesis, at the beginning of gastrulation. Deletions of this receptor cause early embryonic lethality, due to a defect in

germband extension. There is a desynchronization between ectodermal elongation and endoderm and mesoderm invaginations (Colas et al., 1995; Colas et al., 1999b). The mother deposits the cofactor for tryptophan hydroxylase, tetrahydrobiopterin, while the genes required for serotonin synthesis are zygotic. Mutants that lack serotonin have the same phenotype as embryos deficient in the 5-HT2$_{Dro}$, which suggests that serotonin, acting through this receptor, is required for normal gastrulation in the early embryo (Colas et al., 1999a).

The mechanisms that regulate tissue-specific glycan expression are beginning to yield to genetic analyses. Presented here is the emergence of signaling pathways that regulate neural-specific glycosylation in the developing *Drosophila* embryo. Both Tollo and biogenic amine signaling pathways are present very early in embryogenesis. Therefore, signaling, initiated early in development, may stimulate downstream events that, at the appropriate time, trigger Tollo signaling through biogenic amines to differentiating neurons to drive *sff* expression and ultimately Sff activity in the Golgi to decorate proteins with HRP-epitopes. Future work will be aimed at determining the players downstream and upstream of generating the cue to express HRP-epitopes. A relationship between biogenic amine signaling and the regulation of glycosylation is unprecedented and has intriguing implications for diseases with altered monoamine levels, such as depression and bipolar disorder.

ACKNOWLEDGEMENTS

I thank Heather-Flanagan Steet for help with the confocal analysis of the NMJ. Kazuhiro Aoki provided invaluable assistance with the analysis of the N-glycans by mass spectrometry as well as biogenic amine measurement by HPLC. Brian Dong and Khoi Nguyen collected larval brains for N-glycan analysis. Samule Lee performed the viability experiment, and Yong-kyu Kim

provided assistance in learning adult brain dissection. Michael Tiemeyer generated the graphics used for the model figure.

REFERENCES

Aoki, K., Perlman, M., Lim, J., Cantu, R., Wells, L., and Tiemeyer, M. (2007). Dynamic developmental elaboration of N-linked glycan complexity in the *Drosophila melanogaster* embryo. J Biol Chem *282*, 9127-9142.

Benevolenskaya, E., Frolov, M., and Birchler, J. (1998). The *sugarless* mutation affects the expression of the white eye color gene in *Drosophila melanogaster*. Mol Gen Genet *260*, 131-143.

Binari, R., Stavelely, B., Johnson, W., Godavarti, R., Sasisekharan, R., and Manoukian, A. (1997). Genetic evidence that heparin-like glycosaminoglycans are involved in wingless signaling. Development *124*, 2623-2632.

Blenau, W., and Baumann, A. (2001). Molecular and pharmacological properties of insect biogenic amine receptors: lessons from *Drosophila melanogaster* and *Apis mellifera*. Arch. Insect Biochem. and Phys. *48*, 13-38.

Borycz, J., Borycz, J., Kubow, A., Lloyd, V., and Meinhertzhagen, I. (2008). *Drosophila* ABC transporter mutants white, brown and scarlet have altered contents and distribution of biogenic amines in the brain. J Exper. Biol. *211*, 3454-3466.

Buznikov, G., Shmuckler, Y., and Lauder, J. (1996). From oocyte to neuron: do neurotransmitters function in the same way throughout development? Cell. Mol. Neurobiol. *16*, 537-559.

Campbell, J., and Nash, H. (2001). Volatile general anesthetics reveal a neurobiological role for the white and brown genes of *Drosophila melanogaster*. J Neurobiol *49*, 339-349.

Colas, J., Launay, J., Kellermann, O., Rosay, P., and Maroteaux, L. (1995). *Drosophila* 5-HT2 serotonin receptor: coexpression with fushi-tarazu during segmentation. Proc Natl Acad Sci USA *92*.

Colas, J., Launay, J., and Maroteaux, L. (1999a). Maternal and zygotic control of serotonin biosynthesis are both necessary for *Drosophila* germband extension. Mech. Dev. *87*, 67-76.

Colas, J., Launay, J., Vonesch, J., Hickel, P., and Maroteaux, L. (1999b). Serotonin synchronizes convergent extension of ectoderm with morphogenetic gastrulation movements in *Drosophila*. Mech. Dev. *87*, 77-91.

Crump, J., Zhen, M., Yishi, J., and Bargmann, C. (2001). The SAD-1 kinase regulates presynaptic vesicle clustering and axon termination. Neuron *29*, 115-129.

Diegelmann, S., Zars, M., and Zars, T. (2006). Genetic dissociation of acquisition and memory strength in the heat-box spatial learning paradigm in *Drosophila*. Learn Mem. *13*, 72-83.

Ewart, G., and Howells, A. (1998). ABC transporters involved in the transport of eye pigment precursors in *Drosophila melanogaster*. Meth Enzymol *292*, 213-224.

Fiebich, B., Akundi, R., Lieb, K., Candelario-Jalil, E., Gmeiner, D., Haus, U., Muller, W., Stratz, T., and Munoz, E. (2004). Antiinflammatory effects of 5-HT_3 receptor antagonists in lipopolysacharid-stimulated primary human monocytes. Scand. J. Rheumatol *119*, 28-32.

Finocchiaro, L., Callebert, J., Launay, J., and Jallon, J. (1988). Melatonin biosynthesis in *Drosophila*: its nature and its effects. J. Neurochem *50*, 383-387.

Grammatikakis, N., Grammatikakis, A., Toneda, M., Yu, Q., Baneriee, S., and Toole, B. (1995). A novel glycosaminoglycan-binding protein is the vertebrate homologue of the cell cycle control protein Cdc37. J Biol Chem *270*, 16198-16205.

Haerry, T., Heslip, R., Marsh, J., and O'Connor, M. (1997). Defects in glucuronate biosynthesis disrupt Wingless singaling in *Drosophila*. Development *124*, 3055-3064.

Hardie, S., and Hirsh, J. (2006). An improved method for the separation and detection of biogenic amines in adult *Drosophila* brain extracts by high performance liquid chromatography. J NEurosci Met *153*, 243-249.

Hsouna, A., Lawal, H., Izevbaye, I., Hsu, T., and O'Donnell, J. (2007). *Drosophila* dopamine sythesis pathway genes regulate tracheal morphogenesis. Dev. Biol. *308*, 30-43.

Inoue, E., Mochida, S., Takagi, H., Higa, S., Deguchi-Tawarada, M., Takao-Rikitsu, E., Inoue, M., Yao, I., Takeuchi, K., Kitajima, I., *et al*. (2006). A presynaptic kinase associated with synaptic vesicles and the active zone cytomatrix that regulates neurotransmitter release. Neuron *50*, 261-275.

Kaufmann N, DeProto J, Ranjan R, Wan H, and D, V.V. (2002). *Drosophila* liprin-alpha and the receptor phosphatase Dlar control synapse morphogenesis. Neuron *28*, 27-38.

Kidd, M., Gustafsson, B., Drozdov, I., and Modlin, I. (2009). IL1beta-and LPS-induced serotonin secretion is increased in EC cells derived from Crohn's disease. Neurogastroenterol Motil *21*, 439-450.

Kopczynski, C., Davis, G., and Goodman, C. (1996). A Neural Tetraspanin, Encoded by late bloomer, That Facilitates Synapse Formation. Science *271*, 1867-1870.

Krishnakumar, S., Burton, D., Rasco, J., Chen, X., and O'Donnell, J. (2000). Functional interactions between GTP cyclohydrolase I and tyrosine hydroxylase in *Drosophila*. J Neurogenet *14*, 1-23.

Langhans, W. (2007). Symposium on 'Eating, illness and the gut: is there a disorder in the house?' Signals generating anorexia during acute illness. Proceedings of the Nutrition Society *66*, 321-330.

Lauder, J. (1988). Neurotransmitters as morphogens. Prog. Brain Res. *73*, 365-387.

Lauder, J. (1993). Neurotransmitters as growth regulatory signals: role of receptors and second messengers. Trends Neurosci. *16*, 233-240.

Lloyd, T., Verstreken, P., Ostrin, E., Phillippi, A., Lichtarge, O., and Bellen, H. (2000). A genome-wide search for synaptic vesicle cycle proteins in *Drosophila*. Neuron *26*, 45-50.

Lloyd, V., Sinclair, D., Alpern, M., and Grigliatti, T. (2002). *Enhancer of garnet*/δAP-3 is a cryptic allele of the *white* gene and identifies the intracellular transport system for the white protein. Genome *45*, 296-312.

Mackenzie, S., Howells, A., Cox, G., and Ewart, G. (2000). Sub-cellular localisation of the White/Scarlet ABC transporter to pigment granule membranes within the compound eye of *Drosophila melanogaster*. Genetica *108*, 239-252.

Meredith, E., Chamba, A., Holder, M., Barnes, N., and Gordon, J. (2005). Close encounters of the monoamine kind: immune cells betray their nervous disposition. Immun *115*, 289-295.

Monastirioti, M. (1999). Biogenic amine systems in the fruit fly *Drosophila melanogaster*. Microscopy research and technique *45*, 106-121.

Newell-Litwa, K., Seong, E., Burmeister, M., and Faundez, V. (2007). Neuronal and non-neuronal functions of the AP-3 sorting machinery. J. Cell Sci. *120*, 531-541.

Nichols, C., Ronesi, J., Pratt, W., and Sanders-Bush, E. (2002). Hallucinogens and *Drosophila*: linking serotonin receptor activation to behavior. J Neurosci. *115*, 979-984.

Ooi, C., Moreira, J., Dell'Angelica, E., Poy, G., Wassarman, D., and Bonifacino, J. (1997). Altered expression of a novel adaptin leads to the defective pigment ganule biogenesis in the *Drosophila* eye color mutant *garnet*. EMBO J *16*, 4508-4518.

Patel, N. (1994). Imaging neuronal subsets and other cell types in whole-mount *Drosophila* embryos and larvae using antibody probes. Methods Cell Biol *44*, 445-487.

Pendelton, R., Rasheed, A., Roychowdhury, R., and Hillman, R. (1998). A new role for catecholamines: ontogenesis. TiPS *19*, 248-251.

Phillips, J., and Forrest, H. (1980). Ommochromes and pteridines. In The genetics and biology of *Drosophila*, M. Ashburner, and T. Wright, eds. (New York: Academic Press), pp. 542-623.

Regnier-Vigouroux, A., and Huttner, W. (1993). Biogenesis of small synaptic vesicles and synaptic-like microvesicles. Neurochem Res *18*, 59-64.

Sacre, S., Lo, A., Gregory, B., Simmonds, R., Williams, L., Feldmann, M., Brennan, F., and Foxwell, B. (2008). Inhibitors of TLR8 reduce TNF production from human rheumatoid synovial membrane cultures. J. Immunol. *181*, 8002-8009.

Savvateeva, E., Popov, A., Kamyshev, N., Bragina, J., Heisenberg, M., Senitz, D., Kornhuber, J., and Riederer, P. (2000). Age-dependent memory loss, synaptic pathology and altered brain plasticity in the *Drosophila* mutant *cardinal* accumulating 3-hydroxykynurenine. J Neural Transm *107*, 581-601.

Savvateeva, E., Popov, A., Kamyshev, N., Iliadi, K., Bragina, J., Heisenberg, M., Kornhuber, J., and Riederer, P. (1999). Age-dependent changes in memory and mushroom bodies in the *Drosophila* mutant *vermillion* deficient in kynurenine pathway of tryptophan metabolism. Ross. Fizol. Im I M. Sechenova *85*.

Schmucker, D., Clemens, J., Shu, H., Worby, C., Xiao, J., Muda, M., Dixon, J., and Zipursky, S. (2000). *Drosophila* Dscam is an axon guidance receptor exhibiting extraordinary molecular diversity. Cell *101*, 671-684.

Seppo, A., Matani, P., Sharrow, M., and Tiemeyer, M. (2003). Induction of neuron-specific glycosylation by Tollo/Toll-8, a *Drosophila* Toll-like receptor expressed in non-neural cells. Development *130*, 1439-1448.

Shoup, J. (1966). The development of pigment granules in the eyes of wild type and mutant *Drosophila melanogaster*. J Cell Biol *29*, 223-249.

Shuey, D., Sadler, T., Tamir, H., and Lauder, J. (1993). Serotonin and morphogenesis. Transient expression of serotonin uptake and binding protein during craniofacial morphogenesis in the mouse. Anat. Embryol. *187*, 75-85.

Simon, A., Daniels, R., Romero-Calderon, R., Grygoruk, A., Chang, H., Najibi, R., Shamouelian, D., Salzar, E., Solomon, M., Ackerson, L.*, et al.* (2009). *Drosophila* vesicular monoamine transporter mutants can adapt to reduced or eliminated vesicular stores of dopamine and serotonin. Genetics *181*, 525-541.

Simpson, F., Peden, A., Christopoulou, L., and Robinson, M. (1997). Characterization of the adaptor-related protein complex, AP-3. J Cell Biol *137*, 835-845.

Yavarone, M., Shuey, D., Tamir, H., Sadler, T., and Lauder, J. (1993). Serotonin and cardiac morphogenesis in the mouse embryo. Teratology *47*, 573-584.

Zhang, S., and Odenwald, W. (1995). Misexpression of the white (w) gene triggers male-male courtship in *Drosophila*. Proc Natl Acad Sci USA *92*, 5525-5529.

CHAPTER 4

FUTURE DIRECTIONS AND CONCLUSIONS

The current work identifies Sugar-free frosting as a regulator of neural-specific glycosylation in the *Drosophila* embryo. Work branching from the initial Sff project has identified *white* as a genetic interactor with *sff*, and biogenic amines as additional modulators of neural-specific glycosylation. The future directions and implications for this research are discussed below.

Solidifying the roll of sff in neural Golgi trafficking

The identification of *sugar-free frosting* as the *Drosophila SAD* kinase involved the mapping of the EMS-induced mutation to the genetic locus. One of the necessary experiments to confirm *sff* is *SAD* kinase was to introduce a wild-type copy into the mutant and test for rescue of the phenotype. Already begun, a genetic construct carrying the coding region for *SAD* kinase (*CG6114*) has been transformed into *Drosophila* embryos. Linked to the upstream activating sequence (UAS), expression is driven upon binding of the transcription factor Gal4. Gal4 can be fused to any tissue-specific promoter. Crossing UAS-*SAD* to ELAV-Gal4 drives SAD expression in all neural cells. When crossed into an *sff* mutant background, the anti-HRP staining phenotype (as well as any other phenotypes) should be rescued. Although our genetic and phenotypic data lend confidence to *sff* being *SAD* kinase, the rescue experiment should vanquish any doubts that remain.

This work has placed SAD kinase into a previously unidentified role—modulation of Golgi trafficking, specifically, in directing protein glycosylation. As previously discussed, the glycosylation of proteins is initiated in the endoplasmic reticulum (see chapter 1).

Immature glycoproteins are then trafficked to the Golgi apparatus, where the glycans are processed to their mature form. The Golgi consists of membranous stacks, called cisternae. There are two models of how cargo move through the Golgi (Pfeffer, 2007). In one model, vesicles bud from one compartment and fuse with the next, carrying cargo along the route. This trafficking involves tethering molecules like the coiled-coiled domain proteins the Golgins, Rab GTPases, and soluble N-ethylmaleimide-sensitive factor attachment protein receptors (SNARES) (Behina and Munro, 2005). A second model is the cisternal maturation model, which assumes that that stacks move as a whole from cis to trans, with the proteins being processed as the stack travels (Pfeffer, 2007). This latter model also involves vesicular transport, as the glycosyltransferases would require retrograde transport back to the starting cisternae. It is important to note that these models are not mutually exclusive and in reality Golgi trafficking may represent a combination of the two.

In mammalian cells the Golgi stacks are linked into a ribbon structure, but in *Drosophila* they appear as discrete puncta. It was initially thought that the processing of glycans occurred in a gradient manner, with the earlier enzymatic processing events occurring in the cis Golgi and later, more complex processing occurring in the trans Golgi (Nilsson et al., 2009). However, this hypothesis has been challenged, with evidence that GlcNAcT-1 and Sialyltransferase are both localized to the same trans cisternae (Nilsson et al., 2009). Therefore several enzymatic events may occur without the need to transport the substrate to another location, implying that enzymes must "compete" for substrates. However given the small number of biologically relevant structures in relation to an immense possibility of theoretical structures, processing occurs in a highly specified fashion, arguing that there still must be other mechanisms regulating glycosylation events in the Golgi. Several mechanisms that have been put forth include the

presence of multi-enzyme complexes, competition for loading of glycosyltransferases into retrograde transport vesicles, and determination of glycosyltransferase position according to their transmembrane length (Nilsson et al., 2009). Finally, given the results presented in previous chapters, the involvement of kinases and other proteins in these events is likely to contribute to the regulation of glycan processing in the Golgi.

The substrates for Sff/SAD at the neuronal synapse are likely to be different from those at the Golgi. At the presynaptic membrane, SAD has been shown to phosphorylate RIM, a protein that forms a triad with Munc13 and Rab3 to prime synaptic vesicles for release (Inoue et al., 2006). The process of vesicle trafficking at the Golgi is not unlike that that of the synapse. Both require appropriate Rab molecules as well as structural coiled-coil domain proteins to serve as scaffolds. Candidates for Sff/SAD substrates at the Golgi include proteins that interact with Rabs like Golgins, and coiled coil domain proteins (Burguete et al., 2008; Short et al., 2005). Based on our current results it is unclear if Sff/SAD affects trafficking of substrates or glycosyltransferases or both. Experiments are planned to identify substrates by creating a kinase that accepts an orthogonal ATP with a sulfo group, allowing substrates to be uniquely tagged (Liu et al., 1998a; Liu et al., 1998b; Shah et al., 1997).

Our initial look at Golgi trafficking involved staining the embryonic nervous system with antibodies against Golgi compartment markers and a protein that is HRP-modified, although our results clearly indicate that the traffic of glycoproteins is altered in the sff mutant, a closer look at the structure of the Golgi would prove useful. Electron microscopy of synaptic vesicles in the *C. elegans SAD-1* mutant revealed mis-alignment of the vesicles at the cytomatrix active zone; a similar view of the *Drosophila* Golgi of the *sff/SAD* mutant may illustrate a similar phenotype (Crump et al., 2001). Another useful tool to further elucidate Sff/SAD's function at the Golgi is

to visualize the protein by antibody staining. All data points to Sff/SAD activity at the Golgi but immunohistochemistry in embryos will confirm the localization. Unfortunately, all current SAD antibodies generated in mouse and *C. elegans* are to regions of poor conservation to *Drosophila* SAD kinase so more specific antibodies would need to be generated (Hung et al., 2007; Kishi et al., 2005).

We have performed complete characterization of the N-linked glycans in the *sff* mutant, but we have yet to examine whether O-linked glycans or glycolipid prevalences are affected by the *sff* mutation. The O-linked glycan profile of wild-type embryos has already been published by our laboratory and glycolipid analysis methods are currently being developed (Aoki et al., 2008). Since Sff functions to drive Golgi compartmentation, it is likely that other glycan structures are affected. Also, characterization so far has focused on the embryo. A preliminary examination of larval and adult neural tissues has already been performed, but a complete characterization to assess the function of Sff throughout development would be useful. So far the results indicate that many of the trends seen in the embryo extend to later stages of development.

Another question that needs to be addressed is whether SAD's role in the regulation of glycan expression is conserved in higher organisms. An analysis of the N-glycans of *SAD* double knockout mice will be an important future experiment (Kishi et al., 2005). If the phenotype is similar, vertebrate cell culture can be used to address similar questions being sought using *Drosophila*. However, cell culture would not allow the study of cell-cell interactions that may be involved or how the glycan expression of an entire tissue is regulated. There has been very little progress in the determination of the regulators of glycan expression, so work on

sff/SAD, and genes like it, will help define the mechanisms underlying tissue-specific glycosylation patterns.

Defining the relationship between sugar-free frosting and white

In chapter three, the effect of a mutation in *white* on the phenotypes associated with the *sff* mutation was presented. Based on the current findings, many questions remain about how *sff* and *white* interact. It was suggested that signaling pathways involving Sff/SAD might be mis-sorting the White protein. Since male courtship behavior is a consequence of defective white trafficking, sff^{B22} males should be tested (Zhang and Odenwald, 1995). Also, other alleles of white may be crossed into an sff^{B22} background to elucidate any dosage dependent effects (w^{1118} is a null allele). Similarly, other pigment genes, such as *brown* or *garnet*, could be examined to more clearly define the relationship between *sff* and genes involved in pigment biosynthesis and its trafficking events. As with Sff, an antibody against the White protein would prove extremely useful in determining White's function in glycosylation and in neural cells. The White protein is one of the most studied genes in *Drosophila*; in fact it was the first identified mutation (Morgan, 1910). However, little work has been done to determine White's function, although a myriad of genetic interactors have been identified and countless mutant alleles are available. As stated in the discussion for chapter three, *white* is regulated by *sugarless*, creating a link between *white* and glycosylation. Future work will try to solidify White's relationship to glycosylation and further determine White's neural function, and the role Sff plays in contributing to those functions.

Elucidating the role of biogenic amine signaling in the regulation of glycosylation

A very interesting discovery was made during the course of this research project. That is the involvement of biogenic amines in the regulation of tissue-specific glycosylation, a notion that

was initially stumbled upon by a weak genetic interaction between *sff* and *tryptophan hydroxylase*. Also, treatment of sff^{B22} adults with drugs that raise biogenic amine levels restored their locomotor behavior. More intriguingly, it was discovered that treatment of embryos with a monoamine oxidase inhibitor affects anti-HRP epitope expression. Future work in *Drosophila* could include examining the glycan profiles of mutations of genes involved in biogenic amine synthesis and action, like Tyrosine hydroxylase and vesicular monoamine transporters. Testing with other drugs may also help to narrow down the specific amine responsible; our current hypothesis suggests serotonin. The relationship between glycosylation and neurotransmitters is a novel finding and the future implications are very exciting. For instance, the role of glycosylation in disorders stemming from altered biogenic amine levels such as depression, bipolar disorder, and migraine, has not been examined. An effort has already been initiated to extend these studies to higher organisms and preliminary results reveal that a vertebrate cell line treated with phenelzine or the addition of biogenic amines has altered N-glycosylation patterns.

Final remarks

The addition of glycan structures to nascent polypeptides is a complex process and much is still not understood. The blueprints for selecting which glycan structure is added still remain somewhat elusive, despite the well-defined NXS/T amino acid sequon that determines placement. The possible combinations of glycoforms is staggering compared to the actual glycoforms that are present for a single protein (Dennis et al., 2009). Adding another layer of complexity is the fact that neighboring cells can express different glycosylation patterns, and in terms of tissue glycosylation the complexity is astounding. Granted glycosyltransferases have restricted expression patterns, which limits specific structures to specific locations and cell populations. But the fact remains that very little is known about the overarching signaling

pathways that control tissue-specific glycosylation. The work presented here on *sugar-free frosting* has shed some light on how neural-specific glycan expression is regulated in the *Drosophila* embryo. Nonetheless, this small step will hopefully help us to expand our knowledge of glycosylation in other tissues and organisms. There are many levels in which glycan expression can be regulated, such as the control of glycosyltransferase transcript and protein levels. The work presented is a more intriguing mode of regulation, and that is by the modulation of vesicular transport through the Golgi. There are several pathways that impinge on Sff/SAD function, allowing the external environment to have minute control of how substrates are glycosylated, allowing a shift in the transport of substrates to different Golgi compartments (**Figure 4.1**). Very likely there are other kinases that serve similar functions in other tissues in *Drosophila* and in other organisms, opening up new avenues of research into how glycosylation is regulated. Despite the almost overwhelming questions that remain unanswered as to how the regulated complexity of glycosylation is determined, in terms of neural-specific glycosylation in *Drosophila,* this work has provided three answers: white, biogenic amines, and most importantly Sugar-free frosting/SAD kinase.

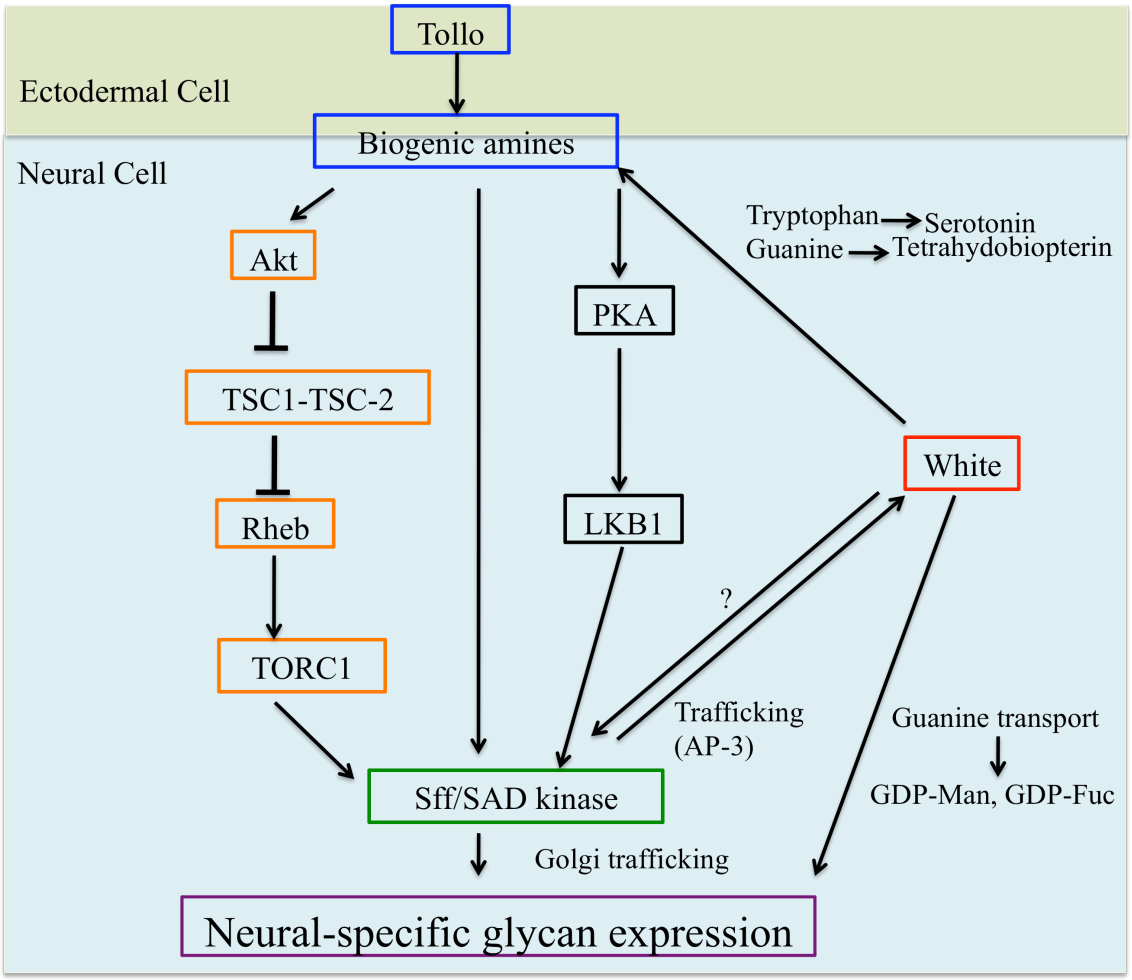

Figure 4.1 Pathways impinging on Sff/SAD kinase that contribute to the regulation of neural-specific glycosylation. Work presented in chapter 2 demonstrates that Sff/SAD kinase modulates vesicle trafficking at the Golgi, essential for neural-specific glycan expression. Work from other groups has demonstrated that pathways initiated by extracellular signals activate Akt and PKA signaling to increase *SAD* kinase protein levels. The pathways have been shown to be important for SAD's function in neuronal polarity; their role in the regulation of neural-specific glycan expression have not yet been examined. Another pathway, initiated by Tollo in a neighboring ectodermal cell, also impinges on Sff/SAD function leading to glycan-expression. Tollo signaling activates the release of biogenic amines that signal to the neural cell. Biogenic amine signaling (through their respective receptors) may lie upstream of Akt and PKA pathways that converge on Sff/SAD. Chapter 3 introduced White as interacting with Sff/SAD and hypothesized that Sff/SAD kinase may also be trafficking AP-3 vesicles carrying White. White also affects *sff*/SAD expression through a yet undefined mechanism. White can also influence glycan expression by modulating GDP-mannose and GDP-fucose levels through transport of guanine. White function may also impact biogenic amines as tryptophan is the precursor for the synthesis of serotonin, and guanine is converted dihydroneopterin triphosphate, which is converted to tetrahydrobiopterin, an essential cofactor for Tyrosine and Tryptophan Hydroxylases. Thus defined pathways are emerging that regulate neural-specific glycan expression in *Drosophila*.

REFERENCES

Aoki, K., Porterfield, M., Lee, S., Dong, B., Nguyen, K., McGlamry, K., and Tiemeyer, M. (2008). The diversity of O-linked glycans expressed during *Drosophila melanogaster* development reflects stage- and tissue-specific requirements for cell signaling. J Biol Chem *283*, 30385-30400.

Behina, R., and Munro, S. (2005). Organelle identity and the signposts for membrane traffic. Nature *438*.

Burguete, A.S., Fenn, T.D., Brunger, A.T., and Pfeffer, S.R. (2008). Rab and Arl GTPase family members cooperate in the localization of the golgin GCC185. Cell *132*, 286-298.

Crump, J., Zhen, M., Yishi, J., and Bargmann, C. (2001). The SAD-1 kinase regulates presynaptic vesicle clustering and axon termination. Neuron *29*, 115-129.

Dennis, J., Nabi, I., and Demetriou, M. (2009). Metabolism, cell surface organizaiton, and disease. Cell *139*, 1229-1241.

Hung, W., Hwang, C., Po, M., and Zhen, M. (2007). Neuronal polarity is regulated by a direct interaction between a scaffolding protein, neurabin, and a presynaptic SAD-1 kinase in *Caenorhabditis elegans*. Development *134*, 237-249.

Inoue, E., Mochida, S., Takagi, H., Higa, S., Deguchi-Tawarada, M., Takao-Rikitsu, E., Inoue, M., Yao, I., Takeuchi, K., Kitajima, I*., et al.* (2006). A presynaptic kinase associated with synaptic vesicles and the active zone cytomatrix that regulates neurotransmitter release. Neuron *50*, 261-275.

Kishi, M., Pan, Y., Crump, J., and Sanes, J. (2005). Mammalian SAD kinases are required for neuronal polarization. Science *307*, 929-932.

Liu, Y., Shah, K., Yang, F., Witucki, L., and Shokat, K. (1998a). A molecular gate which controls unnatural ATP analogue recognition by the tyrosine kinase v-Src. Bioorganic and Medicinal Chemistry *6*, 1219-1226.

Liu, Y., Shah, K., Yang, F., Witucki, L., and Shokat, K. (1998b). Engineering Src family protein kinases with unnatural nucleotide specificity. Chemistry and Biology *5*, 91-101.

Morgan, T. (1910). Sex limited inheritance in *Drosophila*. Science *32*, 12-122.

Nilsson, T., Anu, C., and Bergeron, J.J. (2009). Sorting out glycosylation enzymes in the Golgi apparatus. FEBS Letters *583*, 3764-3769.

Pfeffer, S. (2007). Unsolved mysteries in membrane traffic. Annu rev Biochem *76*, 629-645.

Shah, K., Liu, Y., Diermengian, C., and Shokat, K. (1997). Engineering unnatural nucleotide specificity for Rous Sarcoma Virus tyrosine kinase to uniquely label its substrates. PNAS *95*, 3565-3570.

Short, B., Haas, A., and Baar, F. (2005). Golgins and GTPases, giving identity and structure to the Golgi apparatus. Biochim Biophys Acta *1744*, 383-395.

Zhang, S., and Odenwald, W. (1995). Misexpression of the white (w) gene triggers male-male courtship in *Drosophila*. Proc Natl Acad Sci USA *92*, 5525-5529.